IMPERIAL COLLEGE OF SCIENCE, TECHNOLOGY AND MEDICINE

University of London

# VIBRATION ANALYSIS OF MISTUNED BLADED SYSTEMS

by

**Kenan Yuce SANLITURK**

A thesis submitted to the University of London for the degree of Doctor of Philosophy.

Department of Mechanical Engineering
Imperial College of Science, Technology and Medicine
London SW7

February 1992

*To My Family*

# ABSTRACT

*The existence of small dimensional variations between blades on the same rotor or stator is called mistuning and causes a phenomenon which can drastically change the vibration characteristics of the mistuned assembly from those of the corresponding tuned system. This thesis aims to improve the basic understanding of the response characteristics of mistuned bladed systems and reports both deterministic and statistical studies on this topic.*

*An exact analytical solution, applicable to any number of blades, is presented for the forced vibration of tuned bladed disc assemblies which are modelled using a lumped-parameter technique. This method of analysis is also extended for alternate and single-blade mistuning cases. The latter case is considered to be a result of a blade with a crack and it is modelled using experimentally-derived crack-dependent stiffness and damping properties. This study led to the formulation of a general method for fatigue life prediction of engineering components subjected to dynamic loads.*

*Although such deterministic results are useful in many respects, their application is limited because of the inherent randomness of structural properties of blades due to manufacturing tolerances. As a first step towards the statistical solution of the mistuning problem, an analytical method is developed to investigate the effects of random variations in stiffness and/or damping properties on vibration characteristics of a single-degree-of-freedom system. Cumulative probability distributions of damped natural frequencies and frequency response functions of such systems are obtained directly from the corresponding probability density functions of stiffness and/or damping properties.*

*The general random mistuning problem is addressed using statistical sampling theory. Blade-to-blade variations are considered to be random with a Gaussian distribution and answers to some very important mistuning-related questions are sought on a statistical basis. The findings of this thesis help to reconcile conflicting conclusions which were previously reached by many researchers on both qualitative and quantitative matters related to the consequences of mistuning, most notably the identification of critical blades and the increase in forced response due to mistuning.*

*Finally, a method to determine acceptable blade-to-blade variations for blade response levels to remain within A% of the tuned system or design values is developed. This method is successfully used to find the relationship between the allowable response increase due to mistuning and the allowable manufacturing tolerance.*

# ACKNOWLEDGEMENTS

I am grateful to both of my supervisors, Prof. D. J. Ewins and Dr. M. Imregun, for their continual guidance, stimulus and encouragement during the course of this project.

I would like to thank Mr. D. A. Robb and Dr. P. Cawley for their helpful advice and discussions on some aspects of the work. Thanks are also due to present and past members of the Imperial College Dynamics Section for many useful discussions and exchange of ideas in particular to Miss. W. J. Visser and Mr. H. Yiu.

I am indebted to the Rolls-Royce plc. for their technical assistance. I also thank Mr. J. Bennett of Rolls-Royce for his informative discussion on mistuning.

Finally, I gratefully acknowledge the financial support given by the Turkish Government over the period in which this work was carried out.

# NOTATION

| | |
|---|---|
| $a$ | Crack length |
| $A$ | Cross-sectional area |
| $a_o$ | Initial crack length |
| $c$ | Viscous damping coefficient |
| CD | Coefficient of dispersion (Standard deviation/Mean) |
| $C_o$ | Material constant |
| $E$ | Young's modulus |
| $f(t)$ | General force signal |
| $F_o$ | Magnitude of engine order excitation |
| $g_i$ | $i^{th}$ functional relation |
| $G_j$ | $j^{th}$ blade's first cantilever frequency |
| $\bar{G}$ | Mean of blades' first cantilever frequencies |
| $i$ | $\sqrt{-1}$ |
| $k$, $K$ | Blade stiffness |
| $k_1$ | Cracked blade stiffness |
| $K_d$ | Sectorial disc stiffness |
| $k_g$ | Grounding stiffness |
| $k_H$ | High frequency blade stiffness |
| $K_I$ | Stress intensity factor |
| $K_{Ic}$ | Critical stress intensity factor |
| $k_j$ | $j^{th}$ blade stiffness |
| $k_L$ | Low frequency blade stiffness |
| $k_r$ | Modal stiffness |
| $K_s$ | Shroud stiffness |
| $L$ | Length |
| $m$ | Number of degrees of freedom |

| | |
|---|---|
| $m, M$ | Blade mass |
| $M_d$ | Sectorial disc mass |
| $m_r$ | Modal mass |
| $n$ | Material constant, Number of functional relations or equations |
| $N$ | Number of blades |
| $N_c$ | Fatigue life |
| ND | Nodal diameter |
| $n_I$ | Number of data within a subinterval |
| $N_I$ | Number of subintervals |
| $N_m$ | Number of modes |
| $N_s$ | Sample size |
| $p$ | Probability density function (pdf) |
| $P$ | Cumulative density function (cdf) |
| $\hat{q}$ | Sample mean of response amplitude |
| $r$ | Engine order of excitation |
| $R$ | Stress ratio |
| $s$ | Number of excitation frequencies, distance in Appendix IV |
| $t$ | Time |
| $u$ | Number of unknown structural parameters |
| $v$ | Total number of unknowns |
| $w$ | Number of coordinates at which real and imaginary parts of the response levels are known, thickness in Appendix IV |
| $x$ | Independent variable in chapter 5, response elsewhere |
| $x, y, z$ | Response |
| $X, Y, Z$ | Response amplitude |
| $x_j$ | $j^{th}$ blade response |
| $X_j$ | $j^{th}$ blade response amplitude |
| ${}_IX_j$ | Imaginary part of $j^{th}$ blade response amplitude |

| | |
|---|---|
| ${}_{M}X_j$ | Magnitude of $j^{th}$ blade response amplitude |
| ${}_{R}X_j$ | Real part of $j^{th}$ blade response amplitude |
| $y$ | Dependent Variable in chapter 5, response elsewhere |
| $Y$ | Crack shape function |
| $y_j$ | $j^{th}$ disc sector response |
| $Y_j$ | $j^{th}$ disc sector response amplitude |
| ${}_{I}Y_j$ | Imaginary part of $j^{th}$ disc sector response amplitude |
| ${}_{R}Y_j$ | Real part of $j^{th}$ disc sector response amplitude |
| $\alpha$ | Receptance |
| $\beta_{ij}$ | Stress parameter |
| $\gamma_j$ | jth element of unknown vector $\{\gamma\}$ |
| $\eta$ | Hysteretic damping ratio |
| $\eta_1$ | Cracked blade hysteretic damping ratio |
| $\eta_r$ | Modal damping |
| $\lambda$ | Eigenvalue |
| $\theta_r$ | Interblade phase angle ($2\pi r/N$) |
| $\rho$ | Density |
| $\sigma$ | Standard deviation |
| $\sigma_{nom}$ | Nominal stress |
| $\omega, \omega_{ex}$ | Excitation frequency |
| $\omega_d$ | Damped natural frequency |
| $\omega_o$ | Undamped natural frequency |
| $\omega_r$ | Natural frequency for the $r^{th}$ mode |
| $\omega_{res}$ | Resonant frequency |
| $\zeta$ | Viscous damping ratio |

**Vectors and matrices**

| | |
|---|---|
| $\{f\}$ | Harmonic force vector |

| | |
|---|---|
| $\{\hat{f}\}$ | Force amplitude vector |
| $\{q\}$ | Response vector |
| $\{\hat{q}\}$ | Response amplitude vector |
| $\{R\}$ | Residual vector |
| $\{U_j\}$ | Real and imaginary parts of $j^{th}$ sector response levels at various excitation frequencies |
| $\{\delta\gamma\}$ | Correction vector for the unknown vector |
| $\{\gamma\}$ | Unknown vector |
| $\{\Lambda\}$ | Eigenvalue vector |
| $\{\sigma\}$ | Stress vector |
| $[A]$ | Strain to stress transformation matrix |
| $[B]$ | Response to strain transformation matrix |
| $[D]$ | Hysteretic damping matrix |
| $[K]$ | Stiffness matrix |
| $[M]$ | Mass matrix |
| $[S]$ | Matrix which contains the derivatives of the functional relations with respect to unknown structural parameters and response levels. |
| $[Z]$ | Dynamic stiffness matrix |
| $[\alpha]$ | Receptance matrix |
| $[\psi]$ | Eigenvector matrix |

# TABLE OF CONTENTS

# CHAPTER 1

# INTRODUCTION

**About This Chapter**

*This chapter describes the nature of the problem, gives a brief review of related literature and outlines the objectives of this thesis.*

## 1.1 The Nature of the Problem

Perhaps one of the most challenging tasks facing today's engineers is the design of turbomachinery components which require exceptionally high reliability. For example, a jet engine may contain thousands of blades and a failure of an early stage blade may cause catastrophic results, hence even the failure of a single blade is not allowable in many turbomachinery applications. Moreover, trends in turbomachinery technology have been to increase performance and efficiency and to reduce overall weight often by increasing operating speeds. Together with weight and dimensional optimization of turbomachinery components, these modifications have led to an alarming number of vibration-related fatigue failures and this in turn has made the attainment of the required reliability an extremely difficult task.

In order to prevent hazardous fatigue failures and to ensure the required reliability, it is necessary to predict the dynamic characteristics of a bladed disc assembly within engineering accuracy. However, dynamic analysis of such systems is complicated, the difficulties involved falling into one of the three main categories:

i) the geometry of the assembly is very complex and interface boundary conditions (structure-to-fluid, blade-to-disc and blade-to-shroud) are not well defined;

ii) the operating conditions are very hostile and the excitation forces are difficult to evaluate; and

iii) small dimensional variations, mainly due to manufacturing tolerances, exist between individual blades on the same stage and this phenomenon can change drastically the vibration characteristics of mistuned assemblies from those of their tuned counterparts, thus making the calculations based on tuned system unreliable. This blade-to-blade variation, known as mistuning, constitutes the focal point of this thesis.

There are three main sources of mistuning in bladed disc systems.

i) The first is mechanical mistuning, or the presence of small variations in mass or stiffness properties of individual blades, which is due mainly to manufacturing tolerances. However, other factors can also influence this type of mistuning: uneven wearing of blades during service, leading to mass variations; discrepancies in material properties mainly due to randomness in heat treatment processes, leading to stiffness variations and defects and/or fatigue cracks causing stiffness reduction. The existence of this type of mistuning is normally accompanied by a scatter of individual blade natural frequencies.

ii) The second is damping mistuning, resulting from variations in damping properties of individual blades. Such differences may occur either due to variations in blade-to-disc and/or blade-to-blade frictional forces (especially of blade roots and shrouds interfaces) or due to defects and/or fatigue cracks which can change both the uniformity and the overall level of energy dissipation in individual blades.

iii) The third is aerodynamic mistuning which results from variations in external forces acting on individual blades due to changes in amplitude and phase angle of the aerodynamic forces acting on each blade.

It should be noted that the presence of one type of mistuning may activate further mistuning of some other type. For instance, mechanical mistuning (i) may also produce a non-uniform pressure distribution around the blade, (iii). This, in turn, may cause energy dissipation levels to be different from blade to blade.

It is of paramount importance for engine designers to know the consequences of mistuning, and particularly the amount of increase in the forced response level over that of the corresponding tuned system and the critical blade(s) which is(are) more likely to experience the highest stresses when the system is mistuned. Although many studies have been made on mistuned assemblies to address these questions and further consequences of mistuning, various researchers do not seem to agree on many crucial points. In order to highlight these discrepancies, some of the conclusions which have been reached in the past on the degree of worsening effect of mistuning have been listed below:

- *"The presence of slight detuning - small blade imperfections, typical of those found in gas turbines today - can cause resonant stress level of up to 20% above the optimum."* **Ewins** (1969)

- *"The analyses reported here indicate that individual turbine blades in Configuration A may respond at 1.95 times the response for a perfectly tuned wheel."* **Srinivasan** and **Frye** (1976)

- *"The maximum factor by which the stress can increase on any blade due to mistuning is approximately* $1/2(1+\sqrt{N/2})$*."* **Whitehead** (1976)

- *"The particular arrangement of a set of blades is as important as each blade's individual degrees of mistune in determining the spread of resonant responses. In the cases studied here, the spread varied from 66 to 120 percent of the mean depending on how the given set of blades were distributed around the disc."* **Ewins** and **Han** (1984)

- *"The maximum stress in the 100 rotors simulated was 2.18, more than twice as large as for a tuned disk."* **Griffin** and **Hoosac** (1984)

- *"In a numerical simulation of a 30-bladed disc with random mistuning, an amplitude of more than 350% relative to the tuned case was found."* **Afolabi** (1988a)

Conclusions as to the identity of the critical blade(s) which experience(s) the maximum response level(s) show a similar trend.

- *"The blade experiencing the maximum stress level is not necessarily that of worst mistune"*

  **El-Bayoumy** and **Srinivasan** (1975)

- *"By correlating the maximum blade amplitude with the blade's "blade alone" frequency it was found that those blade most likely to exhibit the largest vibrations were those that had blade-alone frequencies nearly equal to the frequency that the system would resonate at if the blades were identical."* **Griffin** and **Hoosac** (1984)

- *"The highest response was always experienced by a blade of extreme mistune."*

  **Ewins** and **Han** (1984)

- *"In the specific case studies examined here, the blades having the largest deviation from the tuned state are more likely to be found on the envelopes of min-max response amplitudes."*

  **Afolabi** (1985a)

## 1.2 Survey of Mistuning Studies

Over the last several decades, hundreds of research reports and papers have been published on turbomachinery vibration. No attempt will be made here to undertake a complete review of all the related literature as it is beyond the scope of this thesis. The interested reader is referred to excellent review articles by **Rao** (1973), **Rao** (1977), **Leissa** (1981), **Ramamurti** and **Balasubramanian** (1984), **Rao** (1987) on blade vibration, **Srinivasan** (1984), **Omprakash** and **Ramamurti** (1988) on bladed disc vibration, **Ibrahim** (1987) on structural dynamics with parametric uncertainties and, to the latest survey by **Ewins** (1991) on the effects of blade mistuning on vibration response. However, it is proposed to present a review of mistuning studies related to the forced response effects and to the statistical aspects of the problem.

From the author's standpoint, mistuning studies on bladed discs fall into two categories: deterministic studies and statistical studies.

### 1.2.1 Deterministic Studies

**Tobias** and **Arnold** (1957) were the first to consider imperfections in rotating discs and to study disc vibration under static and rotating conditions, their work providing a useful early insight into the effects of mistuning. Recognition of the fact that some blades have higher response levels than their tuned counterparts dates back to **Whitehead** (1966) who reported a theoretical investigation of blade mistuning effects on blade vibration induced by wakes. He considered purely aerodynamic coupling between blades and suggested that the worst blade's amplitude can increase up to $1/2(1+\sqrt{N})$ times that of the tuned system where N is the total number of blades on a disc. Ten years later (1976), he published another paper in which he incorporated the presence of mechanical coupling between blades through root fixings and showed that the upper limit would be $1/2(1+\sqrt{N/2})$ with mechanical coupling.

**Wagner** (1967) developed a model for turbomachinery vibration with a flexible disc and blades consisting of lumped masses and springs and demonstrated the existence of large variations in maximum blade stresses. **Dye** and **Henry** (1969) proposed a simple but representative lumped parameter model for bladed discs and studied the effects of various types of mistuning patterns. They found that the case of single blade mistuning was the most dangerous pattern leading up to 180% stress increase, an observation in line with Whitehead's work.

**Ewins**' contributions to the understanding of bladed disc vibration and mistuning effects have been remarkable. **Ewins** was amongst the earliest researchers (1966) who studied the effects of mistuning and developed a receptance method to analyse tuned and mistuned bladed discs by coupling disc, blades and shrouds. Later, in 1969, he reported a detailed study of the vibration characteristics of detuned systems and estimated the amount of maximum resonant response increase for light damping. He also proposed a method for the experimental simulation of the excitation which exists under operating conditions. A summary of the vibration characteristics of bladed disc assemblies was reported in 1973. He also conducted experimental studies on a bladed disc model and simulated engine order excitation using air jets in a spinning rig **Ewins** (1976). The study made by **Ewins** and **Rao** (1976) took into account the effect of damping levels on the forced response analysis of bladed discs. In 1980, **Ewins** reported a comprehensive review of the major techniques used in bladed disc vibration analysis and of mistuning effects. **Ewins** and **Han** (1984) analysed the effects of several mistuning configurations and a blade with extreme mistune was found to experience the highest response levels. This conclusion was also shared by **Afolabi** (1982) and (1985a). However, in his latest papers, **Afolabi** reported that contrasting characteristics could be observed in bladed disc response at different segments of the eigenvalue spectrum [**Afolabi** (1985b, 1988b)].

**El-Bayoumy** and **Srinivasan** (1975) analysed the influence of mistuning on blade vibration using an axisymmetric plate model for the disc and a lumped parameter model for the blades. They reported that the amount of overstressing due to mistuning depends on the frequency distribution and the deviation of blade cantilever frequencies from the mean value. Later, **Srinivasan** and **Frye** (1976) conducted experiments on two different engines and presented experimental results. The phenomenon of double modes and mode splitting was addressed by **Stange** and **MacBain** (1983) who carried out experiments using holographic interferometry and strain gage measurements under rotating and nonrotating conditions in order to determine the resonant response amplitudes and modal characteristics of a deliberately mistuned bladed disc. Later, **MacBain** and **Whaley** (1984) extended the work of **Tobias** and **Arnold** (1957) and **Ewins** (1969) and derived an analytical expression for the maximum forced resonant response. **Fabunmi** (1980) studied the vibration response of a mistuned axial compressor rotor under various harmonic excitations. He estimated the mass, stiffness and damping parameters of his theoretical model by analysing holographically-measured modes of the rotor.

The influence of irregularities between individual blades' contact surfaces was addressed by **Muszynska** and **Jones** (1981 and 1983), **Griffin** (1980), **Sinha** and **Griffin** (1984), **Griffin** and **Sinha** (1985), **Menq et al**. (1986) and **Wang** and **Yau** (1990). They pointed out that a major part of the damping in bladed disc systems is supplied by friction and suggested that mistuning caused by such irregularities in friction force could lead to significant variations in individual blade response.

Considerable research has been devoted to aeroelastic aspects of mistuning and a short summary will be given here. The model proposed by **Whitehead** (1966) was further developed by **Srinivasan** (1980) to incorporate mechanical coupling and he made a series of parametric studies with emphasis on mistuning. **Imregun** (1984) investigated the effects of mistuning on flutter by using a lumped parameter structural model and two-dimensional unstalled cascade aerodynamics theories for flat plates. **Srinivasan** and **Fabunmi** (1984) proposed a model to define the blades' properties at several spanwise stations. **Kaza** and **Kielb** (1982a, 1982b, 1984, 1985), **Kielb** and **Kaza** (1983, 1984) and **Kaza et al**. (1987) investigated mistuning effects on the stability of bladed disc systems. Initially, they used a simple blade section model in their analysis. Later, they formulated the aeroelastic equations of motion for an arbitrarily mistuned cascade with flexible, pretwisted and nonuniform blades. **Crawley** and **Hall** (1984) suggested an inverse design procedure for determining the minimum amount of positive mass mistuning required to ensure a given stability margin. **Bendikson** (1984) used a perturbation method to study the effect of mistuning on the flutter boundary. It is worth noting that, unlike those drawn from structural mistuning studies, aeroelastic investigations have been consistent in predicting that mistuning has a stabilizing effect on flutter.

### 1.2.2 Statistical Studies

Although deterministic studies are useful in understanding the effects of mistuning, the answers to practical mistuning-related questions can only really be found on a statistical basis: that is to say, in terms of blade population characteristics rather than individual blade properties. Statistical investigations of the mistuning problem are relatively new and can broadly be divided into two groups:

i) analytical studies, where the structural parameters are considered as actual statistical variables and,

ii) numerical studies, where statistical results are generated from deterministic data in which structural parameters are selected by random sampling from a given population.

***i) Analytical Studies***

**Bliven** (1969) considered random structural imperfections of elastic beams and derived statistical properties of the transverse vibration natural frequencies based upon a lumped parameter approach. **Huang** (1982) proposed a method for estimating the mean and variance of the natural frequencies and the response amplitudes of blades. He modelled a bladed disc as a closed ring composed of a stiffened string supported by transverse springs. He assumed the natural frequencies of the blades to be random variables and derived differential equations for the motion of the bladed disc in terms of these random coefficients. He suggested a spectral method to solve the resulting equations. **Sinha** (1986) used an approximate analytical technique to calculate the statistics of the forced response levels of a mistuned bladed disc assembly. His method was based on the assumption that the response levels of mistuned blades were linear combinations of the random parameters and that the distribution of response levels was Gaussian. This method was later improved to include some higher-order terms by **Sinha** and **Chen** (1989) but the simplifying assumptions were still retained. Another analytical method for predicting the cumulative probability and probability density functions of natural frequency and response levels of single-degree-of-freedom (SDOF) individual blades was provided by **Singh** (1988). Later, **Singh** and **Ewins** (1988) extended this work to a multi-degree-of-freedom (MDOF) spring-mass-dashpot system simulating a bladed disc. **Kissel** (1988) and **Pierre** (1990) studied the effects of random disorder on the dynamics of one-dimensional periodic or nearly-periodic structures and showed the existence of strong vibration localization because of such randomness. **Wei** and **Pierre** (1990) applied various methods such as an analytical first-order statistical perturbation method, a numerical Monte Carlo simulation technique and a hybrid method to find the statistics of the response amplitudes of mistuned blades.

***ii) Numerical Studies***

**Sogliero** and **Srinivasan** (1979) proposed a method for calculating the failure probability of mistuned rotors subjected to stationary Gaussian white noise excitation. They determined the blade cumulative damage using a method based on the S-N curve. **Griffin** and **Hoosac** (1984) used a numerical simulation technique for the statistical investigation of mistuning effects on the response of large bladed disc assemblies and they determined the cumulative probability distribution of the resonance response levels. This analysis was further extended by **Basu** and **Griffin** (1986) who also included aerodynamic coupling and who studied the effects of changing various system parameters such as flowing gas density, the number of blades on the disc and the engine order of excitation. Recently, **Griffin** (1991) suggested a strategy for determining the number and the position of critical blades which should be instrumented in a typical turbomachinery vibration rig.

## 1.3 Objectives of the Research

The overall objective of this research is to improve our basic understanding of the response characteristics of mistuned bladed disc systems. Although the vibration of mistuned bladed disc assemblies has been studied by many authors, there are still a number of unanswered questions. Accordingly, the specific objectives of this thesis are to address questions such as:

i) Which are the critical blade(s) on an assembly - i.e., those experiencing the maximum stress level(s)?

ii) What is the maximum amount of stress increase due to mistuning?

iii) What is the expected life of a blade under vibration when a defect in one of the blades starts to propagate?

iv) The blade distribution on a stage being a statistical process within prescribed tolerance limits - what are the statistical characteristics of forced response levels for a given degree of mistuning? and - what is the probability of the maximum blade response being between two prescribed limits?

v) What degree of blade-to-blade variation should be imposed for A% allowable response increase with respect to the tuned system?

It should be noted that question (iv) is the statement of direct problem for mistuning studies while (v) is that of the inverse problem.

## 1.4 Preview of the Thesis

This thesis aims to improve the basic understanding of the response characteristics of mistuned bladed systems and presents new methods for determining the vibration response and fatigue life of mistuned blades via direct and inverse methods.

Chapter 2 presents an exact analytical solution for the forced vibration of tuned bladed disc assemblies which are modelled using a lumped-parameter technique. The method of analysis developed for tuned systems has been extended to the cases of alternate and single-blade mistuning in chapter 3. Single-blade mistuning was considered to be of interest because it would arise as a result of a fatigue-cracked blade and was modelled using experimentally-measured stiffness and damping changes produced by representative fatigue cracks. Chapter 4 presents a general method for fatigue life prediction of engineering components subjected to dynamic loads. It is based on the determination of the stress intensity factor using frequency response functions. The application of the method is illustrated in the case of a bladed disc with single blade mistuning caused by a fatigue crack.

Chapters 5 to 7 are devoted to statistical investigations of the mistuning problem. As a first step, an analytical method is developed in chapter 5 to investigate the effects of random variations in stiffness and/or damping properties on the vibration characteristics of a SDOF system. The general random mistuning problem is addressed in chapter 6 where statistical sampling theory is used. Blade-to-blade variations are considered to be random with a Gaussian distribution and answers to some very important mistuning-related questions are sought on a statistical basis. In chapter 7, an inverse method is proposed to determine acceptable blade-to-blade variations so that blade response levels remain within A% of those of the tuned system. Finally, chapter 8 summarizes the conclusions reached in this study and proposes a number of possible areas for further research.

# CHAPTER 2

# AN ANALYTICAL SOLUTION FOR THE FORCED RESPONSE OF TUNED BLADED DISC ASSEMBLIES

**About This Chapter**

*It is believed that the understanding of the vibration behaviour of tuned bladed disc assemblies is vital for that of mistuned systems. Accordingly, this chapter is devoted to an analysis of tuned bladed disc assemblies and presents an exact analytical solution for forced vibration levels of such assemblies represented by a lumped-parameter model. The response equations, which are explicit functions of structural parameters, exciting frequency and interblade phase angle, can be used to determine the response levels due to any engine-order type of excitation and to identify all the resonance and antiresonance frequencies of the assembly without requiring an eigensolution. It is further shown that the results obtained are applicable to any number of blades, a feature which makes the proposed solution ideal for parametric studies of turbine and compressor stages.*

## 2.1 Introduction

The prediction of the vibration properties and forced response levels of turbomachinery blades is an essential part of bladed disc assembly design. Although more powerful but expensive analysis techniques exist, it is useful to conduct case studies based on lumped parameter models since such simple but representative models allow an easy and cost effective way of determining some invariant properties of the assembly dynamics. The simplicity of this approach has attracted many researchers and the methods of determining the natural frequencies, mode shapes and forced response levels of bladed disc assemblies are now well established. However, when a disc has many blades, say over 100, the size of the problem may become very large, even for parametric studies using a lumped parameter model. Perhaps this is the reason why many researchers have focused their attention on those rotors that have relatively few blades and have neglected damping (structural and/or aerodynamic) in their work.

The main purpose of this chapter is to address this shortcoming and to present an analytical solution which is valid for any number of blades. Although analytical solutions present a natural alternative to costly numerical techniques, the number of available solutions is very limited. Some approximate solutions for bladed disc assemblies comprising non-linear friction damping, where linear matrix operations are not applicable, have been obtained by **Muszynska** and **Jones** (1983), **Griffin** (1980) and **Sinha et al**. (1985).

Solution techniques for forced response level predictions of tuned or mistuned rotors do not differ from each other in principle in the sense that the response of all blades are computed simultaneously for both cases; an approach which cannot be justified for the tuned case since all blades have identical responses. Indeed, systems with a circular symmetry have a special vibratory behaviour which is characterized by patterns of pure nodal diameters and circles. When such systems are subjected to an $r^{th}$ engine order (rEO) excitation, which is believed to be the main source of forcing in bladed disc assemblies [**Armstrong et al**. (1966), **Whitehead** (1966), **Ewins** (1969)], only the r nodal diameter modes are excited [**Ewins** (1973)]. A close inspection of results from previous studies [**Afolabi** (1982) **Imregun** (1984)] suggests that there should be a simple and closed form expression for response levels to a specific EO excitation.

Although the scope of this chapter is restricted to tuned rotors in order to develop the methodology, the solution technique presented here has promising implications for mistuned bladed disc studies. In chapter 3, the same approach is applied for the analyses of alternate and single-blade mistuning.

## 2.2 Model Description

A number of lumped parameter models of increasing complexity, depicted in Figs. 2.1 to 2.3, were used to represent tuned bladed discs. Model A, shown in Fig. 2.1, assumes the disc to be rigid and represents each blade as a lumped mass, the coupling between one blade and its neighbours being modelled by springs representing massless shrouds. Model B, shown in Fig. 2.2, is identical to the original lumped parameter model of a compressor rotor proposed by **Dye** and **Henry** (1969); a single mass being used to model the blade while the sectorial mass of the disc is lumped at the root, the flexibility of which is also included. Model C, shown in Fig. 2.3, is an extension of Model B in that each blade is now represented by two lumped masses and springs. Although damping is not shown in the models, it can easily be incorporated into the solutions obtained here as viscous and/or hysteretic type.

The specific values of the lumped parameters used in these models can be calculated for a given bladed disc assembly using a semi-empirical method described in **Afolabi** (1982).

## 2.3 A Review of the State-of-the-Art of Forced Response Calculations

A brief review of the existing lumped parameter-based methods to predict the response levels of bladed discs will be given here since the proposed method is based on the same modelling principle.

The general equation of motion for a general multi-degree-of-freedom system subjected to harmonic excitation is given by:

$$[M]\{\ddot{q}\} + [C]\{\dot{q}\} + ( [K] + i\,[D] )\,\{q\} = \{\hat{f}\}\, e^{i\omega t} \tag{2.1}$$

If a harmonic solution of the form is assumed

$$\{q\} = \{\hat{q}\}\, e^{i\omega t} \tag{2.2}$$

Eq. (2.1) becomes:

$$( [K] + i\,[D] - \omega^2\,[M] + i\,\omega\,[C] )\,\{\hat{q}\} = \{\hat{f}\} \tag{2.3}$$

and the response level is obtained from

$$\{\hat{q}\} = ( [K] + i\,[D] - \omega^2\,[M] + i\,\omega\,[C] )^{-1}\{\hat{f}\} \tag{2.4}$$

or

$$\{\hat{q}\} = [Z]^{-1}\{\hat{f}\} = [\alpha]\{\hat{f}\} \tag{2.5}$$

Although the analytical derivation of Eq. (2.4) is simple, it has several disadvantages as discussed by **Ewins** (1984). The major drawback is that its application is too expensive for large-order systems because it requires the inversion of a system matrix at each frequency. Alternative equations have been derived by making use of the system's modal properties. Customarily, these methods have been derived for special cases that the system has either hysteretic or viscous type of damping but not both. In the case of hysteretic damping, Eq. (2.3) is reduced to :

$$( [K] + i\,[D] - \omega^2\,[M] )\,\{\hat{q}\} = \{\hat{f}\} \tag{2.6}$$

Setting the force vector to zero in Eq. (2.6) leads to a complex eigenproblem the solution of which contains the complex eigenvalues $\{\Lambda\}$ of the form

$$\Lambda_r = \omega_r^2\,( 1 + i\,\eta_r ) \tag{2.7}$$

where $\omega_r$ and $\eta_r$ are the natural frequency and the damping loss factor for the $r^{th}$ mode. Using the eigenvector matrix $[\psi]$ which satisfies the orthogonality properties:

$$[\psi]^T\,[M]\,[\psi] = [\,\grave{}m_r\grave{}\,] \tag{2.8a}$$

$$[\psi]^T\,[K]\,[\psi] = [\,\grave{}k_r\grave{}\,] \tag{2.8b}$$

any element of the receptance matrix can be written explicitly in a series form as:

$$\alpha_{jk} = \sum_{r=1}^{N_m} \frac{{}_r\psi_j\,{}_r\psi_k}{m_r(\omega_r^2 - \omega^2 + i\,\eta_r\,\omega_r^2)} \tag{2.9}$$

where $N_m$ is the number of modes. Once the receptance matrix at a specific frequency is computed using Eq. (2.9), the response levels at that frequency can be obtained via Eq. (2.5).

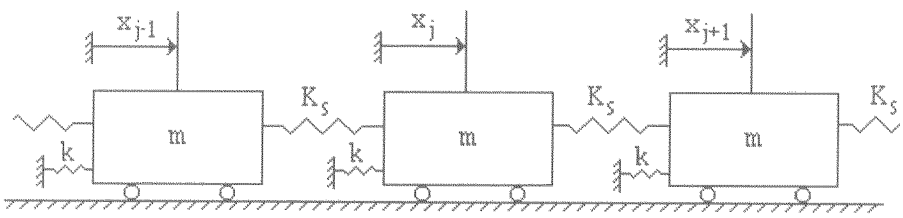


**Fig. 2.1** Model A.

In the case of viscous damping, a similar procedure is followed but the size of the complex eigenproblem is doubled in order to make the problem linear. When both types of damping are present in the model, direct matrix inversion seems to be appropriate since an expression for the elements of the receptance matrix in the form of Eq. (2.9) either does not exist or is too lengthy to use.

## 2.4 Symbolic Inversion of the Dynamic Stiffness Matrix

The receptance matrix $[\alpha]$ can be found by *symbolic inversion* of the dynamic stiffness matrix $[Z]$ and the response levels can be computed easily for a given force vector $\{\hat{f}\}$. This symbolic inversion constitutes the basis of the formulation presented in this chapter and a dedicated software package *Mathematica* [**Wolfram** (1988)] was used for this purpose.

### 2.4.1 Solution for Model A

Introducing both hysteretic and viscous damping to the model shown in Fig. 2.1, the equation of motion for the $j^{th}$ blade can be written as:

$$m \ddot{x}_j + c \dot{x}_j + k ( 1+ i\eta ) x_j + K_S ( x_j - x_{j-1} ) + K_S ( x_j - x_{j+1} ) = f_j(t) \qquad (2.10)$$

where the external forcing $f_j(t)$ here represents a particular EO excitation which is sinusoidal in time and differs only in phase from blade to blade. It can be shown that for an $r^{th}$ EO excitation:

$$f_j(t) = F_o \, e^{i(\omega t + \theta_r (j-1))} \tag{2.11}$$

where

$$\theta_r = \frac{2\pi r}{N} \tag{2.12}$$

$F_o$ = magnitude of forcing

$N$ = total number of blades

$\theta_r$ = interblade phase angle of forcing

It is important to note that the interblade phase angle for the $r^{th}$ nodal diameter mode of vibration is the same as $\theta_r$. Assuming a harmonic solution and setting $F_o$ to unity allows the equations of motion be written in recurrence form:

$$AX_j + BX_{j-1} + BX_{j+1} = \hat{f}_j = e^{i\theta_r (j-1)} \tag{2.13}$$

where

$$A = k + 2\,K_s - m\,\omega^2 + i\,(\,\omega\,c + k\,\eta\,)$$
$$B = -\,K_s \tag{2.14}$$

and $X_j$ is the vibration amplitude for the $j^{th}$ blade. Irrespective of which damping elements are in the model, Eq. (2.13) takes the same form, the expressions for coefficients A and B changing with the configuration. The equation of motion in recurrence form can be written as:

$$[Z]\,\{\hat{q}\} = \{\hat{f}\} \tag{2.15}$$

where

$$[Z] = \begin{vmatrix} A & B & 0 & 0 \cdots 0 & 0 & 0 & B \\ & A & B & 0 \cdots 0 & 0 & 0 & 0 \\ & & A & B \cdots 0 & 0 & 0 & 0 \\ & & & \cdot & & & \\ & & & \cdot & & & \\ & \text{Symmetric} & & & & A & B \\ & & & & & & A \end{vmatrix}_{N\mathrm{x}N} \tag{2.16}$$

$$\{\hat{q}\} = \{\, X_1,\ X_2,\ X_3,\ X_4,\ \ldots\ldots\ldots\ldots,\ X_N\,\}^T \tag{2.17}$$

$$\{\hat{f}\} = \{1,\ e^{i\theta_r},\ e^{i2\theta_r},\ e^{i3\theta_r},\ \ldots\ldots\ ,\ e^{i(N-1)\theta_r}\}^T \tag{2.18}$$

and the solution of Eq. (2.15) is given by:

$$\{\hat{q}\} = [Z]^{-1}\,\{\hat{f}\} = [\alpha]\,\{\hat{f}\} \tag{2.19}$$

Since the system is tuned we need only to find the response amplitude of any one of the blade, say $X_1$:

$$X_1 = \sum_{j=1}^{N} \alpha_{1,j}\,\hat{f}_j \tag{2.20}$$

In order to obtain an analytical formulation for the response level, the receptance matrix was determined by inverting symbolically the dynamic stiffness matrix of Eq. (2.16) using *Mathematica*. This was performed for a number of discs each with a relatively small number of blades since the symbolic matrix inversion is much more costly than its numerical counterpart. Not surprisingly, all the elements of the receptance matrix were found to be functions of the coefficients A and B, and very lengthy expressions were obtained depending on the size of the dynamic stiffness matrix. Initially, an attempt was made to perform the summation of Eq. (2.20) by using the generalized force vector $\{\hat{f}\}$ of Eq. (2.18). However, *Mathematica* was unable to simplify the resulting lengthy response expression and it was necessary to form the vector $\{\hat{f}\}$ for each specific EO excitation. The order of excitation was increased from zero to the maximum possible number which is equal to N/2 for an even number of blades and (N-1)/2 for an odd number of blades.

Unlike the individual elements of the receptance matrix, the expressions for the response levels were found to be very simple functions of the coefficients A and B for each EO excitation. The results for all three test cases are tabulated in Table 2.1 for each possible EO excitation. The most important finding from these results, and many others which are not presented here, is that for a given value of interblade phase angle, $\theta_r$, the solution for blade responses is invariant, which indicates that response levels for a disc with any number of blades can be expressed as a function of $\theta_r$. The following expression was derived by observation of several test cases under varying EO excitations.

$$X_1 = \frac{1}{A + 2\,B\,\cos(\theta_r)} \tag{2.21}$$

The general expression given in Eq. (2.21) for a blade's vibration amplitude is verified in **Appendix I** where the same result is obtained analytically using Circulant Matrix Theory. The magnitude of the response level for $r^{th}$ EO excitation can be written explicitly as a function of the structural parameters and the excitation frequency by substituting Eq. (2.14) into Eq. (2.21):

**Table 2.1** Response levels for Model A.

| No of blades N | Engine order r | Phase angle $\theta_r$[°] | Response amplitude $X_1$ |
|---|---|---|---|
| 4 | 0 | 0 | $\frac{1}{A+2B}$ |
| | 1 | 90 | $\frac{1}{A}$ |
| | 2 | 180 | $\frac{1}{A-2B}$ |
| 6 | 0 | 0 | $\frac{1}{A+2B}$ |
| | 1 | 60 | $\frac{1}{A+B}$ |
| | 2 | 120 | $\frac{1}{A-B}$ |
| | 3 | 180 | $\frac{1}{A-2B}$ |
| 8 | 0 | 0 | $\frac{1}{A+2B}$ |
| | 1 | 45 | $\frac{1}{A+\sqrt{2}B}$ |
| | 2 | 90 | $\frac{1}{A}$ |
| | 3 | 135 | $\frac{1}{A-\sqrt{2}B}$ |
| | 4 | 180 | $\frac{1}{A-2B}$ |

$$|X_1| = \frac{1}{\sqrt{(k + 2K_s(1-\cos(\theta_r)) - m\,\omega^2)^2 + (\omega c + k\eta)^2}} \tag{2.22}$$

The natural frequencies of the system can easily be obtained from Eq. (2.22) by solving for $\omega$ to maximise the response level.

### 2.4.2 Solution for Model B

Having obtained an analytical expression for the vibration response level of the simpler system, it was decided to repeat the calculations for the extended model, B, which is

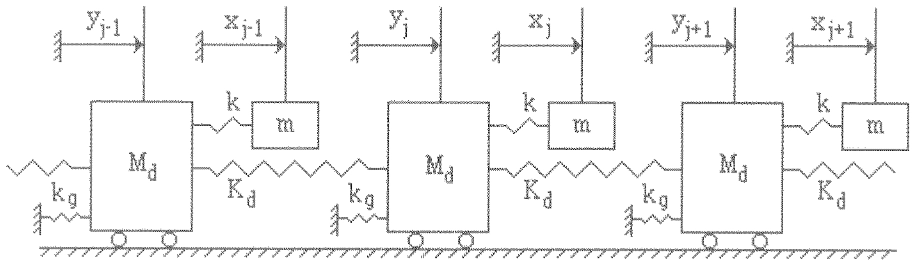


**Fig. 2.2** Model B.

shown in Fig. 2.2. As before, blade stiffness k was assumed to include structural damping while aerodynamic damping was represented by a dashpot attached between ground and the blade. The following are the equations of motion for the $j^{th}$ blade and the corresponding disc segment:

$$m\,\ddot{x}_j + c\,\dot{x}_j + k\,(1+i\eta)\,(x_j - y_j) = f_j(t)$$
$$M_d\,\ddot{y}_j + k\,(1+i\eta)\,(y_j - x_j) + k_g y_j + K_d(2y_j - y_{j+1} - y_{j-1}) = 0 \qquad (2.23)$$

The harmonic response assumption enables the equations of motion to be written in recurrence form:

$$AX_j + BY_j = e^{i\theta_r(j-1)} = \hat{f}_j$$
$$BX_j + CY_j + DY_{j-1} + DY_{j+1} = 0 \qquad (2.24)$$

where

$$A = k - m\omega^2 + i(\eta k + \omega c)$$
$$B = -k(1 + i\eta)$$
$$C = 2K_d + k_g + k - M_d\omega^2 + i\eta k \qquad (2.25)$$
$$D = -K_d$$

The dynamic stiffness matrix can be expressed as:

$$[Z] = \begin{vmatrix} A & B & 0 & 0 & 0 & 0 \cdots 0 & 0 & 0 \\ & C & 0 & D & 0 & 0 \cdots 0 & 0 & D \\ & & A & B & 0 & 0 \cdots 0 & 0 & 0 \\ & & & C & 0 & D \cdots 0 & 0 & 0 \\ & & & & & \vdots & & \\ & \text{Symmetric} & & & & & A & B \\ & & & & & & & C \end{vmatrix}_{2N\mathrm{x}2N} \tag{2.26}$$

and the response and force vectors are respectively:

$$\{\hat{q}\} = \{ X_1,\ Y_1,\ X_2,\ Y_2, \ldots\ldots\ldots\ldots, X_N,\ Y_N \}^T \tag{2.27}$$

$$\{\hat{f}\} = \{1, 0, e^{i\theta_r}, 0, e^{i2\theta_r}, 0, \ldots\ldots, e^{i(N-1)\theta_r}, 0\}^T \tag{2.28}$$

As mentioned before, since the system is tuned the vibration response levels for one sector only, say $X_1$ and $Y_1$, need to be determined:

$$X_1 = \sum_{j=1}^{2N} \alpha_{1,j}\, \hat{f}_j \qquad \text{and} \qquad Y_1 = \sum_{j=1}^{2N} \alpha_{2,j}\, \hat{f}_j \tag{2.29}$$

Following the approach described in the previous section, simple expressions for response levels for several discs under all possible EO of excitations were obtained. The results for two discs with different numbers of blades are given in Table 2.2. As before, the following functions were found to represent the response levels for Model B for any interblade phase angle and for any number of blades.

$$X_1 = \frac{C + 2D\cos(\theta_r)}{- B^2 + A(C + 2D\cos(\theta_r))} \tag{2.30}$$

**Table 2.2** Response levels for Model B.

| No of blades N | Engine order r | Phase angle $\theta_r$[°] | Response amplitude $X_1$ | Response amplitude $Y_1$ |
|---|---|---|---|---|
| 6 | 0 | 0 | $\frac{C + 2D}{-B^2 + A(C + 2D)}$ | $\frac{-B}{-B^2 + A(C + 2D)}$ |
| | 1 | 60 | $\frac{C + D}{-B^2 + A(C + D)}$ | $\frac{-B}{-B^2 + A(C + D)}$ |
| | 2 | 120 | $\frac{C - D}{-B^2 + A(C - D)}$ | $\frac{-B}{-B^2 + A(C - D)}$ |
| | 3 | 180 | $\frac{C - 2D}{-B^2 + A(C - 2D)}$ | $\frac{-B}{-B^2 + A(C - 2D)}$ |
| 8 | 0 | 0 | $\frac{C + 2D}{-B^2 + A(C + 2D)}$ | $\frac{-B}{-B^2 + A(C + 2D)}$ |
| | 1 | 45 | $\frac{C + \sqrt{2}D}{-B^2 + A(C + \sqrt{2}D)}$ | $\frac{-B}{-B^2 + A(C + \sqrt{2}D)}$ |
| | 2 | 90 | $\frac{C}{-B^2 + AC}$ | $\frac{-B}{-B^2 + AC}$ |
| | 3 | 135 | $\frac{C - \sqrt{2}D}{-B^2 + A(C - \sqrt{2}D)}$ | $\frac{-B}{-B^2 + A(C - \sqrt{2}D)}$ |
| | 4 | 180 | $\frac{C - 2D}{-B^2 + A(C - 2D)}$ | $\frac{-B}{-B^2 + A(C - 2D)}$ |

$$Y_1 = \frac{-B}{-B^2 + A(C + 2D\cos(\theta_r))} \tag{2.31}$$

### 2.4.3 Solution for Model C

After obtaining the required solutions for the two simpler models, the same approach was applied to the more general model shown in Fig. 2.3. As before, the equations of motion are written in recurrence form.

$$\begin{aligned} &AX_j + BY_j = a\,\hat{f}_j \\ &BX_j + CY_j + DZ_j + GY_{j-1} + GY_{j+1} = b\,\hat{f}_j \\ &DY_j + EZ_j + FZ_{j-1} + FZ_{j+1} = 0 \end{aligned} \tag{2.32}$$

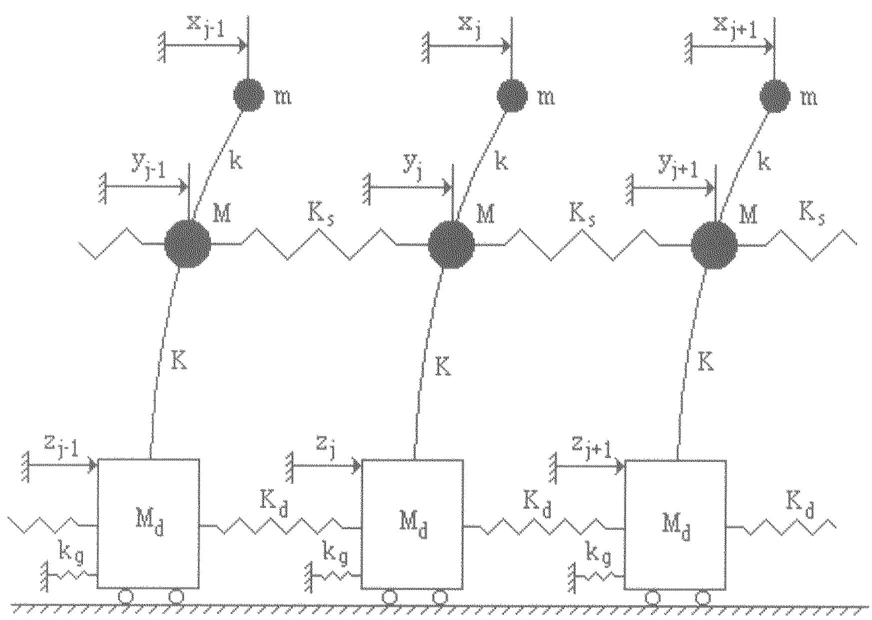


**Fig. 2.3** Model C.

where a and b represent the proportion of the external force applied to the blade upper and lower masses in the model such that a+b=1. It was decided to obtain the analytical solution for the following two cases:

i ) external forces are acting on the upper masses only ( a=1, b=0 )

ii) external forces are acting on the lower masses only ( a=0, b=1 )

and the principle of superposition can be applied to provide the solution for the general case. Again, the receptance matrix was obtained via symbolic matrix inversion and the response levels, $X_1$,$Y_1$ and $Z_1$, were determined by multiplying the receptance matrix by the appropriate force vectors. Expressions for the response levels for various values of $\theta_r$ are not tabulated as previously, to preserve space, and the results obtained as a function of $\theta_r$ are presented directly. For case (i), these are:

$$X_{1X} = \frac{D^2 - (C + 2G\cos(\theta_r))(E + 2F\cos(\theta_r))}{\text{Denom}} \tag{2.33}$$

$$Y_{1X} = \frac{B(E + 2F\cos(\theta_r))}{\text{Denom}} \tag{2.34}$$

$$Z_{1X} = \frac{-BD}{\text{Denom}} \tag{2.35}$$

where

$$\text{Denom} = B^2 (E + 2F\cos(\theta_r)) + A (D^2 - (C + 2G\cos(\theta_r))(E + 2F\cos(\theta_r))) \tag{2.36}$$

Similarly, for case (ii), the response levels are:

$$X_{1Y} = Y_{1X} \tag{2.37}$$

$$Y_{1Y} = \frac{-A(E + 2F\cos(\theta_r))}{\text{Denom}} \tag{2.38}$$

$$Z_{1Y} = \frac{AD}{\text{Denom}} \tag{2.39}$$

Using the principle of superposition, the total vibration amplitude at each coordinate can now be written as:

$$X_1 = a\,X_{1X} + b\,X_{1Y} \tag{2.40}$$

$$Y_1 = a\,Y_{1X} + b\,Y_{1Y} \tag{2.41}$$

$$Z_1 = a\,Z_{1X} + b\,Z_{1Y} \tag{2.42}$$

Having found the response levels, it is now possible to obtain the natural frequencies of the system as well as the antiresonances using transfer functions in each coordinate direction. For simplicity, we shall derive expressions for the natural frequencies of the undamped case. It is also worth noting that the antiresonances of the undamped system can be obtained more easily than can the natural frequencies since the order of the polynomial in the numerator is less than that of the denominator.

***Natural Frequencies of Undamped Bladed Disc***

For the undamped case, the coefficients in Eq. (2.32) can be written explicitly as:

$$\begin{aligned}
A &= k - \lambda m \\
B &= -k \\
C &= k + K + 2K_s - \lambda M = T_1 - \lambda M \\
D &= -K \\
E &= K + k_g + 2K_d - \lambda M_d = T_2 - \lambda M_d \\
F &= -K_d \\
G &= -K_s
\end{aligned} \tag{2.43}$$

where $\lambda = \omega^2$. Substituting these coefficients into Eq. (2.36) and equating the resulting expression to zero yields the frequency equation for the r nodal diameter modes.

$$\lambda^3 + a_1 \lambda^2 + a_2 \lambda + a_3 = 0 \tag{2.44}$$

where

$$\begin{aligned}
a_1 &= \{2m\cos(\theta_r)(MK_d + K_sM_d) - T_1M_dm - T_2mM - kMM_d\}/(mMM_d) \\
a_2 &= \{2K_d\cos(\theta_r)(2K_sm\cos(\theta_r) - T_1m - kM) - 2K_s\cos(\theta_r)(kM_d + T_2m) + \\
&\quad + mT_2k + M_dT_1k - M_dk^2 - mK^2 + T_1T_2m\}/(mMM_d)
\end{aligned} \tag{2.45}$$

$$a_3 = \{2k\cos(\theta_r)\,(K_dT_1 + K_sT_2 - K_dk - 2K_dK_s\cos(\theta_r)) + $$
$$+ kK^2 - T_1T_2k + T_2k^2\}/(mMM_d)$$

The solution of Eq. (2.44) is given in **Appendix II**. The three real roots correspond to the zero, one and two nodal circle modes associated with interblade phase angle, $\theta_r$.

## 2.5 Numerical Example

A computer program based on the modal summation technique was written to check the validity of the Eqs. (2.21), (2.30) and (2.31) numerically and the results obtained were compared with the derived analytical solutions using a hand calculator. Perfect agreement was obtained in all cases.

Now, we shall focus on some of the numerical results for model C. Again, the system was assumed to be undamped for the sake of simplicity. Two separate programs were developed. In the first one, the natural frequencies were determined using an eigensolution and the response levels were obtained using modal summation. In the second program, algebraic expressions derived in the previous section were used directly. The structural parameters used are listed in Table 2.3.

The CPU time required to determine all natural frequencies of a 30-bladed disc via this first program was approximately 12 minutes on a IBM PC-AT compatible micro computer. On the other hand, the results from the second program were almost instantaneous using the same computer. Natural frequencies of the system for several

**Table 2.3** Structural parameters for 30-bladed disc.

| | |
|---|---|
| $m$ =0.115 kg | $K$ = 24.171*$10^6$ N/m |
| $M$ = 0.321 kg | $K_s$ = 8.000*$10^6$ N/m |
| $M_d$ = 0.72 kg | $K_d$ = 2.600*$10^6$ N/m |
| $k$ = 0.317*$10^6$ N/m | $k_g$ = 60.000 N/m |

**Table 2.4** Some of the resonance and antiresonance frequencies of 30-bladed disc.

| Nodal diameter | Phase angle $\theta_r$[°] | Natural frequency [Hz] | | | | | | Antireso-nance [Hz] |
|---|---|---|---|---|---|---|---|---|
| | | Eigensolution | | | Analytical solution | | | |
| | | 0 Circle | 1 Circle | 2 Circle | 0 Circle | 1 Circle | 2 Circle | First one at blade tip |
| 3 | 36 | 163.57 | 286.22 | 1674.19 | 163.57 | 286.22 | 1674.19 | 198.24 |
| 4 | 48 | 206.14 | 298.91 | 1680.18 | 206.14 | 298.91 | 1680.18 | 249.92 |
| 5 | 60 | 233.24 | 324.68 | 1687.40 | 233.24 | 324.68 | 1687.40 | 300.74 |
| 6 | 72 | 246.11 | 361.74 | 1695.52 | 246.11 | 361.74 | 1695.52 | 349.33 |
| 7 | 84 | 251.97 | 402.17 | 1704.17 | 251.97 | 402.17 | 1704.17 | 394.75 |

different nodal diameter patterns as obtained from both methods are presented in Table 2.4, from which it is immediately seen that both sets of results are identical. The first antiresonance frequency of the blade tip EO response, which cannot be predicted from an eigensolution, was also calculated from the analytical formulation and is included in that table.

It was assumed that the external forces were acting at the blade tips (i.e., a=1, b=0 ) and a 5th EO excitation was applied (i.e., $\theta_r$=60°.) The response curves corresponding to the coordinates X, Y and Z are shown in Fig. 2.4. The response levels obtained from the two methods are once again identical. In order to plot each curve shown in Fig. 2.4, the response levels were computed at 450 frequencies. The CPU time required was about 50 minutes for the first program including an eigensolution. However, the same results were obtained in about 3 seconds using the second program based on the analytical solution.

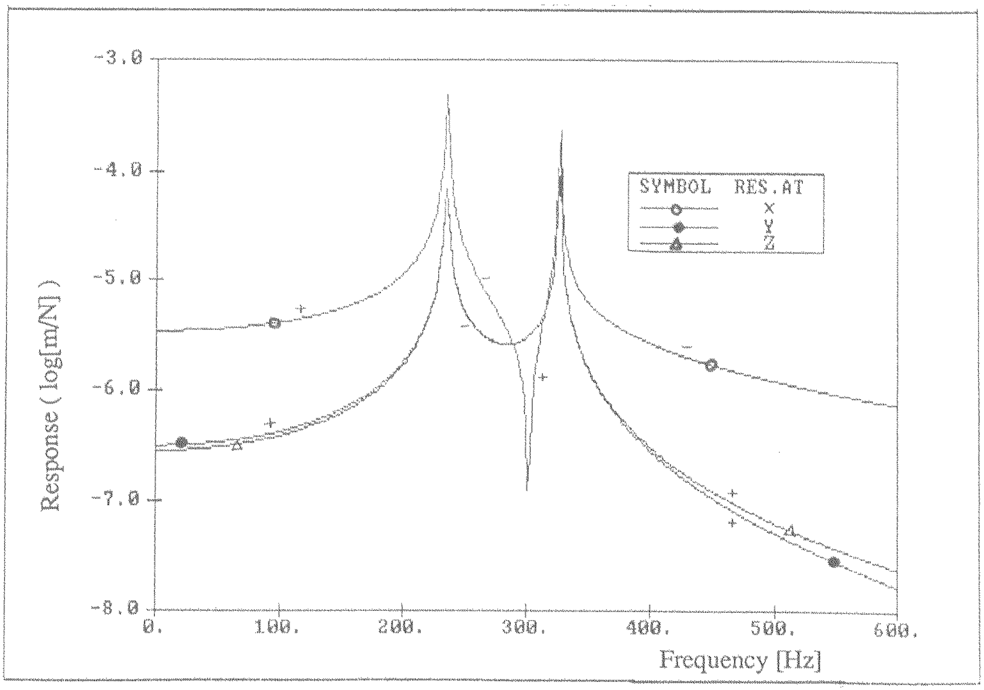


**Fig. 2.4** Response of the 30-bladed disc to 5EO excitation.

## 2.6 Concluding Remarks

i) An analytical formulation for the calculation of tuned system response levels has been presented and its validity has been checked using other available prediction techniques.

ii) The proposed formulation brings major savings in computational time since it is based on closed form analytical expressions.

iii) The analysis of tuned bladed discs with large numbers of blades does not bring any complexity nor additional computational cost in response predictions whatsoever.

iv) Since the proposed analytical solutions of response levels are given as functions of symbolic coefficients in the equations of motion, both viscous and hysteretic damping can be included easily into the formulation.

v) The analytical solutions for response levels have been found to be a function of the ratio r/N, more conveniently represented by the interblade phase angle $\theta_r=2\pi r/N$. This has very important implications for the prediction of the response levels: there is no need to conduct studies by changing r and N individually, a single parameter $\theta_r$ can be used to assess the response levels directly. Again, this represents an enormous saving in computing time since (a) far fewer cases need to be investigated and (b) the dynamic behaviour of large systems can be deduced from that of much smaller systems.

vi) The antiresonance frequencies in any coordinate response, which cannot be identified from an eigensolution, can also be determined using the proposed formulation.

# CHAPTER 3

# FORCED VIBRATION ANALYSIS OF MISTUNED BLADED DISC ASSEMBLIES

**About This Chapter**

*The effects of two types of bladed disc assembly mistuning, namely alternate and single blade mistuning, are examined in this chapter by extending the method used in chapter 2 for tuned assemblies. Single-blade mistuning is considered to be a result of a cracked blade and is modelled using experimental data on stiffness and damping changes produced by fatigue cracks. The results presented in this chapter show that the position of the critical blade and the amount of resonant response increase over the corresponding tuned system depend on both the interblade phase angle and the amount of mistuning present. The results also suggest that, as in the case of tuned bladed discs, the dynamic behaviour of mistuned bladed discs with large numbers of blades can be inferred by studying systems with much smaller numbers of blades.*

## 3.1 Introduction

Vibration-induced fatigue in bladed disc assemblies has always been a primary concern and dynamic stresses which can cause fatigue failures need to be predicted accurately for safe and economical design. Among many difficulties in doing so, mistuning and its consequences still remain as unknown quantities in stress calculations. Although studies consistently indicate that mistuning causes large stress increases relative to the tuned state, the answers to the following two important questions still remain to be satisfactorily answered:

i) which blade(s) experience(s) the maximum stress level? and

ii) what is the maximum amount of dynamic stress increase over the tuned state?

As pointed out in chapter 1, some researchers suggest that the worst blade, the one experiencing the largest vibration amplitude, is most likely to be the one with the greatest mistune while others suggest the worst blade to be a "mean" blade. Nor is there any agreement about the magnitude of the dynamic stress increase over the corresponding tuned system, either. Many different levels of stress increase have been suggested: 20% increase by **Ewins** (1969), 350% of tuned case by **Afolabi** (1988a) and a factor of $1/2(1+\sqrt{N/2})$ by **Whitehead** (1976) where N is the number of blades. Although different modelling techniques can be expected to give different quantitative results, qualitatively the results are expected to show the same general trends rather than being in contradiction as in determining the critical blade.

This chapter deals with two specific types of mistuning, namely alternate and single-blade mistuning. The alternate mistuning considered here addresses the case where two sets of identical blades are mounted on a disc in an alternating fashion (Fig. 3.1.a). Single-blade mistuning, as the name implies, is considered as the case where the

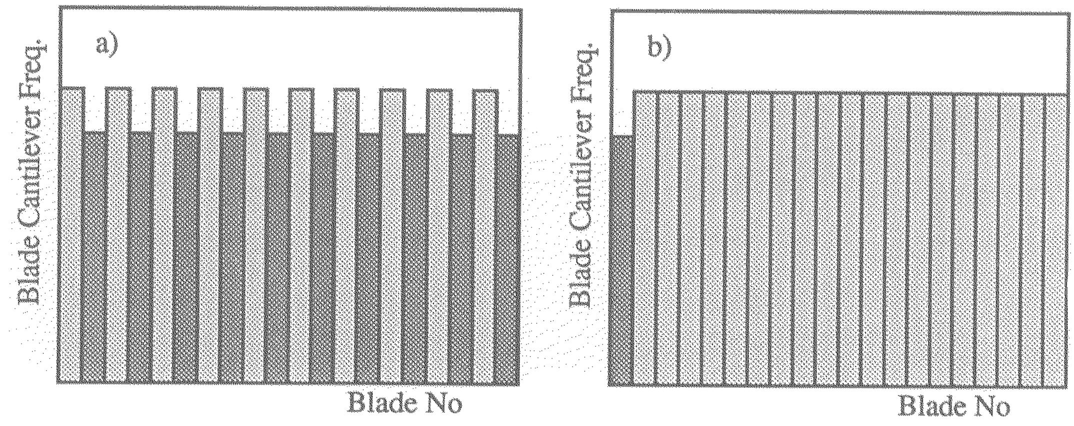


**Fig. 3.1** Mistuning types studied. (Only cantilever frequency variation is shown)

properties of one blade are different from those of others as shown in Fig. 3.1.b. In both cases, it is assumed that the corresponding disc sectors are tuned. For the alternate mistuning case, an analytical solution which is applicable to a disc with any number of blades has been obtained and used for predicting forced response levels. For the analysis of the single-blade mistuning case, a combination of analytical and numerical solutions is applied to find the required response levels.

## 3.2 Description of the Model and Solution Technique

The basic **Dye** and **Henry** (1969) model used in the previous chapter is extended by including hysteretic and viscous damping to represent both aerodynamic and structural sources of energy dissipation. Referring to Fig. 3.2, the equations of motion for the $j^{th}$ blade and disc sector can be written as:

$$m\,\ddot{x}_j + c\dot{x}_j + k_j^*\,(x_j - y_j) = f_j(t)$$
$$M_d\,\ddot{y}_j + k_j^*\,(y_j - x_j) + k_g\,y_j + K_d\,(2\,y_j - y_{j+1} - y_{j-1}) = 0 \tag{3.1}$$

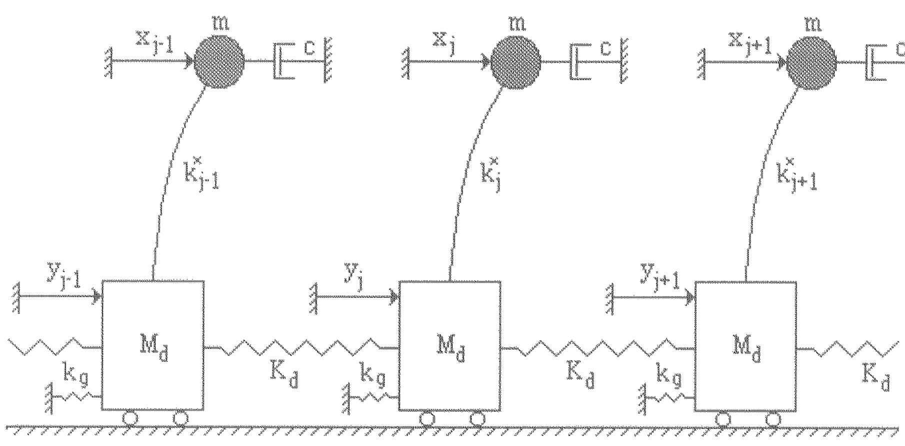


**Fig. 3.2** Lumped parameter model of mistuned bladed disc assembly.

where $k_j^* = k_j\,(1 + \eta_j)$ and the external force $f_j(t)$ represents a particular engine order (EO) of excitation which is sinusoidal in time and differs only in phase from blade to blade.

The method of solution used in this chapter is similar to that described in chapter 2 where forced response levels were obtained directly via:

$$\{\hat{q}\} = [Z]^{-1}\{\hat{f}\} = [\alpha]\,\{\hat{f}\} \tag{3.2}$$

Once again, symbolic inversion of the dynamic stiffness matrix [Z] constitutes the basis of the formulation and the dedicated software package, *Mathematica* [**Wolfram** (1988)], was used for this purpose.

**Table 3.1** Tuned system model parameters.

| | | | | |
|---|---|---|---|---|
| $\frac{1}{2\pi}\sqrt{\frac{k}{m}} = 182$ Hz | $\frac{\sqrt{k/m}}{\sqrt{k_g/M_d}} = 60$ | $\frac{\sqrt{K_d/M_d}}{\sqrt{k/m}} = 14$ | $\eta = 0.2\%$ | $\zeta = 1.0\%$ |

The equivalent tuned system model parameters, summarized in Table 3.1, were used in both the alternate and single-blade mistuning cases.

## 3.3 Alternate Mistuning

The Fourier analysis of some research fan data provided by a well-known aero engine manufacturer showed that a significant degree of alternate mistuning already existed in more than 80% of the assemblies studied, probably due to dynamic balancing considerations. This clearly shows that even though alternate mistuning seems to be a simplistic special case, the understanding of its consequences has important practical implications. An extensive study on alternate mistuning was carried out by **Griffin** and **Hoosac** (1984) who suggested that building a bladed disc by selecting alternate blades from two distinct populations which have different mean frequencies could be a possible way of reducing the worsening effect of mistuning caused by random mistuning. Results presented in this chapter indicate that some of their findings related to alternate mistuning are valid under specific circumstances only, and may not be applicable to the general case.

### 3.3.1 Formulation

The solution procedure requires the dynamic stiffness matrix to be written in symbolic form. This can be done by assuming a harmonic solution which allows the equations of motion be written in the form:

$$[\,Z\,]\,\{\hat{q}\} = \{\hat{f}\} \tag{3.3}$$

where the response vector $\{\hat{q}\}$, force vector $\{\hat{f}\}$ and dynamic stiffness matrix $[Z]$ are:

$$\{\hat{q}\} = \{X_1, Y_1, X_2, Y_2, X_3, Y_3, \ldots\ldots, X_N, Y_N\}^T \tag{3.4}$$

$$\{\hat{f}\} = F_o \{1,0,e^{i(\theta_r)},0,e^{i(2\theta_r)},0,e^{i(3\theta_r)},0,......,e^{i((N-1)\theta_r)},0\}^T \tag{3.5}$$

$$[Z] = \begin{vmatrix} A_L & B_L & 0 & 0 & 0 & 0 \cdots 0 & 0 & 0 \\ & C_L & 0 & D & 0 & 0 \cdots 0 & 0 & D \\ & & A_H & B_H & 0 & 0 \cdots 0 & 0 & 0 \\ & & & C_H & 0 & D \cdots 0 & 0 & 0 \\ & & & & & \cdot & & \\ & & & & & \cdot & & \\ & \text{Symmetric} & & & & & A_H & B_H \\ & & & & & & & C_H \end{vmatrix}_{2N\times 2N} \tag{3.6}$$

respectively, where subscripts $_L$ and $_H$ refer to low (odd) and high (even) frequency blades respectively. The solution procedure has already been described in the previous chapter and analytical results for response levels will be given without further explanation. Because of the symmetry inherent in this type of mistuning, the magnitude of the $j^{th}$ blade response level is identical to that of the $(j+2)^{th}$ blade (i.e., $|X_j| = |X_{j+2}|$, $|Y_j| = |Y_{j+2}|$). Therefore, we shall give an analytical solution only for the $(j)^{th}$ and the $(j+1)^{th}$ blades where j is an odd number corresponding to low-frequency blades:

$$X_j = F_o \frac{-B_H^2 C_L + A_H C_L C_H - 2\cos(\theta_r) B_L B_H D - 4\cos^2(\theta_r) A_H D^2}{\Delta} e^{i(j-1)\theta_r} \tag{3.7}$$

$$X_{j+1} = F_o \frac{-B_L^2 C_H + A_L C_L C_H - 2\cos(\theta_r) B_L B_H D - 4\cos^2(\theta_r) A_L D^2}{\Delta} e^{ij\theta_r} \tag{3.8}$$

$$Y_j = F_o \frac{B_H^2 B_L - A_H B_L C_H + 2\cos(\theta_r) A_L B_H D}{\Delta} e^{i(j-1)\theta_r} \tag{3.9}$$

$$Y_{j+1} = F_o \frac{B_L^2 B_H - A_L B_H C_L + 2\cos(\theta_r) A_H B_L D}{\Delta} e^{ij\theta_r} \tag{3.10}$$

where

$$\Delta = B_L^2\, B_H^2 - A_L\, B_H^2\, C_L - A_H\, B_L^2\, C_H + A_L\, A_H\, C_L\, C_H - 4\cos^2(\theta_r)\, A_L\, A_H\, D^2 \tag{3.11}$$

Assuming that only the stiffness properties of the two set of blades are different, the coefficients in the above solution can be written explicitly as:

$$\begin{aligned}
A_L &= k_L - m\,\omega^2 + i\,(\eta\, k_L + \omega\, c) \\
B_L &= -k_L\,(1 + i\,\eta) \\
C_L &= 2\,K_d + k_g + k_L - M_d\,\omega^2 + i\,\eta\, k_L \\
A_H &= k_H - m\,\omega^2 + i\,(\eta\, k_H + \omega\, c) \\
B_H &= -k_H\,(1 + i\,\eta) \\
C_H &= 2\,K_d + k_g + k_H - M_d\,\omega^2 + i\,\eta\, k_H \\
D &= -K_d
\end{aligned} \tag{3.12}$$

Eqs. (3.7) to (3.12) show that apart from the structural parameters and excitation frequency, the response levels of discs with alternate mistuning, like those of tuned rotors, depend only on interblade phase angle ($\theta_r = 2\pi\, r/N$) rather than the engine order of excitation, r, or the number of blades, N, separately. Therefore, the closed form analytical solution given above is applicable to a disc with any number of blades under excitation of any EO.

### 3.3.2 Case Study

First, results obtained from the analytical solution, Eqs. (3.7) to (3.10), were compared with those found numerically by studying discs with small numbers of blades. Identical results were obtained and, predictably, the analytical solution brought huge savings in computation time. These equations were then used to find the increase in forced response due to alternate mistuning. The normalized magnitudes, obtained by dividing the resonant response levels of high- and low-frequency blades by that of the equivalent tuned blade, are plotted in Fig. 3.3 against the amount of mistuning (defined as the ratio of the cantilever frequency difference of high and low frequency blades to the cantilever frequency of tuned blade) for various values of interblade phase angle ($\theta_r=2\pi r/N$). The critical blade is seen to be the low-frequency blade if $\theta_r$ is less than $90^o$ and, as $\theta_r$ increases, the critical blade changes depending on the amount of mistuning.

These results show that, even for this simple type of mistuning, the position of the critical blade cannot be related to its cantilever frequency without detailed knowledge of the excitation characteristics and the amount of mistuning. It is also worth noting that results presented here are in agreement with previous published work. For example, **Ewins** (1969) showed that the critical blade at certain degree of mistuning may not be the critical one at some other degrees of mistuning. Moreover, **Griffin** and **Hoosac** (1984) found a trend very similar to that given in Fig. 3.3 for $\theta_r = 10^o$. Results presented in Fig.3.3 show that this trend is valid for a range of interblade phase angles only hence it cannot be generalized. Another set of results, obtained with and without viscous damping, is presented in Fig. 3.4. It is immediately seen that damping has negligible effect on the results presented for the alternate mistuning case.

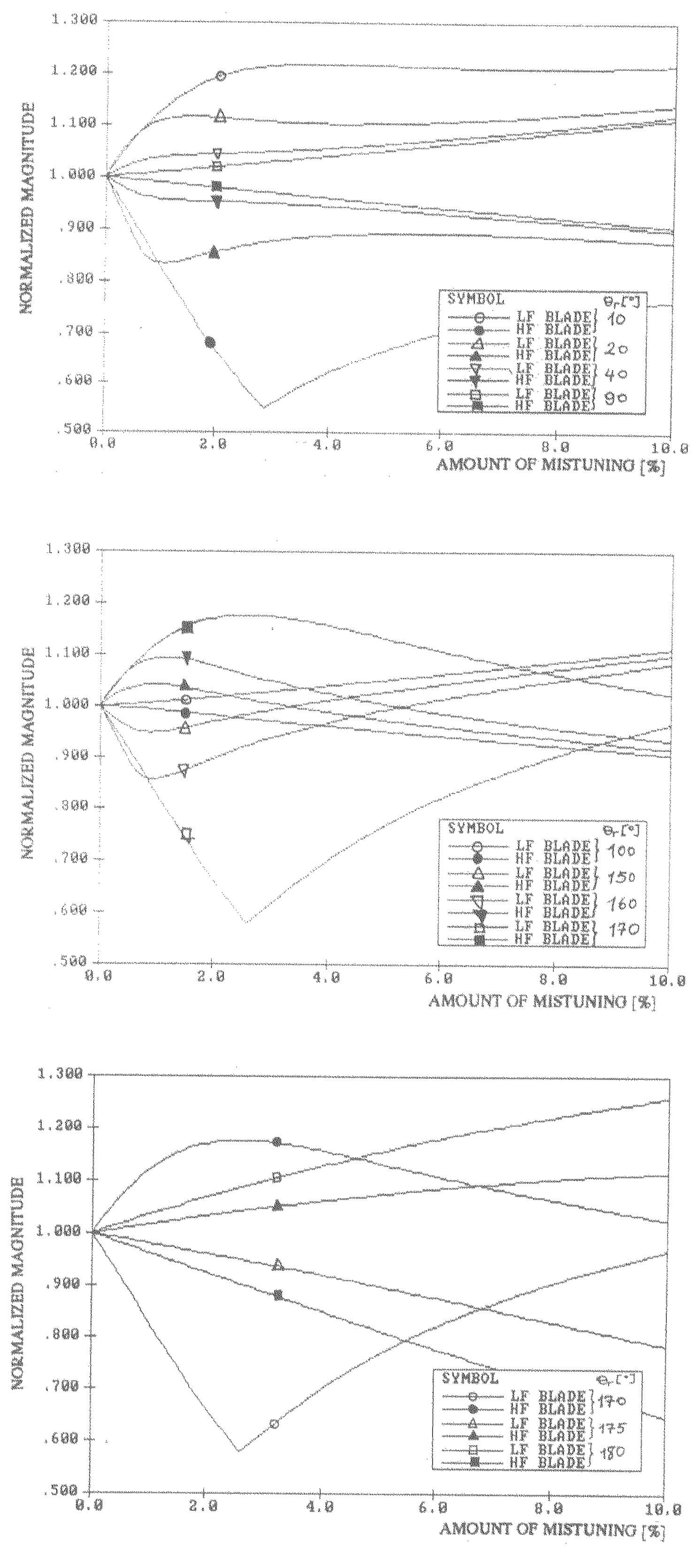


Fig. 3.3 Normalized resonant response versus amount of mistuning.

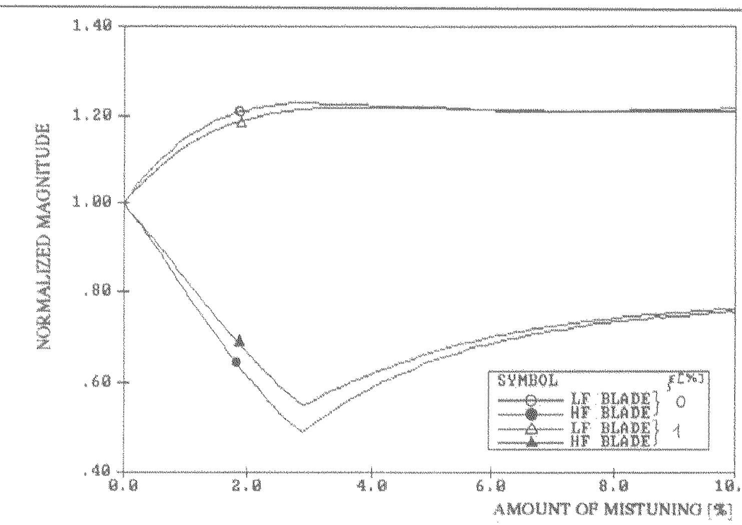


**Fig. 3.4** Effect of damping modelling on normalized resonant response for alternate mistuning case.

## 3.4 Single Blade Mistuning

Single-blade mistuning is usually considered to be an academic case rather than a realistic problem. However, a practical problem arises when a defect starts to propagate in one of the blades of a rotor stage which is otherwise made of nominally-identical blades. This situation is addressed in this section.

### 3.4.1 Formulation

Assuming that the first blade is mistuned (Fig. 3.1.b), the dynamic stiffness matrix can be written as follows:

$$[Z] = \left|\begin{matrix} A_1 & B_1 & 0 & 0 & 0 & 0 \cdots 0 & 0 & 0 \\ & C_1 & 0 & D & 0 & 0 \cdots 0 & 0 & D \\ & & A & B & 0 & 0 \cdots 0 & 0 & 0 \\ & & & C & 0 & D \cdots 0 & 0 & 0 \\ & & & & & \cdot & & \\ & & & & & \cdot & & \\ & \text{Symmetric} & & & & & A & B \\ & & & & & & & C \end{matrix}\right|_{2N\times 2N} \qquad (3.13)$$

where

$$\begin{aligned}
A_1 &= k_1 - m\,\omega^2 + i\,(\eta_1 k_1 + \omega c) \\
B_1 &= -k_1\,(1 + i\,\eta_1) \\
C_1 &= 2\,K_d + k_g + k_1 - M_d\,\omega^2 + i\,\eta_1 k_1 \\
A &= k - m\,\omega^2 + i\,(\eta k + \omega c) \\
B &= -k\,(1 + i\,\eta) \\
C &= 2\,K_d + k_g + k - M_d\,\omega^2 + i\,\eta\,k \\
D &= -K_d
\end{aligned} \tag{3.14}$$

$k_1$ and $\eta_1$, which are functions of the crack depth, represent the stiffness and structural damping of the first blade while all other parameters of the system are assumed to be those of the tuned state.

The symbolic inversion technique was applied to Eq. (3.2) in an attempt to find a general solution. However, it was not possible to obtain a closed-form solution applicable to any number of blades. Instead, analytical solutions for those discs with a small number of blades (maximum 12) were found for various EO excitations. The solution for a 6-bladed disc under 1 EO excitation is given here for illustration purposes.

$$\begin{aligned}
X_1 = F_o(&-B^6C_1+3AB^4CC_1-3A^2B^2C^2C_1+A^3C^3C_1-B^5B_1D+2AB^3B_1CD-A^2BB_1C^2D- \\
&2AB^4D^2+AB^3B_1D^2+4A^2B^2CD^2-A^2BB_1CD^2-2A^3C^2D^2+3A^2B^2C_1D^2- \\
&3A^3CC_1D^2+4A^2BB_1D^3+4A^3D^4)/\beta
\end{aligned} \tag{3.15}$$

$$\begin{aligned}
Y_1 = F_o(&B^6B_1-3AB^4B_1C+3A^2B^2C^2B_1-A^3C^3B_1+B^5A_1D-2AB^3A_1CD+A^2BA_1C^2D- \\
&AB^3A_1D^2-3A^2B^2B_1D^2+A^2BA_1CD^2+3A^3CB_1D^2-4A^2BA_1D^3)/\beta
\end{aligned} \tag{3.16}$$

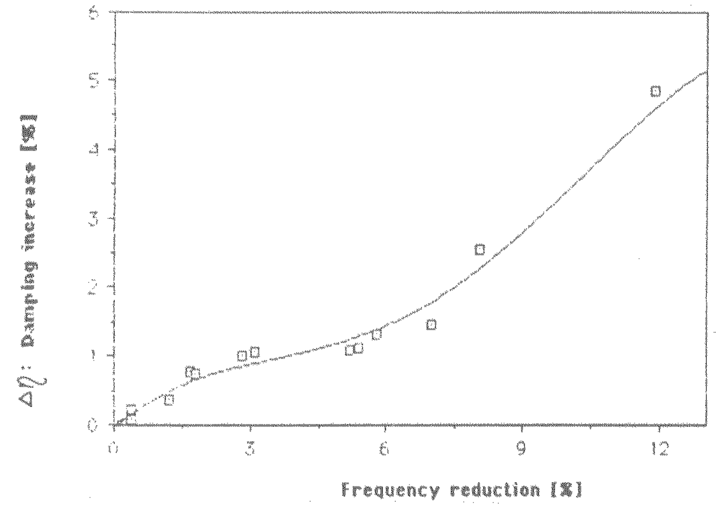


**Fig. 3.5** Experimental data for frequency and damping changes produced by fatigue cracks.

where $X_1$ and $Y_1$ are the deflections of the first blade and disc sector respectively and $\beta$ is given by

$$\beta = (B^6B_1^2-3AB^4B_1^2C+3A^2B^2C^2B_1^2-A^3C^3B_1^2-B^6A_1C_1+3AA_1B^4CC_1-3A^2A_1B^2C^2C_1+A^3C^3C_1A_1-2AB^4A_1D^2-3A^2B^2B_1^2D^2+4A^2B^2D^2A_1C+3A^3CB_1^2D^2-2A^3C^2A_1D^2+3A^2B^2A_1C_1D^2-3A^3A_1CC_1D^2+4A^3A_1D^4) \quad (3.17)$$

### 3.4.2 Case Study

In order to allow a more realistic assessment of the forced response characteristics of bladed disc systems when there is mistuning due to a crack defect in a single blade, the changes in natural frequencies and structural damping values of free-free steel beams due to the presence of fatigue cracks were investigated experimentally.[1] Results from this work are given in **Appendix III** and are used in the case study presented in this section. Measured natural frequency reduction versus damping increase for the first mode of a free-free beam is plotted in Fig. 3.5. This reduction was regarded as a decrease in blade stiffness since a fatigue crack does not cause any mass changes.

[1] A theoretical model to predict the damping increase due to fatigue cracks in beam-like structures was proposed by **Sanliturk** and **Imregun** (1991).

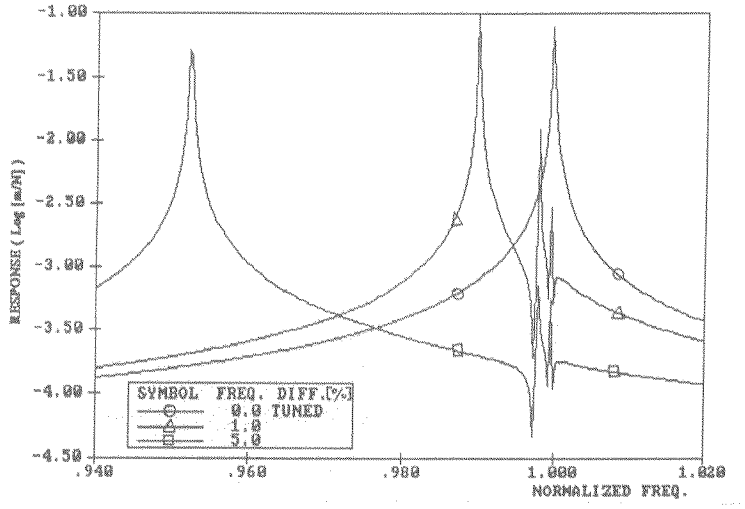


**Fig. 3.6** Response levels of tuned and mistuned blades versus excitation frequency for undamped case. (N=12, r=3)

As mentioned before, a general analytical solution applicable to any number of blades could not be found for the single-blade mistuning case. Instead, solutions for discs with up to and including 12 blades were obtained for various EO excitations. Results referring to discs with more than 12 blades were computed by numerical inversion of the system matrix.

One of the consequences of mistuning is that the $r^{th}$ EO excitation excites several modes, as illustrated for the undamped case of Fig. 3.6 in which the exciting frequency is normalized to the tuned blade-alone cantilever frequency. However, as shown in Fig. 3.7, when proportional damping or damping due to a fatigue crack is introduced, small peaks are suppressed and the response curve becomes smoother, suggesting that damping is responsible for reducing the effect of mistuning. Forced response levels computed for odd numbered blades in the case of a 24-bladed disc with a cracked blade under 5 EO excitation are plotted in Fig. 3.8. All response levels are close to each other except those for the cracked blade which is lower due to the high level of damping introduced to that blade by the fatigue crack. However, the crack tip stresses

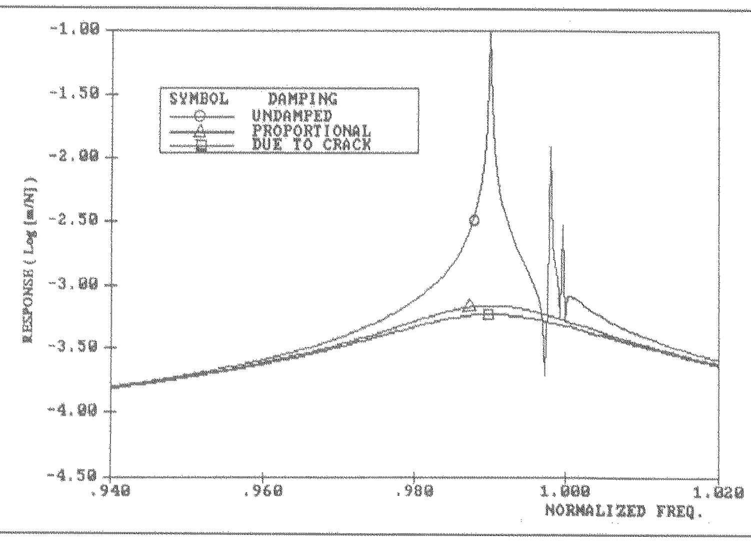


**Fig. 3.7** Effects of damping on response level of mistuned blade.
(N=12, r=3, Mistuning = 1%)

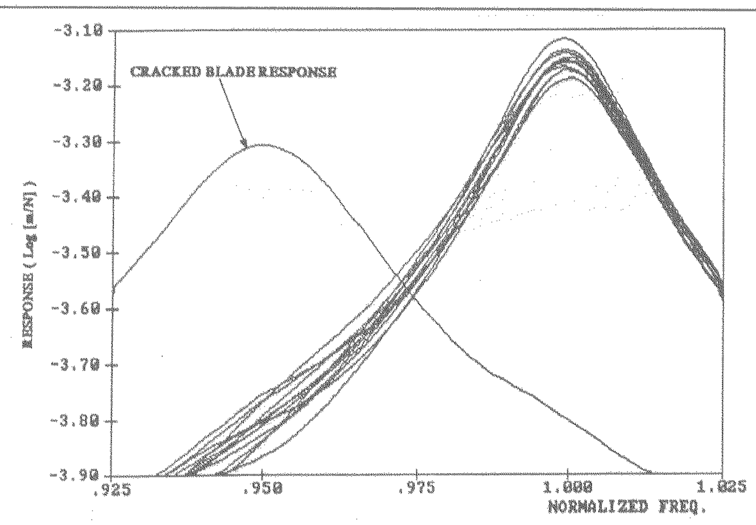


**Fig. 3.8** Response levels of odd numbered blades.
(N=24, r=5, Mistuning = 5%)

may well be large enough for further crack propagation, a situation which is addressed in chapter 4.

Although the response levels are found to be dependent on the number of blades, this dependency is rather weak if the ratio of EO excitation to the blade number (thus, interblade phase angle $\theta_r$) is kept constant. This can easily be seen from the response levels of the cracked blade plotted for $\theta_r$=180° in Figs. 3.9 and 3.10. Results suggest

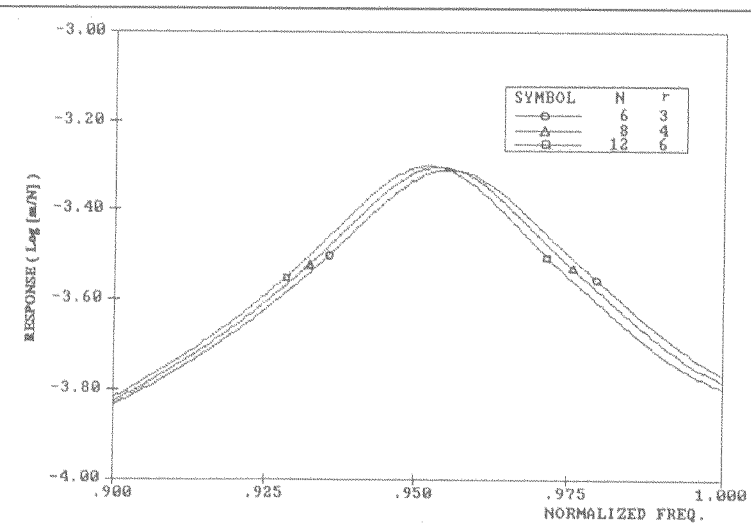


**Fig. 3.9** Response level of cracked blade versus excitation frequency. ($\theta_r = 180^o$)

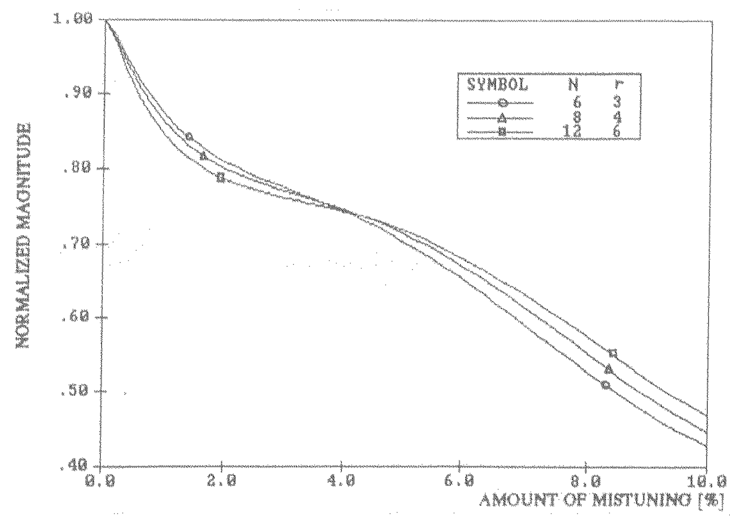


**Fig. 3.10** Normalized resonant response level versus amount of mistuning. ($\theta_r = 180^o$)

that the interblade phase angle can still be used to predict the *state* of the response levels of such bladed disc assemblies. Finally, the normalized resonant response of the mistuned blade was found in terms of the amount of mistuning for various $\theta_r$ values and the results are presented in Fig. 3.11. It is clear that including the damping produced by a fatigue crack has a marked effect on the maximum response level of a fatigue-cracked blade.

As in chapter 2, results presented here on alternate and single-blade mistuning also indicate that the disc assembly with a large number of blades responds in a similar way

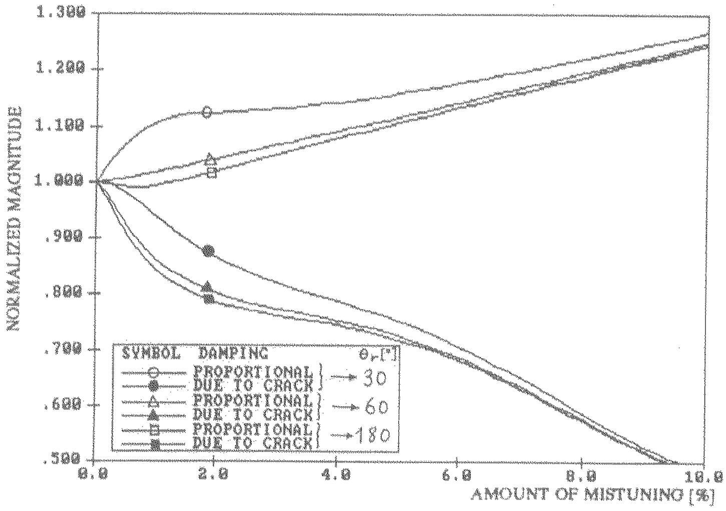


**Fig. 3.11** Normalized resonant response levels versus amount of mistuning for mistuned blade with and without the damping produced by fatigue crack.

to one with only a few blades if $\theta_r$ is the same for both assemblies, hence one can deduce that the behaviour of discs with large numbers of blades can be inferred by studying smaller systems. However, the validity of this argument for the general case of random mistuning needs to be investigated in detail and this is addressed in chapter 6.

## 3.5 Concluding Remarks

i) A closed-form analytical solution has been obtained for forced response levels of alternately mistuned bladed assemblies. The solution is independent of the number of blades and is applicable to excitation of any EO, which makes the solution ideal for parametric studies.

ii) Results presented in this chapter suggest that, as for tuned bladed discs, a simple parameter $\theta_r$, which represents the interblade phase angle, is sufficient to describe the response characteristics of mistuned bladed discs studied in this chapter (i.e., alternate and single-blade mistuning).

iii) The critical blade on an alternately-mistuned bladed disc depends on the characteristics of the exciting force. For a given bladed disc, the worst blade under a certain EO excitation may not be the critical one under some other EO excitations. Accordingly, the critical blade cannot be determined according to its cantilever frequency alone without a priori knowledge of the excitation forces.

iv) Damping caused by a fatigue crack can have a marked effect on the response levels of the cracked blade. These were always found to be lower than those of other blades, due to the high level of damping introduced by such cracks. However, this does not mean that the cracked blade is not the critical one since further crack propagation is possible.

v) The specific mistuning patterns studied here can increase the resonance response levels by up to 20% above that of the corresponding tuned system.

# CHAPTER 4

# FATIGUE LIFE PREDICTION FOR MISTUNED ASSEMBLIES

**About This Chapter**

*Mistuning not only increases blade response levels but also the chance of fatigue failures and, hence, mistuning-related blade fatigue is of considerable importance to turbomachine manufacturers. This chapter deals with the development of a general method for fatigue life prediction of engineering components subjected to dynamic loads. It is based on the determination of the nominal stress at the crack position using frequency response functions and this in turn enables the prediction of dynamic fatigue life under forced vibration. The implementation of the technique is discussed in the case of a bladed disc assembly where single-blade mistuning is caused by a fatigue crack. It is believed that the proposed method has promising implications for safer designs and also for the prediction of inspection intervals, especially in aero engine applications where such considerations are of paramount importance.*

## 4.1 Introduction

Many engineering components operate under dynamic loads which make fatigue resistance a primary design criterion. The designer must ensure that a component or a structure has an adequate fatigue life, especially when crack propagation is a distinct possibility. In order to ensure that an undetected crack does not lead to unexpected failure, the component must be inspected at regular intervals, the length of which is usually based on past experience rather than predictive methods.

Research in fracture mechanics has provided a number of fatigue life prediction methods which are based on various crack propagation criteria [**Ewalds** and **Wanhill** (1986), **Rolfe** and **Barson** (1977), **Pook** (1983), **Fong** (1979), **Stanley** (1977)]. It is possible to determine the number of stress cycles required for a crack to propagate from an initial size to a certain value, provided that the nominal stress or the stress field around the crack is known. However, although crack propagation is usually caused by forced vibration, the stresses used in fatigue life predictions have traditionally been determined by neglecting the inertia and damping forces [**Findly** and **Reed** (1983), **Fisher** and **Sherratt** (1977)]. In other words, it has been inherently assumed that the stress is independent of the frequency of excitation, its pattern following that of the external force. The implications of this assumption are illustrated in Fig. 4.1 where an impact generates a stress variation of similar shape. Although some publications [**Takezono** (1982), **Dowling** (1983), **Alawi** (1989) , **James** (1971) and **Sakamato et al**. (1988)] deal with the effects of excitation frequency and/or complex loads on crack propagation, the problem of including inertia and damping forces into fatigue life models remains largely unaddressed. The exclusion of these forces may still yield acceptable results if the frequency of the applied force is much lower than the natural frequencies of the structure and many high pressure vessel applications fall into this category. However, for most rotating machinery components, particularly bladed discs, this is not the case. For such applications, stresses should be determined dynamically

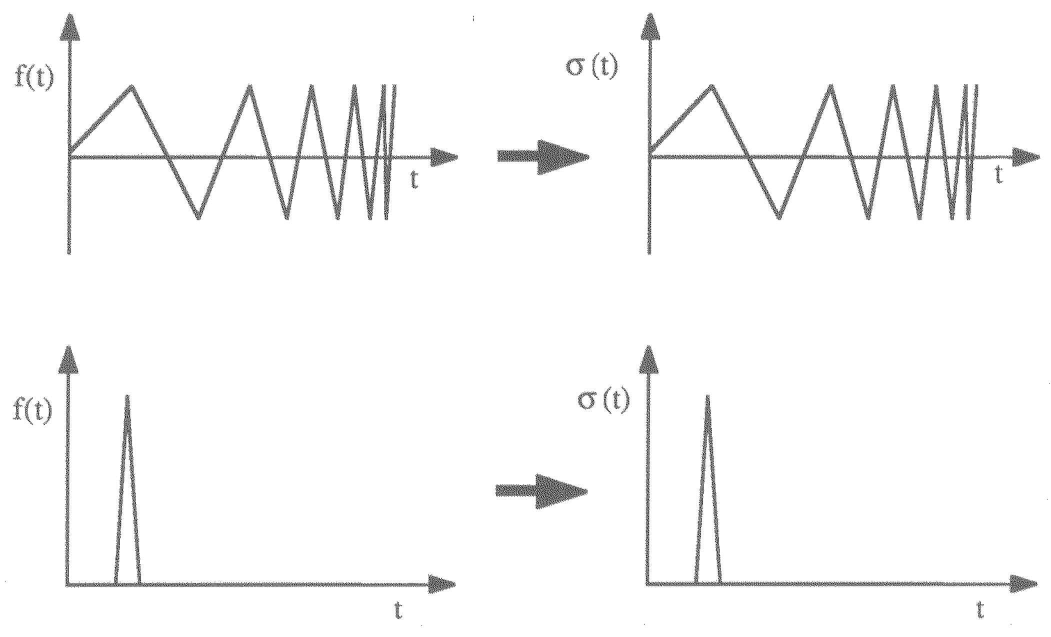


**Fig. 4.1** Implications of neglecting inertia and damping forces in stress analysis.

including not only elastic but also inertia and damping forces. This chapter describes a method which adopts this latter approach.

## 4.2 Basic Theory

The relationship between the stress intensity factor $K_I$ and the crack length $a$ is usually expressed as a shape-dependent function which can be determined either from closed-form solutions [**Paris** and **Sih** (1965), **Newman** and **Raju** (1981), **Tada et al**. (1973) and **Sih** (1973)] or from the empirical relationship:

$$K_I = Y \sigma_{nom} \sqrt{\pi a} \tag{4.1}$$

where

$Y$ = shape factor,

$\sigma_{nom}$ = nominal stress

The crack growth rate can be expressed using semi-empirical formulae

$$\frac{da}{dN_c} = C_o\,(\Delta K_I)^n \qquad \text{Paris law [\textbf{Paris} and \textbf{Erdogan} (1963)]} \tag{4.2}$$

$$\frac{da}{dN_c} = \frac{C_o\,(\Delta K_I)^n}{(1-R)K_{Ic}-\Delta K_I} \qquad \text{Forman equation [\textbf{Forman et al.} (1967)]} \tag{4.3}$$

where

$\Delta K_I$ = stress intensity factor range ($K_{Imax}$ - $K_{Imin}$)

$K_{Ic}$ = critical stress intensity factor

$R$ = stress ratio ($\sigma_{min}/\sigma_{max}$)

$C_o$, $n$ = material constants

Using Eq. (4.3), one can determine the number of stress cycles needed for a crack to propagate from initial length $a_o$ to final length a :

$$N_c = \frac{1}{C_o}\int_{a_o}^{a} \frac{(1-R)K_{Ic}-\Delta K_I}{(\Delta K_I)^n}\,da \tag{4.4}$$

The evaluation of the above integral presents no difficulties if the assumption in Eq. (4.1) is retained, i.e. the nominal stress is considered to be constant irrespective of the frequency of excitation. However, the stress intensity factor can perhaps be more correctly defined using the frequency response functions of the component under study, and these in turn may be crack-dependent. In other words, one can bring two levels of improvement to the formulation of the stress intensity factor by redefining it as (i) frequency-dependent and (ii) frequency- and crack-dependent.

## 4.3 Determination of the Dynamic Stress Intensity Factor

The response of a structure to harmonic excitation can be found from:

$$\{ \hat{q} \} = [ \alpha(\omega) ] \{ \hat{f} \} \tag{4.5}$$

where

$\{\hat{q}\}$ = amplitude of response vector

$\{\hat{f}\}$ = amplitude of force vector

$\omega$ = excitation frequency

$[\alpha]$ = frequency response function (here receptance) matrix

Once the response vector is determined, the required stresses can be calculated from :

$$\{\sigma\} = [A] [B] \{\hat{q}\} \tag{4.6}$$

where [B] and [A] are the transformation matrices from responses to strains and strains to stresses respectively. The stress intensity factor range $\Delta K_I$ can then easily be computed from knowledge of the stress field around the fatigue crack. If the stiffness and damping properties of a structure are likely to depend on the crack size - as is the case in many critical applications - Eqs. (4.5) and (4.6) should be solved for every crack length while evaluating Eq. (4.4).

Although this procedure is applicable to any structure, detailed modelling of complex geometries with fatigue cracks may require prohibitively expensive computing time at the solution stage. Experimental determination of these stresses provides an alternative. However, it might be extremely difficult to measure these stresses around the crack for each loading condition and for varying crack size. One practical solution is to relate the nominal stress at crack position i to the response at point j. That is to say:

$$\sigma_{nom} = \beta_{ij}(\omega) \mid q_j \mid \tag{4.7}$$

where $\beta_{ij}(\omega)$ is a frequency-dependent (but crack-independent) stress parameter which relates response to nominal stress. The derivation of $\beta_{ij}(\omega)$ for a cantilever beam is given in **Appendix IV** and the variations of $q(s_j)$ ,$\sigma(s_i)$ and $\beta_{ij}(\omega)$ with respect to frequency are plotted in Fig. AIV.2.

Eq. (4.7) is equally applicable to both theoretical and experimental data and it presents some additional advantages over obtaining nominal stress using Eq. (4.6). From a computational viewpoint, displacement calculations are more efficient than stress calculations. From an experimental viewpoint, deflection measurements at some point j away from the crack are much easier than stress measurements near the crack tip. However, the experimental determination of $\beta_{ij}(\omega)$ is probably much simpler than its numerical counterpart. In a typical vibration measurement, the stress at a critical location i (i.e. a possible crack location) and deflection at some other point j can easily be recorded and $\beta_{ij}(\omega)$ can be calculated from their ratio.

Once $\beta_{ij}(\omega)$ is known, Eq. (4.7) can be expressed in terms of the frequency response functions via Eq. (4.5)

$$\sigma_{nom} = \beta_{ij}(\omega) \mid \{ \alpha(\omega) \}_j^T \{\hat{f}\} \mid \tag{4.8}$$

where vector $\{ \alpha(\omega) \}_j^T$ represents the transpose of the $j^{th}$ column of the receptance matrix. Substituting Eq. (4.8) into Eq. (4.1) gives the required stress intensity factor:

$$K_I = Y \, \beta_{ij}(\omega) \sqrt{\pi a} \mid \{ \alpha(\omega) \}_j^T \{\hat{f}\} \mid \tag{4.9}$$

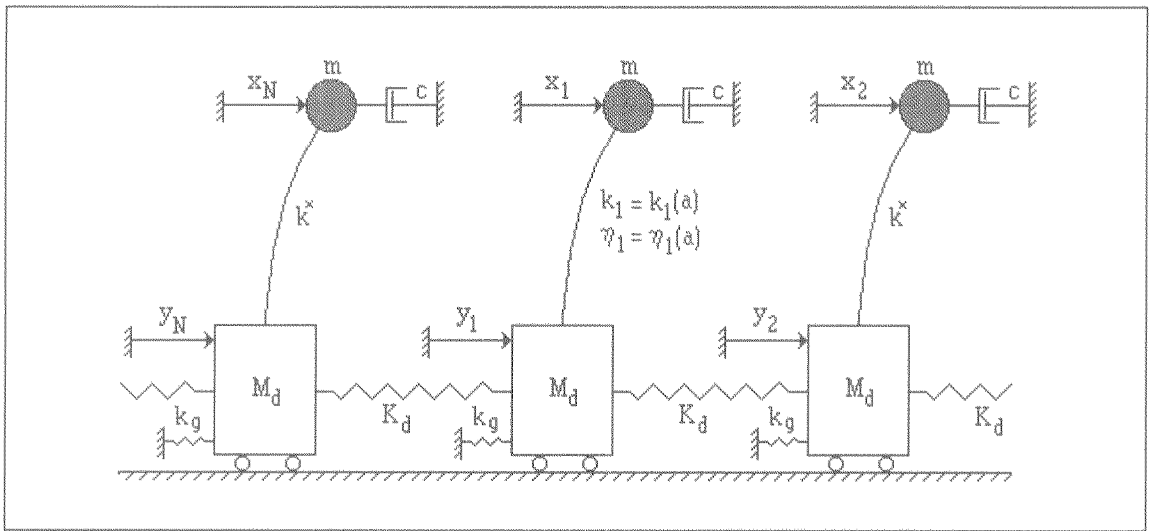


**Fig. 4.2** Lumped parameter of a bladed disc with a cracked blade.

## 4.4 Bladed Disc Assembly with a Cracked Blade

It is now proposed to illustrate the above described technique in the case of a bladed disc with single-blade mistuning. Such a situation arises when a defect initiates and starts to propagate in one of the blades during operation. A lumped parameter model, shown in Fig. 4.2, is used to represent the bladed disc assembly where all sectors are identical except for that representing the blade with a fatigue crack. In addition to the dashpots between blades and ground, which represent aerodynamic damping, hysteretic damping of the blade material is also included in the model. The equations of motion for the $j^{th}$ blade and disc sector can be written as:

$$m\,\ddot{x}_j + c\dot{x}_j + k_j\,(1 + \eta_j)\,(x_j - y_j) = f_j(t)$$
$$M_d\,\ddot{y}_j + k_j\,(1 + \eta_j)\,(y_j - x_j) + k_g\,y_j + K_d\,(2\,y_j - y_{j+1} - y_{j-1}) = 0 \qquad (4.10)$$

where the external force $f_j(t)$ represents a particular engine order (EO) excitation at the $j^{th}$ blade. Assuming simple harmonic motion, the equations of motion for N blades can be written in matrix form as

$$\{\hat{q}\} = [Z]^{-1}\{\hat{f}\} = [\alpha(\omega)]\{\hat{f}\} \tag{4.11}$$

where

$$\{\hat{q}\} = \{X_1, Y_1, X_2, Y_2, X_3, Y_3, .........., X_N, Y_N\}^T$$

$$\{\hat{f}\} = F_o\,\{[1, 0], [e^{(i\,2\pi r/N)}, 0], [e^{(i\,4\pi r/N)}, 0], ........, [e^{(i\,(N-1)\pi r/N)}, 0]\}^T$$

If it is assumed that the fatigue crack is in the first blade, the dynamic stiffness matrix [Z] is given by Eq. (3.13) since the situation is precisely that derived in the previous chapter. $k_1$ and $\eta_1$, both functions of the crack size, represent the stiffness and structural damping of the first blade. Using Eq. (4.11), the tip response of the cracked-blade can be written as:

$$X_1 = \sum_{p=1}^{2N} \alpha_{1p}\,\hat{f}_p \tag{4.12}$$

The stress intensity factor can now be calculated from Eq. (4.9):

$$K_I = Y\,\beta_{ij}(\omega)\,\sqrt{\pi a}\,\left|\sum_{p=1}^{2N} \alpha_{1p}\,\hat{f}_p\right| \tag{4.13}$$

Eq. (4.3) can now be used for fatigue life prediction. Neglecting the mean stress, we have $R = \sigma_{min}/\sigma_{max} = K_{Imin}/K_{Imax} = -1$ and $\Delta K_I = 2K_I$ since each vibration cycle encompasses compression and tension stresses of equal magnitude.

Substituting Eq. (4.13) into Eq. (4.3) yields:

$$\frac{da}{dN_c} = \frac{C_o \left( 2\, Y\, \beta_{ij}(\omega) \sqrt{\pi a}\, \left| \sum_{p=1}^{2N} \alpha_{1p}\, \hat{f}_p \right| \right)^n}{2 \left( K_{Ic} - Y\, \beta_{ij}(\omega) \sqrt{\pi a}\, \left| \sum_{p=1}^{2N} \alpha_{1p}\, \hat{f}_p \right| \right)} \tag{4.14}$$

and re-arranging the above expression for fatigue life results in:

$$N_c = \frac{2}{C_o} \int_{a_o}^{a} \frac{\left( K_{Ic} - Y\, \beta_{ij}(\omega) \sqrt{\pi a}\, \left| \sum_{p=1}^{2N} \alpha_{1p}\, \hat{f}_p \right| \right)}{\left( 2\, Y\, \beta_{ij}(\omega) \sqrt{\pi a}\, \left| \sum_{p=1}^{2N} \alpha_{1p}\, \hat{f}_p \right| \right)^n}\, da \tag{4.15}$$

It should be noted that $\alpha_{1p}$ is a function of the crack length and hence it needs to be evaluated at each integration step.

## 4.5 Numerical Study

The structural parameters given in Table 3.1 of the previous chapter were also used in the case of a 24-bladed disc.

When a small defect in any one blade starts to propagate under operation, the stiffness and damping properties of that blade become crack-dependent, a phenomenon which makes the assembly markedly mistuned. In this study it is proposed to use the experimental data given in **Appendix III** and plotted in Fig. 4.3 which indicate the degree of stiffness reduction and damping increase caused by fatigue cracks in free-free beams. (A reduction in natural frequency can be interpreted as a loss in stiffness since fatigue cracks do not cause any mass change.)

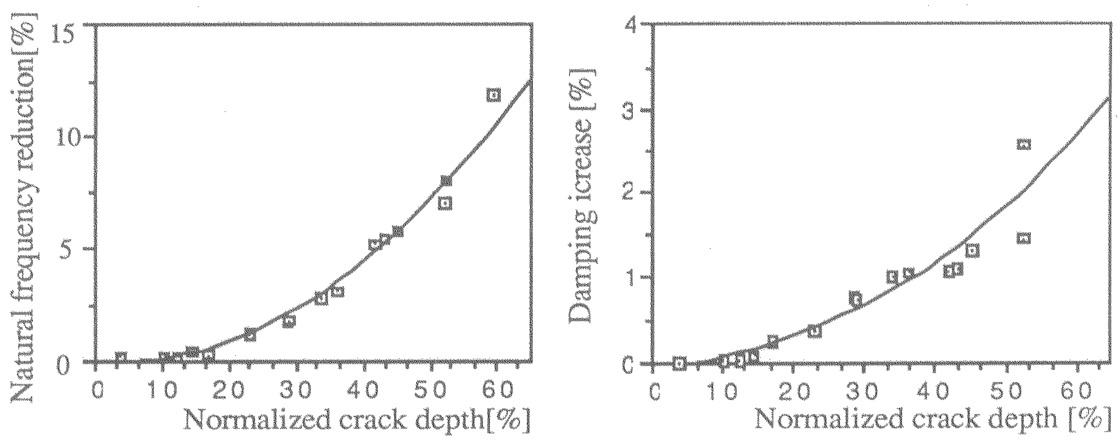


**Fig. 4.3** Natural frequency reduction and damping increase produced by fatigue crack for mode 1 of free-free beam.

The cracked blade's response due to unit-amplitude 5EO excitation was calculated for various crack lengths for a narrow frequency interval which included the 5 nodal diameter mode of the tuned assembly. (It should be noted that a 5EO excitation excites only the 5 nodal diameter mode if the system is perfectly tuned.) The stress parameter $\beta_{ij}(\omega)$ was determined by assuming that the design stress corresponding to this (tuned) case was 500 MPa. All subsequent nominal stress values were computed using this reference value and the results are plotted in Fig. 4.4. The stress levels seem to depend on both the excitation frequency and the crack size and there are three cases to be considered. In the first case where the (normalized) excitation frequency is much lower than unity, crack propagation causes the nominal stress to increase relative to the initial stress level. On the other hand, if the (normalized) excitation frequency is greater than unity, the nominal stress tends to decrease as the crack grows. In the third case, which falls in between the two previous cases, the nominal stress first tends to increase, then reaches a maximum at the new natural frequency of the assembly and finally starts to decrease again as the fatigue crack grows further. This trend can probably be best illustrated by Fig. 4.5 where nominal stress is plotted against normalized crack depth for various values of the excitation frequency.

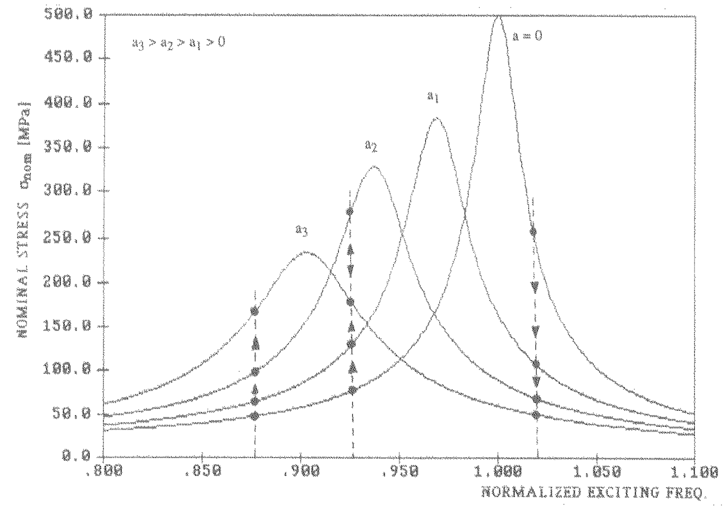


**Fig. 4.4** Nominal stress as a function of excitation frequency for various crack depths.

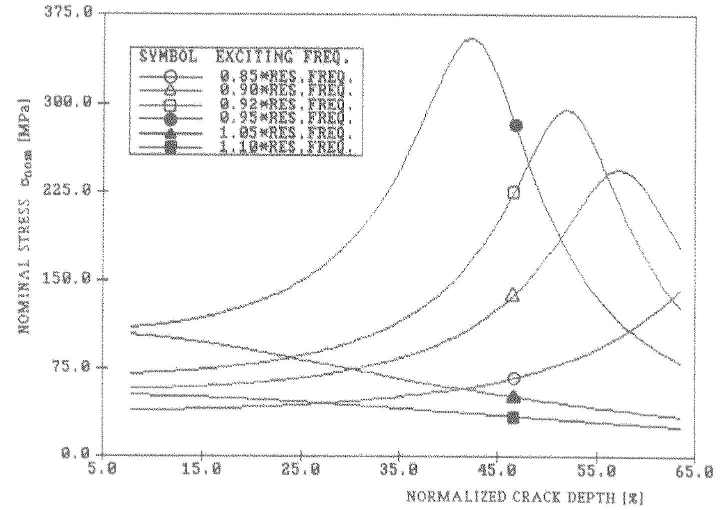


**Fig. 4.5** Effects of excitation frequency on nominal stress.

The remaining stages of fatigue life prediction are illustrated step-by-step in Figs. 4.6 to 4.8. The relationship between the stress intensity factor and the crack depth was obtained using Eq. (4.13) and is plotted in Fig. 4.6. The crack growth rate was calculated using material data given in Table 4.1 and the results are displayed in Fig. 4.7 for various values of the excitation frequency. Again, the crack growth rate is seen to be frequency-dependent. As expected, the maxima in these figures occur when the excitation frequency coincides with a natural frequency of the mistuned system. Also,

**Table 4.1** Crack growth rate data for a structural steel [**Ewalds** and **Wanhill** (1977)].

| | | | |
|---|---|---|---|
| $C_o = 5.01*10^{-12}$ | $n = 3.1$ | $K_{Ic} = 100.0\ MPa\sqrt{m}$ | $\frac{da}{dN_c}$ is in m/cycle |

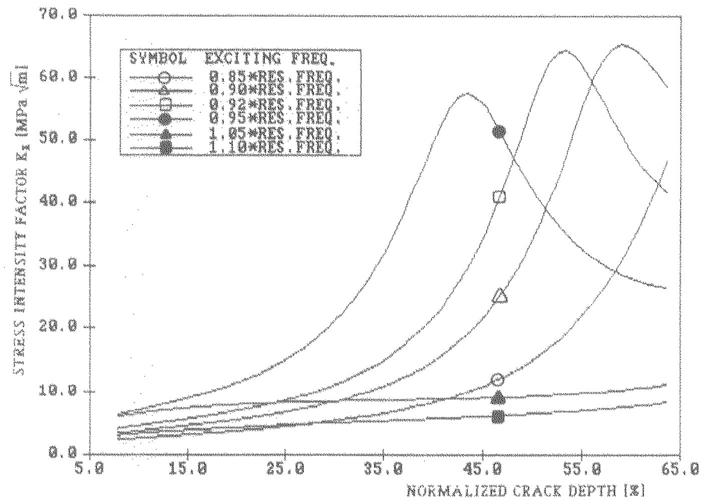


**Fig. 4.6** Stress intensity factor versus crack size for various values of excitation frequency.

the fatigue life was calculated for various values of excitation frequency using Eq. (4.15) and these results are presented in Fig. 4.8.

Finally, it was decided to investigate the extent of the additional effects brought in by using frequency- and/or crack-dependent nominal stress while predicting fatigue life. Three further sets of calculations, corresponding to (i) a frequency- and crack-independent (i.e. constant) nominal stress; (ii) a frequency-dependent but crack-independent nominal stress and (iii) both frequency- and crack-dependent nominal stress, were performed. The variation of fatigue life with excitation frequency is plotted in Fig. 4.9 for all three cases. As expected, the excitation frequency has a marked effect on fatigue life, the variation of which is remarkably similar to the inverse of the frequency response function. The effects of including crack-dependency in the nominal stress calculation is also illustrated in Fig. 4.9 and results suggest that this effect is crack size-dependent.

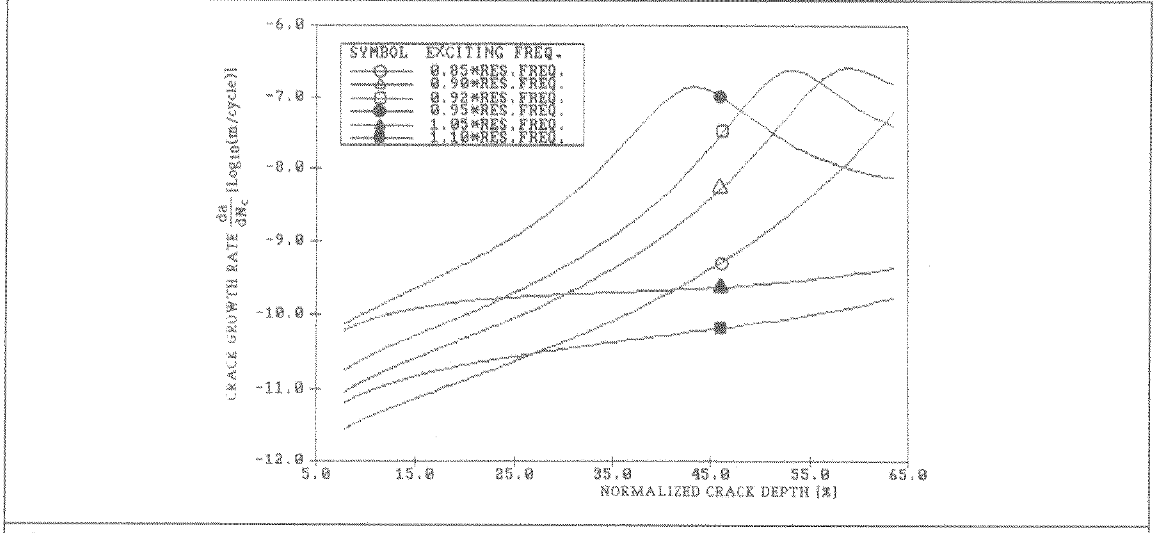


**Fig. 4.7** Crack growth rate versus crack size for various values of excitation frequency.

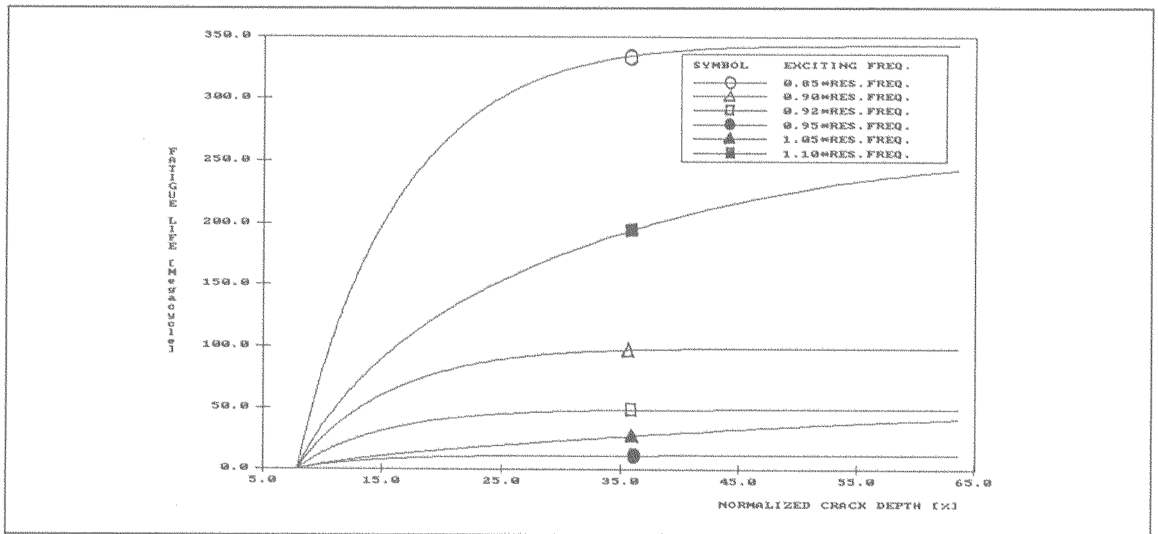


**Fig. 4.8** Fatigue life versus crack size for various values of excitation frequency.

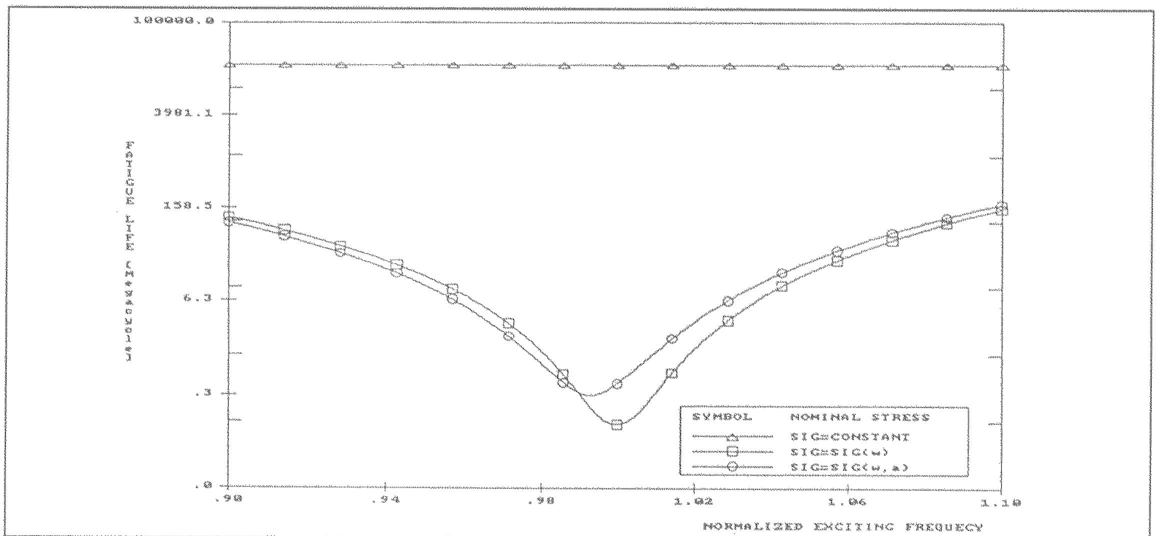


**Fig. 4.9** Effects of using frequency- and/or crack-dependent nominal stress while predicting fatigue life (for a crack to propagate to 35% blade thickness).

## 4.6 Concluding Remarks

i) A method for predicting fatigue life under forced vibration has been presented and it has been shown that the inclusion of frequency- and/or crack-dependence into the stress intensity factor yields significantly lower fatigue life predictions, especially when the excitation frequency is in the vicinity of a natural frequency of one of the modes of vibration.

ii) The technique has been applied to a bladed disc assembly for the case of single-blade mistuning caused by a fatigue crack. The findings suggest that the coincidence of excitation frequency with the new natural frequencies of the system due to fatigue crack should be avoided for prolonged fatigue life.

iii) Although the method is illustrated using a lumped parameter model, it is equally applicable to finite element formulations. However, the computation of the required stress parameter may become prohibitively expensive for complex engineering components in which case experimental data can be used.

# CHAPTER 5

# A PROBABILISTIC ANALYSIS OF SINGLE-DEGREE-OF-FREEDOM SYSTEM VIBRATION

**About This Chapter**

*In earlier chapters, analyses were based on a deterministic approach in that predetermined configurations of mistuned bladed discs were studied to find the consequences of mistuning. Although such an approach is useful in many respects, the application of the findings from such analyses is limited because of the inherent randomness of the blades' structural properties due to manufacturing tolerances. In this chapter, as a first step towards the statistical analysis of mistuning, the effects of random stiffness and damping variations on single-degree-of-freedom system vibration are investigated statistically. An important feature of this study is the determination of the cumulative probability distributions for damped natural frequency and receptance frequency response function without having to compute their probability density distributions since it is shown that those of stiffness and damping can be used directly. The advantage of this approach is not only in the simplicity of the problem formulation but also in the substantial reduction of computational requirements which is achieved.*

## 5.1 Introduction

The most common way of dealing with mistuning-related vibration problems is to use a deterministic approach where answers are sought for a particular mistuning configuration which is hoped to be representative enough of the assembly under study. However, turbomachinery designers need to know the maximum changes in resonant response level which are due to variations in individual blade properties and these are somewhat random quantities with quantifiable statistical bounds. It seems, therefore that it is more appropriate, albeit much more difficult and computationally expensive, to address the problem using a statistical approach. Furthermore, although the determination of accurate damping values is probably the most important requirement for reliable forced response calculations, damping is estimated with much lower accuracy when compared with other modal data, and is a parameter which needs to be considered as one of the random structural parameters. Examples of statistical analyses of blade and bladed disc vibrations already exist in the published literature. **Griffin** and **Hoosac** (1984) studied the effect of mistuning on the response levels of large bladed disc assemblies. **Basu** and **Griffin** (1986) extended this work to include the effects of changing various system parameters such as: gas density, number of blades on the disc, disc stiffness and engine order of excitation. A probabilistic treatment of natural frequency and response level variations of individual blades represented as simple one degree-of-freedom cantilever beams was provided by **Singh** (1988). Later, **Singh** and **Ewins** (1988) applied the same technique to a spring-mass-dashpot system simulating a bladed disc. However, both studies focussed on stiffness variations only and hence damping changes were not included in the analysis as random variable.

The purpose of the present study is twofold. First, it is proposed to investigate cases where both stiffness and damping properties are random variables. In this respect, the present work is an extension of **Singh**'s work (1988) in the sense that a single-degree-of-freedom system is also used here. Secondly, an alternative mathematical formulation is presented: the cumulative probability distributions of damped natural frequency and receptance frequency response function are obtained directly from the probability density functions of stiffness and damping distributions without having to determine the probability density distributions of these two quantities first. One obvious advantage of this approach lies in the substantial reduction of computing requirements.

## 5.2 Theory

A review of probability theory is beyond the scope of this thesis and the interested reader should consult **Parzen** (1960) and **Lin** (1967) for details of these topics. The main objective here is the determination of the statistical characteristics of a function of random variables. Indeed, the statistical behaviour of any such function can be calculated provided that that of the independent variables is known and this is precisely the situation addressed here: the equation of motion for a single-degree-of-freedom system provides the target functional relationship and the independent variables are the structural parameters with known statistical properties.

For the sake of generality, let $x_1,...,x_n$ be the n jointly distributed independent random variables with joint probability density functions (pdf) $p_{x_1,...,x_n}(x_1,...,x_n)$ and let y be the dependent variable.

$$y = g(x_1, ..., x_n) \tag{5.1}$$

It is now possible to find the cumulative density function (cdf) (also called cumulative probability or probability distribution) and the probability density function (pdf) of y, denoted by $P_Y(y)$ and $p_Y(y)$ respectively.

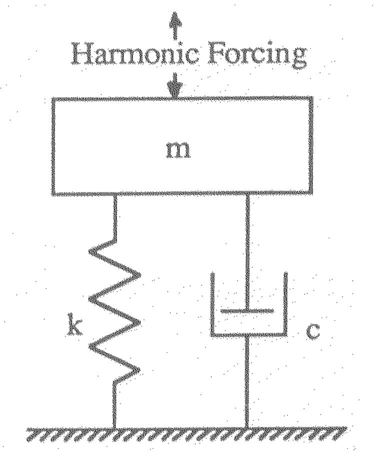


**Fig. 5.1** Single degree-of-freedom model.

$$P_Y(y')=\text{Prob}(y\le y')=\underset{\{(x_1,\ldots,x_n):g(x_1,\ldots,x_n)\le y'\}}{\iiint\ldots\ldots\int} p_{X_1,\ldots,X_n}(x_1,\ldots,x_n)dx_1\ldots dx_n \tag{5.2}$$

$$p_Y(y') = \frac{dP_Y(y')}{dy'} \tag{5.3}$$

Once $P_Y(y')$ is obtained, the probability of y to be within two prescribed limits is

$$\text{Prob}(y_1 \le y \le y_2) = P_Y(y_2) - P_Y(y_1) \tag{5.4}$$

### 5.3 Application to a Single-Degree-of-Freedom System

Referring to the spring-mass-dashpot model of Fig. 5.1, the damped natural frequency and the magnitude of the receptance frequency response function are given by

$$\omega_d = \omega_o\sqrt{1-\zeta^2} = \sqrt{k/m - c^2/4m^2} \tag{5.5}$$

$$\alpha = \frac{1}{\sqrt{(k-m\omega^2)^2 + \omega^2c^2}} \tag{5.6}$$

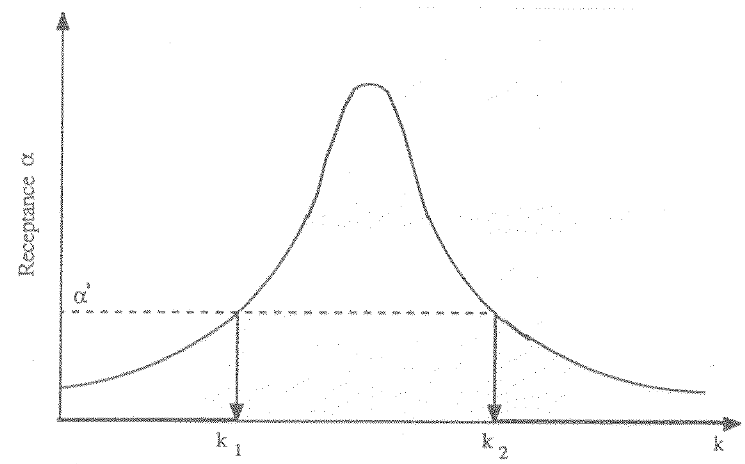


**Fig. 5.2** Receptance as a function of stiffness.

where all symbols have their customary meanings. In Eqs. (5.5) and (5.6) the damped natural frequency, $\omega_d$, and receptance, $\alpha$, are independent variables where $\omega_d$ is a function of three variables (stiffness, mass and damping) while $\alpha$ is a function of four variables, the additional one being the excitation frequency. Since the mass properties and the excitation frequency can be determined with good accuracy, it can be assumed that random variations exist in stiffness and damping properties only. However, this assumption brings no loss of generality since Eq. (5.2) is valid for any number of random variables. Equation (5.6) is plotted in Fig. 5.2 as a function of stiffness, and again in Fig. 5.3 as a function of both stiffness and damping.

In the following sections, an explicit formulation of the cumulative density functions of $\omega_d$ and $\alpha$ will be derived for random variations of (i) stiffness only, (ii) damping only and (iii) both stiffness and damping. Once the cumulative density functions are known, the corresponding probability density distributions can easily be obtained from Eq. (5.3).

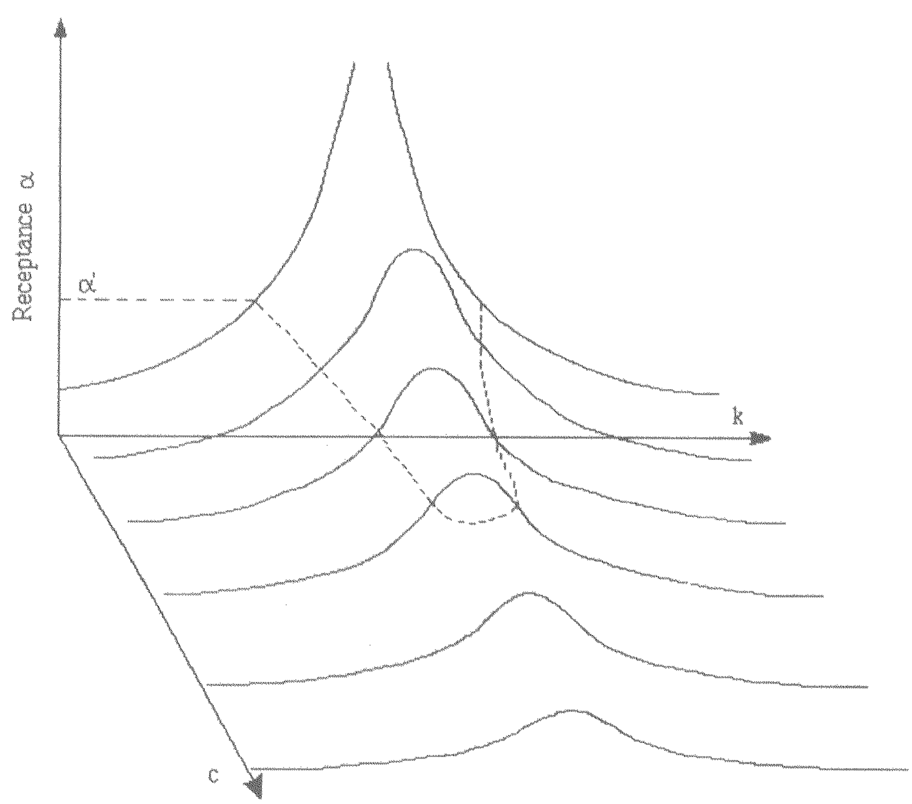


**Fig. 5.3** Receptance as a function of stiffness and damping.

### 5.3.1 Cumulative Probability of Damped Natural Frequency

For case (i), the cumulative probability of the damped natural frequency being less than certain value, say $\omega'$, can be found using Eq. (5.2) as

$$\mathrm{Prob}(\omega_d \le \omega') = \int_{\{k:\ \omega_d(k) \le \omega'\}} p_K(k)dk \qquad (5.7)$$

where $p_K(k)$ is the (known) probability density function of k. Let us consider the integration domain in Eq. (5.7).

$$\omega_d(k) \le \omega' \quad \text{or} \quad \sqrt{k/m - c^2/4m^2} \le \omega' \quad \text{or} \quad k \le m(\omega'^2 + c^2/4m^2) \qquad (5.8)$$

Eq. (5.7) now becomes

$$\mathrm{Prob}(\ \omega_d \le \omega'\ ) = \int_0^{m(\omega'^2 + c^2/4m^2)} p_K(k)dk \tag{5.9}$$

Applying the same procedure to case (ii), we find:

$$\mathrm{Prob}(\omega_d \le \omega') = \int_{2m(k/m-\omega'^2)^{1/2}}^{\infty} p_C(c)dc \tag{5.10}$$

Finally, for case (iii) where both stiffness and damping are random variables:

$$\mathrm{Prob}(\omega_d \le \omega') = \iint_{\{(k,c):\omega_d(k,c)\le\omega'\}} p_{K,C}(k,c)dk\,dc \tag{5.11}$$

where $p_{K,C}(k,c)$ is the joint probability density function of stiffness and damping. As before, inserting the appropriate expressions for the integration limits yields

$$\mathrm{Prob}(\ \omega_d \le \omega'\ ) = \int_0^{\infty} dc \int_0^{m(\omega'^2 + c^2/4m^2)} p_{K,C}(k,c)dk \tag{5.12}$$

### 5.3.2 Cumulative Probability of Receptance

For case (i), the cumulative probability of receptance being less than $\alpha'$ can be written as

$$\mathrm{Prob}(\alpha \le \alpha') = \int_{\{k:\ \alpha(k) \le \alpha'\}} p_K(k)dk \tag{5.13}$$

where the integration domain can be expressed as

$$\{(k-m\omega^2)^2 + \omega^2c^2\}^{-1/2} \le \alpha' \tag{5.14}$$

Solving for k gives

$$k \le k_1 = m\omega^2 - \sqrt{1/\alpha'^2 - \omega^2c^2} \tag{5.15.a}$$

$$k \ge k_2 = m\omega^2 + \sqrt{1/\alpha'^2 - \omega^2c^2} \tag{5.15.b}$$

Using these two expressions, Eq. (5.13) can be rewritten as

$$\mathrm{Prob}(\alpha \le \alpha') = \mathrm{Prob}(k \le k_1) + \mathrm{Prob}(k \ge k_2) = \int_0^{k_1} p_K(k)dk + \int_{k_2}^{\infty} p_K(k)dk \tag{5.16}$$

where $k_1$ and $k_2$ are defined in Eq. (5.15)

For case (ii), the cumulative density function can be derived in a similar fashion as

$$\mathrm{Prob}(\alpha \le \alpha') = \mathrm{Prob}(c \ge c_1) = \int_{1/\omega-(1/\alpha'^2-(k-m\omega^2)^2)^{1/2}}^{\infty} p_C(c)dc \tag{5.17}$$

And finally, for case (iii)

$$\mathrm{Prob}(\alpha \le \alpha') = \int_0^\infty dc \left[ \int_0^{k_1} p_{K,C}(k,c)dk + \int_{k_2}^\infty p_{K,C}(k,c)dk \right] \tag{5.18}$$

It should be noted that the limits of the inner integrals are now functions of the damping parameter c.

## 5.4 Results and Discussion

So far, no assumptions have been made about stiffness and damping distributions. In fact, any pdf representing the stiffness and the damping populations can be used in conjunction with the method described here. However, for the purpose of simplicity, and because of the lack of evidence to the contrary, the stiffness and damping populations were assumed to be normal. Also, it was decided to make these two parameters independent of each other in which case $p_{K,C}(k,c)=p_K(k) \times p_C(c)$ since the individual pdfs are not jointly-distributed.

From the outset, it is worth mentioning that the probability distribution of any non-linear function of normally-distributed random variables is not normal, the deviation from the normal distribution depending on the degree of the non-linearity of the function. In our particular case, the damped natural frequency and the receptance are non-linear functions of the structural parameters and hence their probability distributions will not be normal.

A computer program was written to evaluate the above cdfs (Eqs. (5.9), (5.10), (5.12), (5.16), (5.17), (5.18)) in order to illustrate how random variations in structural parameters affect the damped natural frequency and receptance frequency response function. Although a numerical difficulty was encountered while evaluating Eqs. (5.12) and (5.18), for which the inner integral limits are a function of the outer variable, a solution was found eventually.

Unless otherwise stated, the following parameters were used as mean structural parameters in all numerical examples given here while determining the cdfs and pdfs: $m=1.0$ kg, $k=1000$ N/m and $\zeta=0.03$. The receptance frequency response function was calculated at the nominal system natural frequency.

### 5.4.1 Effects on Damped Natural Frequency

The cumulative probability distribution of the damped natural frequency was calculated for various stiffness populations characterized by their coefficient of dispersion, CD, (which is defined as the ratio of standard deviation to mean) and the results are plotted in Fig. 5.4.a where the damped natural frequency is scaled such that it is unity at mean stiffness. The corresponding probability density curves were computed using Eq. (5.3) and are displayed in Fig. 5.4.b. A close inspection of the curves in Fig. 5.4.b shows that they are not symmetrical and hence are not normal. However, the deviation from a normal distribution is not very significant. Further calculations using a range of damping values showed that the results in Fig. (5.4) were quite general when stiffness was the only random parameter.

The same process was applied to the case of damping being the only random parameter and cumulative probability distributions are shown in Fig. (5.5). The main observation is that damping changes have a very small effect on damped natural frequencies.

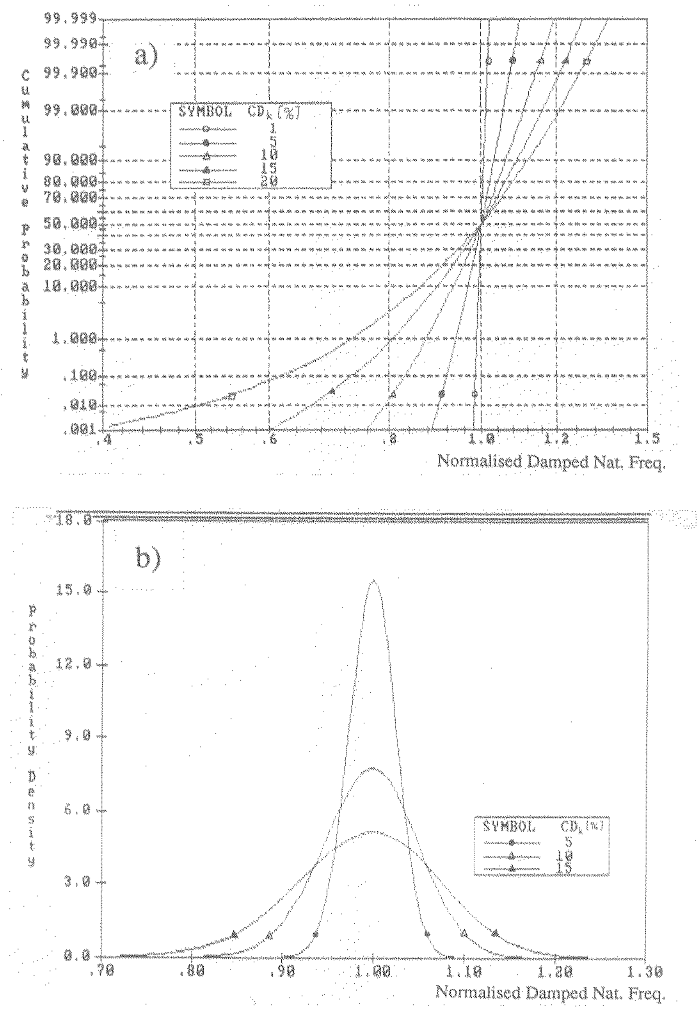


**Fig. 5.4** Cumulative probability and probability density functions of damped natural frequency. (Only k is random variable.)

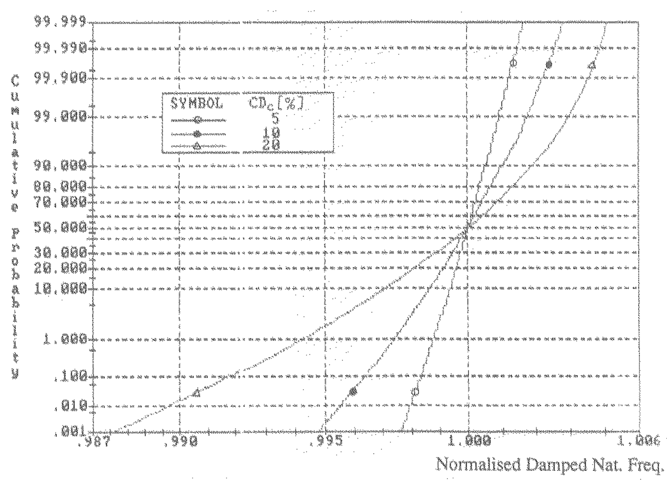


**Fig. 5.5** Cumulative probability of damped natural frequency. (Only c is random variable. $\zeta$=0.1)

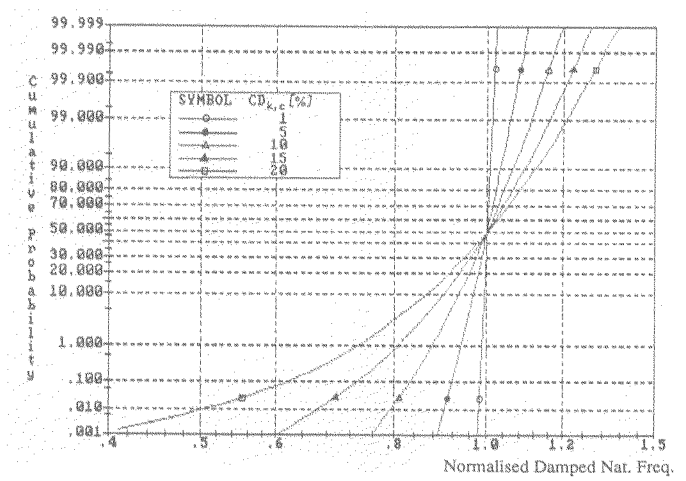


**Fig. 5.6** Cumulative probability of damped natural frequency. (Both k and c are random variables.)

The next step was to investigate the effects of simultaneous variations of stiffness and damping properties on the damped natural frequency and these results are given in Fig. (5.6). Once again, damping changes have very little effect, an expected result in the light of Figs. (5.4) and (5.5).

### 5.4.2 Effects on Receptance

Since the receptance frequency response function is also a function of the exciting frequency, $\omega_{ex}$, its cdf and pdf will vary with the exciting frequency. This is illustrated in Fig. 5.7 where probability density functions corresponding to various values of $\omega_{ex}$ are plotted when stiffness is the only random parameter. It should be noted that the receptance axis in Fig. 5.7 is normalized such that unity represents nominal receptance value at specified exciting frequency. Also, the pdf of the receptance is very sensitive to the position of $\omega_{ex}$ and the sharp increase visible in Fig. 5.7 is due to a nearby resonance. Although it is relatively straightforward to obtain the cdf and pdf of the response at any exciting frequency, changes near resonance are of greatest interest and attention will now be focussed on this particular situation.

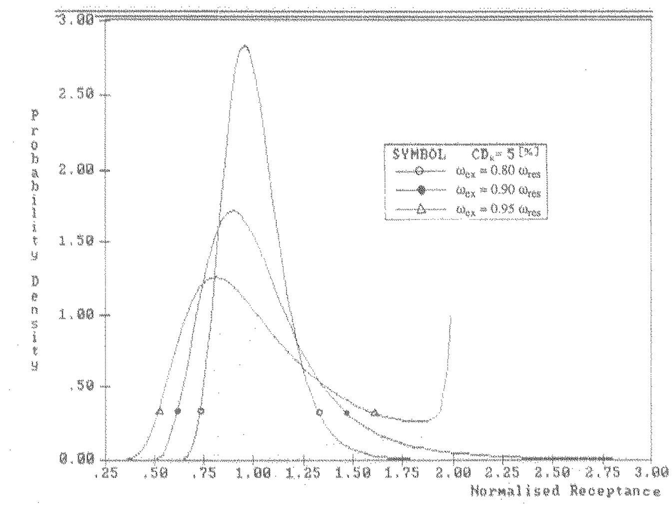


**Fig. 5.7** Probability density function of receptance for various values of exciting frequency. (Only k is random variable.)

The cdf and the pdf of the receptance are plotted in Figs. (5.8.a) and (5.8.b) respectively for the case where the random parameter is stiffness only, the receptance axis being normalized with respect to the value obtained for nominal stiffness. In this case, stiffness variations will cause all normalized receptances to be less than unity since the maximum was only be reached at the nominal value of stiffness when the exciting frequency coincides with the system natural frequency. As can be seen from Fig (5.8.b), response levels spread over a wide range, a concentration of response occurring far away from design value, depending on the standard deviation of stiffness. Further calculations, not reported here, show that the general appearance of the pdf curves does not depend on damping, increasing values of which have the effect of slightly shifting the curves upwards.

The cdf and the pdf of the receptance are plotted in Figs. (5.9.a) and (5.9.b) for the case where the random parameter is damping only, the receptance axis being normalized this time with respect to the value obtained for nominal damping. The immediate feature is the very wide scatter of the response for moderate damping variations. This finding is in complete agreement with **Basu** and **Griffin** (1986) who showed that the *mistuning enhancement ratio* - ratio of maximum blade amplitude of mistuned assemblies to that

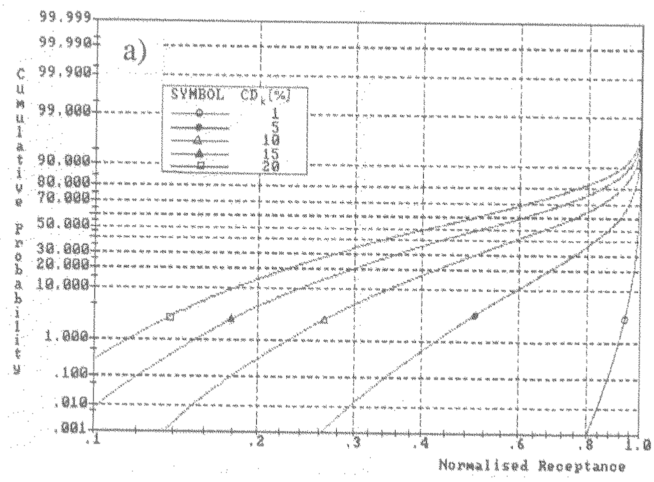


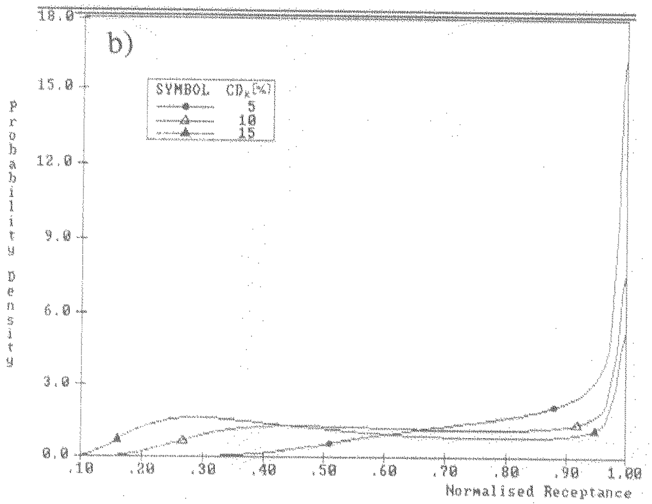


**Fig. 5.8** Cumulative probability and probability density functions of receptance. (Only k is random variable.)

of the tuned system - is very sensitive to small variations in aerodynamic damping. Fig. 5.9.b also reveals that the amount of response increase due to negative changes of damping exceeds by far that of response decrease for equivalent positive changes of damping.

Finally, the cdf and the pdf of the receptance are plotted in Figs. (5.10.a) and (5.10.b) for the case where both stiffness and damping are the random parameters. The receptance pdfs of Fig. 5.10.b have a rather unusual appearance and they bear no

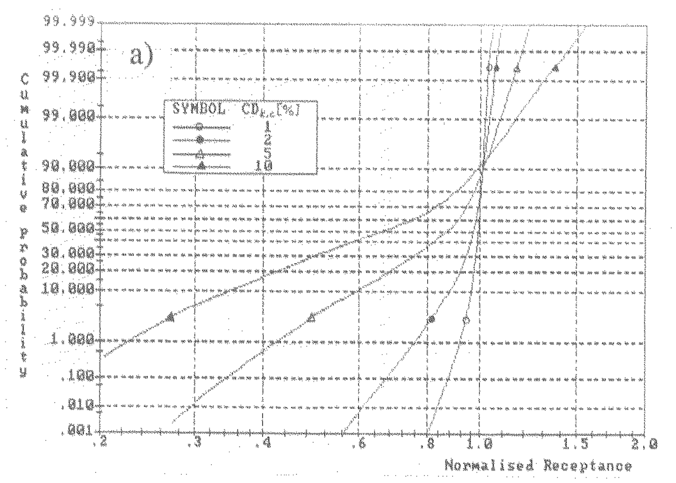


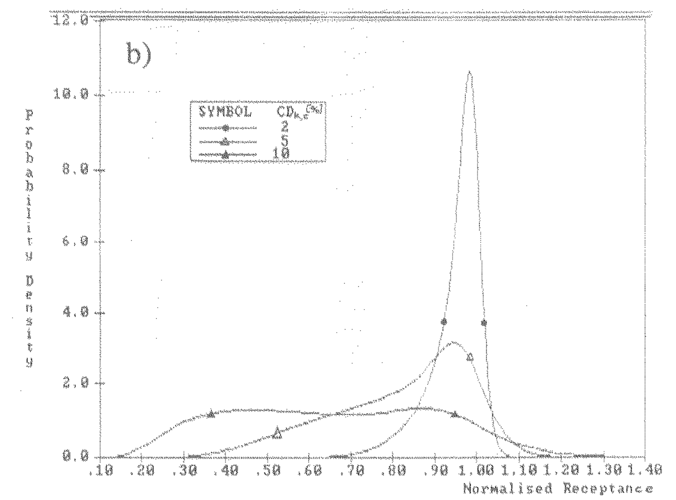


**Fig. 5.10** Cumulative probability and probability density functions of receptance. (Both k and c are random variables.)

## 5.5 Concluding Remarks

i) A probabilistic approach to single-degree-of-freedom system forced vibration has been discussed and a method to compute the cumulative probability distribution for damped natural frequencies and response levels for both stiffness and damping variations has been presented.

ii) Although the formulation is valid for any probability density function for the independent variables, a normal distribution has been assumed for both stiffness and damping changes and it is found that the corresponding natural frequency and receptance probability distributions are not normal.

iii) The factor controlling the amount of scatter in the response levels is the standard deviation and this has practical implications for turbomachinery applications where the individual blade cantilever frequencies, hence stiffness properties, are known. However, there is no obvious justification to assume a normal distribution for damping changes, a topic which merits thorough experimental investigation.

iv) Damping variations have very little effect on the damped natural frequency which is predominantly determined by stiffness and mass properties.

v) Small variations in damping change resonant response levels considerably, negative changes causing large response increases while equivalent positive changes result in only modest response reductions.

vi) The general appearance of probability density distributions of the response depend on exciting frequency and the amount of scatter in the structural parameters.

# CHAPTER 6

# STATISTICAL ANALYSIS OF RANDOM MISTUNING: A DIRECT APPROACH

**About This Chapter**

*This chapter deals with the statistical analysis of the forced response of mistuned bladed discs. Statistical sampling theory is used to calculate the probability and the cumulative density functions of the mistuned blades' resonant response amplitudes, blade-to-blade variations in cantilever frequency being considered to be random with a Gaussian (normal) distribution. Results presented in this chapter make it possible to reconcile conflicting conclusions which have been reached by many researchers on both qualitative and quantitative matters related to the consequences of mistuning, most notably the identification of critical blades and the increase in forced response due to mistuning.*

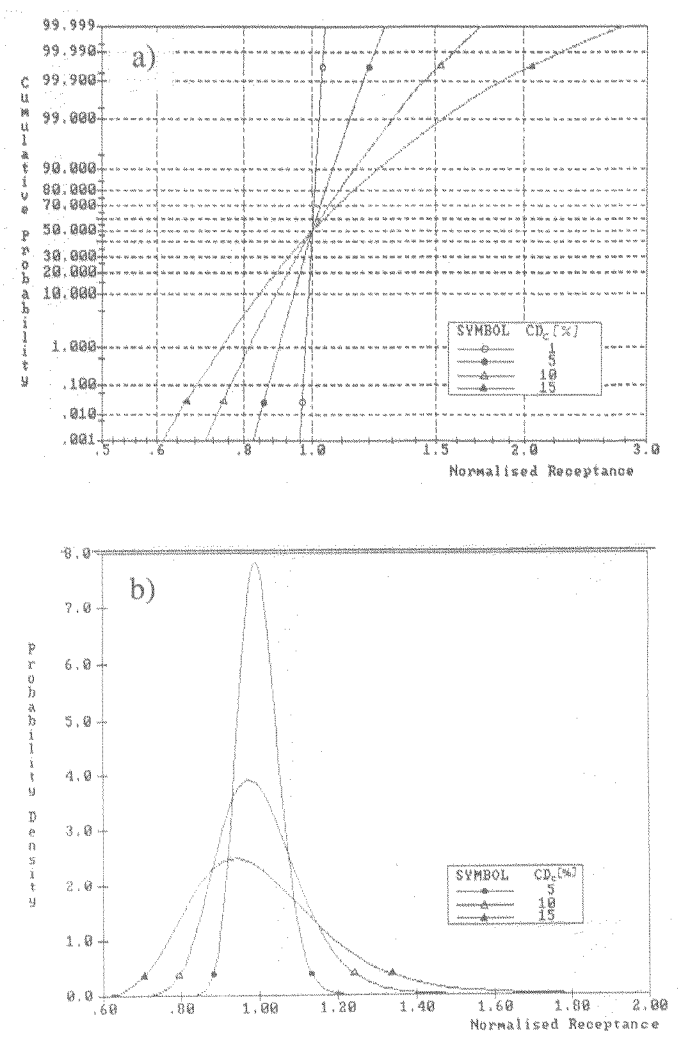


**Fig. 5.9** Cumulative probability and probability density functions of receptance. (Only c is random variable.)

resemblance to the input stiffness and damping pdfs. Their shapes are dominated by the amount of scatter in the input parameters and may well exhibit more than one peak.

## 6.1 Introduction

The traditional way of studying the effects of mistuning is the deterministic approach in which a predetermined configuration of mistuned blades is studied directly. As reviewed in chapter 1, the majority of the research made on mistuning effects, including that described in chapters 3 and 4, falls into this category. Although studies based on this approach can reveal highly complex dynamic behaviour of mistuned bladed systems, results from such studies find a very limited application since building a mistuned bladed disc to specification is almost certainly more difficult than building a perfectly tuned disc. A preferred alternative is to seek statistical answers to mistuning-related questions since all steps from manufacturing blades to assembling a bladed disc are themselves probabilistic processes.

This chapter is concerned with a statistical analysis of the dynamic behaviour of mistuned bladed discs and the main objectives are to find;

i) the probability and the cumulative density functions of the blade response amplitudes so that the maximum response and the critical blade can be determined on a statistical basis; and

ii) the possibility of predicting the vibration characteristics of bladed discs with large numbers of blades by studying systems with fewer blades.

## 6.2 Model Description

The lumped parameter model of chapter 3 will be used in the present statistical investigation of the mistuning problem. The cantilever frequency of each blade is now considered as a random parameter, other parameters used in the simulation being assumed to be constant. Referring to Fig. 3.2, the equations of motion for the $j^{th}$ blade and disc sector can be written as:

$$\ddot{x}_j + 2\zeta G_j \dot{x}_j + G_j^2 (1+ i\eta)(x_j - y_j) = \frac{f_j(t)}{m} \tag{6.1}$$

$$\frac{M_d}{m} \ddot{y}_j + G_j^2 (1+ i\eta) (y_j - x_j) + \frac{k_g}{m} y_j + \frac{K_d}{m} (2y_j - y_{j+1} - y_{j-1}) = 0 \tag{6.2}$$

where $G_j$ $(=\sqrt{k_j/m})$ is the random variable representing the cantilever frequency of the $j^{th}$ blade and the external force $f_j(t)$ represents a particular engine order (EO) excitation. The equations of motion in recurrence form can easily be converted into a linear matrix equation for the steady-state solution for blade and disc sector responses as:

$$\{\hat{q}\} = [Z]^{-1} \{\hat{f}\} \tag{6.3}$$

It should be noted that as a result of the randomness in blade frequencies, the dynamic stiffness matrix, [Z], and consequently the steady-state response vector $\{\hat{q}\}$, are also random quantities.

Except where stated otherwise, the structural parameters shown in Table 6.1 were used in this investigation. Practical experience indicates that a coefficient of dispersion (CD) of 3% (CD is defined as the ratio of standard deviation to the mean value) is representative of blade mistuning in modern gas turbines. Furthermore, experimental data on the first bending mode natural frequency of blades in typical aeroengines suggest that the blade population is approximately Gaussian and this assumption is

**Table 6.1** Structural parameters.

| | | |
|---|---|---|
| $\frac{\bar{G}}{2\pi} = 182$ Hz | $\frac{\sqrt{K_d/M_d}}{\bar{G}} = 2$ | $\frac{\bar{G}}{\sqrt{k_g/M_d}} = 60$ |
| $CD_G = 3.0$ % | $\eta = 0.2\%$ | $\zeta = 1.0$ % |

made throughout this study. Also, it is believed that damping values shown in Table 6.1 are typical of such assemblies.

## 6.3 Theoretical Background

A method to determine the statistical properties of a dependent variable which is a function of several random variables was outlined in the previous chapter in the case of a SDOF system with random stiffness and damping parameters. The same method can be extended and applied to a MDOF system. Supposing that the random function is given by Eq. (6.3), where the response amplitudes $\{\hat{q}\}$ are dependent and the blade natural frequencies are independent random variables, it is possible to find the cumulative distribution function (cdf) and the probability density function (pdf) of any element of the response vector, $\hat{q}_i$, as:

$$P_{\hat{q}_i}(\hat{q}')=\mathrm{Prob}(\hat{q}_i \leq \hat{q}')= \int\int_{\{(g_1,..,g_N):\hat{q}_i \leq \hat{q}'\}} .... \int p_{G_1,G_2,..G_N}(g_1,g_2,..,g_N)\, dg_1 dg_2....dg_N \quad (6.4)$$

$$p_{\hat{q}_i}(\hat{q}') = \frac{dP_{\hat{q}_i}(\hat{q}')}{d\hat{q}'} \quad (6.5)$$

where $p_{G_1,G_2,..G_N}(g_1,g_2,....,g_N)$ is the joint probability density function of the blade first cantilever frequencies and $\hat{q}'$ is any arbitrary value. If we assume that blade frequencies are not jointly distributed (this means that if a blade is drawn randomly from a given population, this does not affect the outcome of the next draw), Eq. (6.4) can be simplified to:

$$P_{\hat{q}_i}(\hat{q}') = \mathrm{Prob}(\hat{q}_i \leq \hat{q}') = \int\int_{\{(g_1,..,g_N):\hat{q}_i \leq \hat{q}'\}} .... \int \left(\prod_{j=1}^{N} p_{G_j}(g_j)\right) dg_1 dg_2....dg_N \quad (6.6)$$

Although the formulation for the pdf and cdf of blade response levels is simple, the evaluation of the multi-dimensional integral above is very difficult since (i) the dimension of the integral is equal to the number of blades, and this is usually very large and (ii) the integral domain is very complicated. Therefore, an appropriate statistical theory had to be used to evaluate the multi-dimensional integral in Eq. (6.6). Statistical sampling theory [**Gibra** (1973), **Davies** (1972), **Ealpole** and **Myers** (1985)] was used for this particular problem since the analytical techniques available are either applicable to specific cases only or are based on unrealistic assumptions. Consequently, the work presented in this chapter falls into the numerical studies category of mistuning investigations.

When sampling theory is used to predict the statistics of a random variable, say $\hat{q}_i$, it requires a large sample drawn from the population as $\hat{q}'_1, \hat{q}'_2, \hat{q}'_3, \ldots, \hat{q}'_{N_s}$ where $N_s$ represents the sample size. If sampled quantities are rearranged in such a way that $\hat{q}'_{(1)} \leq \hat{q}'_{(2)} \leq \hat{q}'_{(3)} \leq \ldots \leq \hat{q}'_{(N_s)}$, sampling theory states that the cumulative density function (cdf) of the random variable $\hat{q}_i$ is:

$$P_{\hat{q}_i}(\hat{q}'_{(j)}) = \mathrm{Prob}(\hat{q}_i \leq \hat{q}'_{(j)}) \approx \frac{j}{N_s+1} \tag{6.7}$$

and the sample mean and the variance are, respectively:

$$\bar{\hat{q}}_i = \frac{1}{N_s} \sum_{j=1}^{N_s} \hat{q}'_j \tag{6.8}$$

$$\sigma^2 = \frac{\sum_{j=1}^{N_s} (\hat{q}'_j - \bar{\hat{q}}_i)^2}{N_s - 1} \tag{6.9}$$

When the cdf is calculated using sampling theory, its accuracy is not good enough to predict the pdf using Eq. (6.5) because of the derivative involved. Instead, the sample range is divided into $N_I$ subintervals as:

$$\Delta\hat{q}' = \frac{\hat{q}'_{max} - \hat{q}'_{min}}{N_I} \tag{6.10}$$

and the value of the pdf is estimated at each subinterval mid-point:

$$p_{\hat{q}_i}(\hat{q}') \approx \frac{1}{\Delta\hat{q}'} \frac{n_I}{N_s+1} \tag{6.11}$$

where $n_I$ is the number of data points which lie within the range $(\hat{q}' - \Delta\hat{q}'/2, \hat{q}' + \Delta\hat{q}'/2]$.

It should be noted that $(N_s-1)$ or $(N_s+1)$ were used in the denominators of Eqs. (6.7, 6.9, 6.11) instead of the more usual $N_s$. This is due to the finite size of the sample set and we shall include a comment made by **Press et al.** (1986)"*...if that difference ever matters to you, then you are probably up to no good anyway - e.g., trying to substantiate a questionable hypothesis with marginal data...*".

### 6.4 Sample Size Determination

One of the critical parameters in any numerical simulation of a statistical process is the sample size $N_s$ on which confidence limits and the accuracy of the statistical findings strongly depend. As $N_s$ gets larger, the accuracy of the estimated parameters improves and, in the limit as $N_s$ approaches infinity, the results become exact. In practice, however, as time and cost factors have to be weighed carefully, one has to choose a reasonable sample size while trying to preserve accuracy.

Finding a compromise between accuracy and a manageable sample size is not always a straightforward task. Although there are mathematical and statistical guidelines, such as the central limit theorem and several theorems related to confidence limits, which can be used to estimate the number of samples required to find the mean of an unknown population for a given confidence interval, there is no simple analytical way of predicting the accuracy of the estimated probability density function (pdf). One possibility is to predict the pdf of a known population for various values of $N_S$ and $N_I$ and then to compare the predicted pdfs with the exact values. From such comparisons, it is possible to infer the required $N_S$ and $N_I$ for determining the unknown population. Such tests were carried out for a normal distribution and the exact and predicted normal distributions are overlaid for various combinations of $N_S$ and $N_I$ in Fig. 6.1. (It is desirable to have $N_S$ as small as possible from the computational cost point of view while a large $N_I$ is required in order to describe the pdf curve at a sufficient number of points. However, a large $N_I$ also requires a large $N_S$ for the same level of accuracy so it is necessary to choose an optimum combination of these two parameters.) As can be seen from Fig. 6.1, exact and predicted values for a normal distribution at 30 points agree well when the sample size is 20,000. It was concluded that $N_S$ =25,000 and $N_I$ =20 would provide an acceptable level of accuracy in determining the unknown distribution of the response levels provided that the distribution curve does not exhibit many maxima.

## 6.5 Statistical Properties of the Forced Response (36-Bladed Disc)

All results presented in this section are for a 36-bladed disc subjected to various engine order excitations. The effects of varying the number of blades on the forced vibration response of mistuned blades is the subject of a later section.

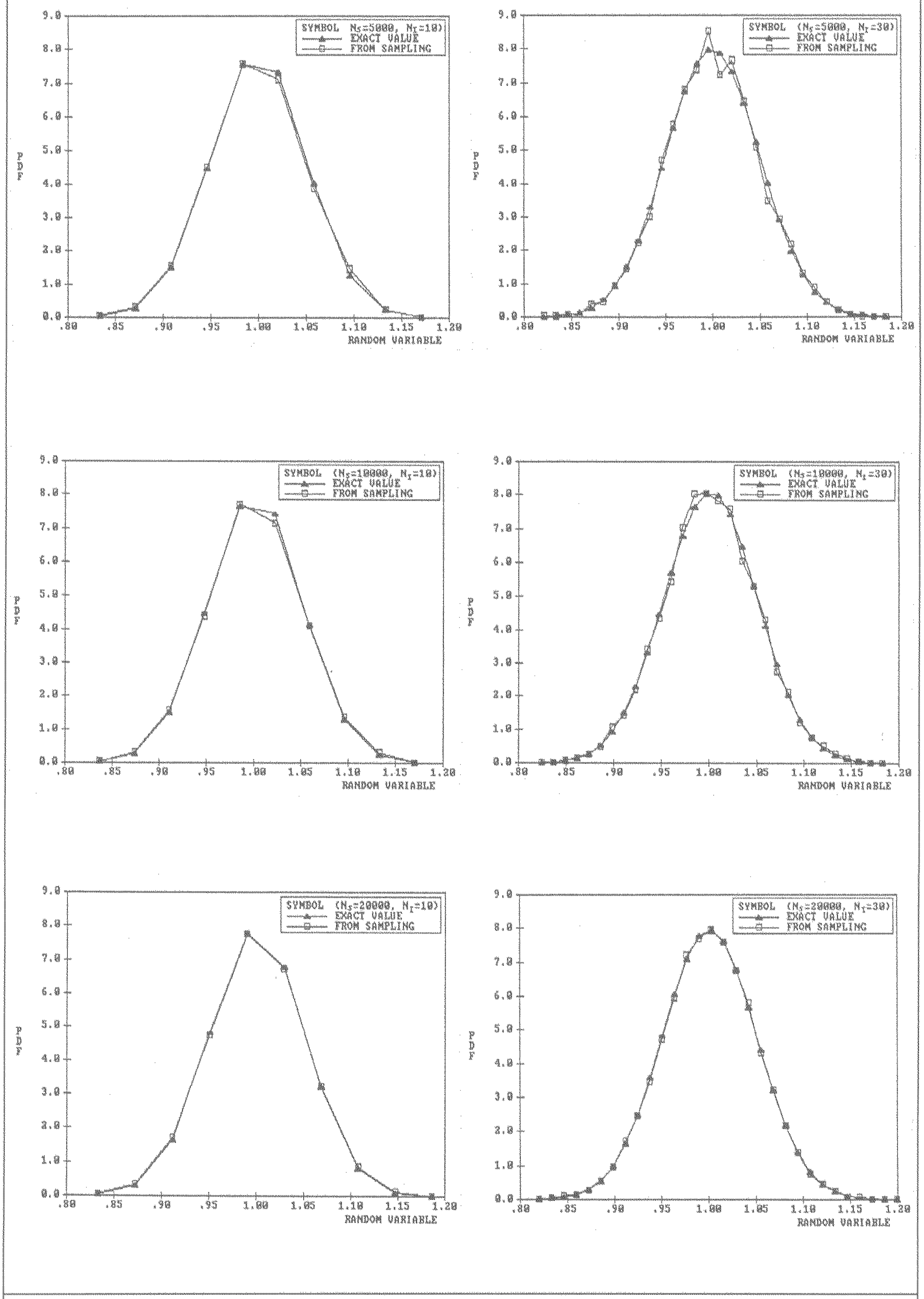


**Fig. 6.1** Determination of sample size $N_S$ and number of subintervals $N_I$.
(Population = Normal, Mean=1.0, CD = 5%)

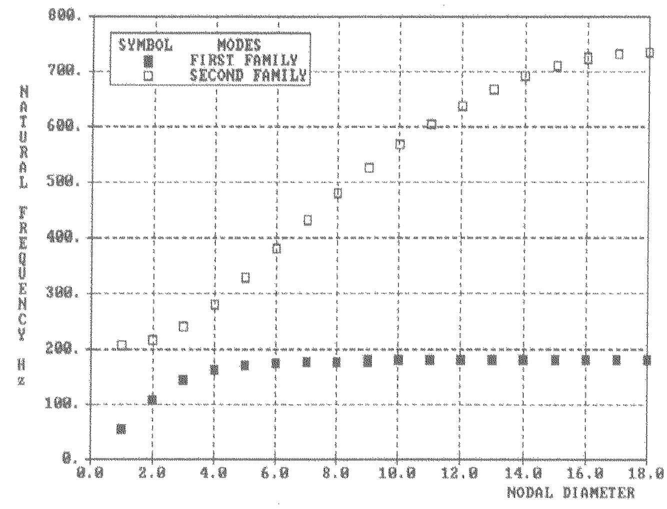


**Fig. 6.2** Natural frequencies of a 36-bladed disc.

The natural frequencies of a tuned 36-bladed disc were calculated using the structural parameters of Table 6.1 and they are shown in Fig. 6.2. It is well known that when the blades are mistuned, the smooth pattern of natural frequency against nodal diameter curves is disturbed and many of the double modes split [**Ewins** (1973)]. Similarly, when minor differences exist between blades on an assembly, mistuned blades do not experience the same response amplitudes as their tuned counterparts. A typical example is presented in Fig. 6.3.a where the response amplitudes of the first 12 blades of a 36-bladed disc under 6 engine order (EO) excitation are plotted. (Responses are normalized to the tuned resonant response and the excitation frequency is normalized to the 6 nodal diameter natural frequency of the tuned assembly.) The corresponding random scatter in the blade first cantilever frequencies, drawn from normal distribution, is shown in Fig. 6.3.b.

As can be seen from Fig. 6.3.a the maximum response levels for individual blades - also referred to as *resonant responses* - occur at different excitation frequencies and attain different maximum (peak) levels, a characteristic feature of mistuned bladed discs.

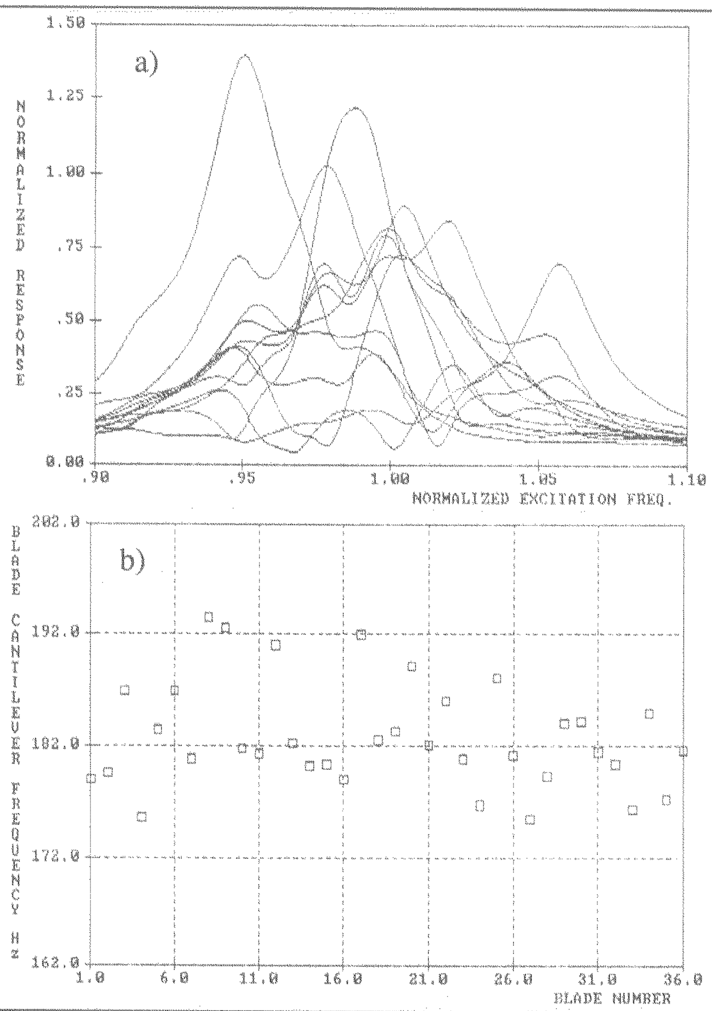


**Fig. 6.3** A typical response levels of mistuned blades and corresponding blade cantilever frequency scatter.

Therefore, finding the resonant responses of all the blades requires the computation of the individual blade responses over a frequency range encompassing all resonances. The determination of this frequency range is not straightforward since it depends both on the amount of mistuning and, as will be shown, on the EO of excitation. After considering various amounts of mistuning and EO excitations, that range was found by trial-and-error. Blade responses over this frequency range were calculated and the maximum amplitude for each blade was recorded together with the corresponding excitation frequency. As mentioned earlier, approximately 25,000 data points were necessary to estimate the probability density function of an unknown population with reasonable accuracy and this in turn necessitated the determination of blade responses for 700 36-bladed discs. The calculations, including those for other mistuned bladed discs with different numbers of blades presented in this chapter, were performed on IBM RS/6000 530 workstation and took several days to complete.

### 6.5.1 Relationship Between Blade Frequency and Resonant Response

In order to find a correlation between the blade responses and their cantilever frequencies, peak response amplitudes, normalized to the tuned resonant response, were plotted against blade frequency normalized to the mean blade first bending frequency for various EO excitations (Figs. 6.4.a to 6.4.f.) A simple inspection of these figures revealed that the relationship between resonant response and blade bending frequency changed with EO excitation and it was thought that the classification of the resonant responses with respect to EO excitation could offer some insight into the effects of mistuning. The resonant response increase due to random mistuning is very small when the excitation EO is very low ($r = 1,2$). As the EO increases, the worsening effect of mistuning also increases and reaches a maximum at which the normalized resonant response exceeds 2.0 and then tends to decrease again ($r = 3$ to $9$ for this case). For 10 to 18 EO excitations, the relationship between resonant response and blade frequency does not show any significant variations. In the general case, the identification of the EO excitation causing the worst mistuning effect is not straightforward. However, preliminary calculations, not reported here, showed that the coupling ratio, $\sqrt{K_d/M_d}/\bar{G}$, was an important parameter, an increase in which caused the worst effect of mistuning to be reached under lower EO excitations.

The results presented in Fig. 6.4 suggest that blades with the highest amplitudes under $r^{th}$ EO excitation are those with individual cantilever frequencies near the $r^{th}$ nodal diameter (rND) natural frequency of the tuned bladed assembly, indicated by an arrow on each figure (Note that 1ND and 3ND tuned natural frequencies are not shown in Figs. 6.4.a and 6.4.b since they are below the minimum individual blade frequency).

This is in agreement with the conclusion drawn by **Griffin** and **Hoosac** (24) who stated that *'...high responding blades are neither the highest nor lowest frequency blades but are those whose blade-alone frequencies are near the tuned system frequency...'*. One should also add that the high-response blades can also be those with the lowest cantilever frequencies (Fig. 6.4.b) when the tuned assembly rND frequency is lower than the lowest blade cantilever frequency.

### 6.5.2 Relationship Between Excitation Frequency and Resonant Response

Another important item of information needed in engine testing is the engine speed (or frequencies) at which the critical blade(s) will vibrate most strongly. Availability of such information can obviate the need to monitor instrumented blades for an unnecessarily wide range of engine speed. The relationship between the maximum amplitude of each blade and the corresponding excitation frequency is plotted in Figs. 6.5.a to 6.5.f. The excitation frequency axis is normalized to the rND natural frequency of the tuned bladed disc: if the assemblies studied were all tuned, all the points would coincide at (1.0,1.0). In fact , under very low EO excitations, (Fig. 6.5.a), all the points are concentrated near (1.0,1.0), showing quasi-tuned assembly characteristics. Results presented in Figs. 6.5.b to 6.5.d show that increasing the EO causes the maximum amplitudes to occur over increasingly wider frequency ranges. The highest responding blades participate in modes with natural frequencies near but slightly lower than the tuned system's rND mode. However, this trend is not clear in Figs. 6.5.e and 6.5.f, making it very difficult to decide at which excitation frequency the engine should be tested under higher EO excitations. This question is further addressed in the next section.

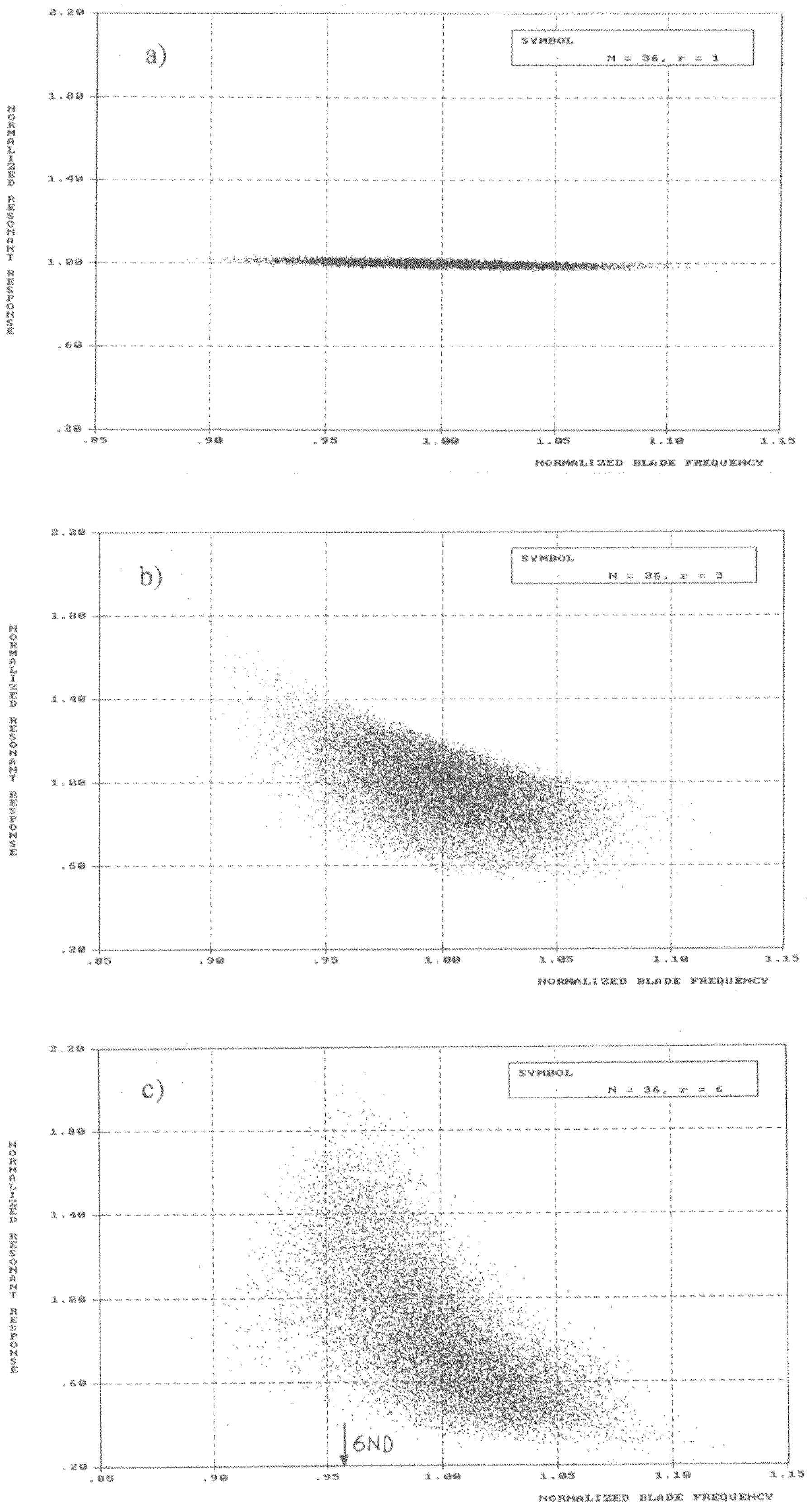


**Fig. 6.4** continued...

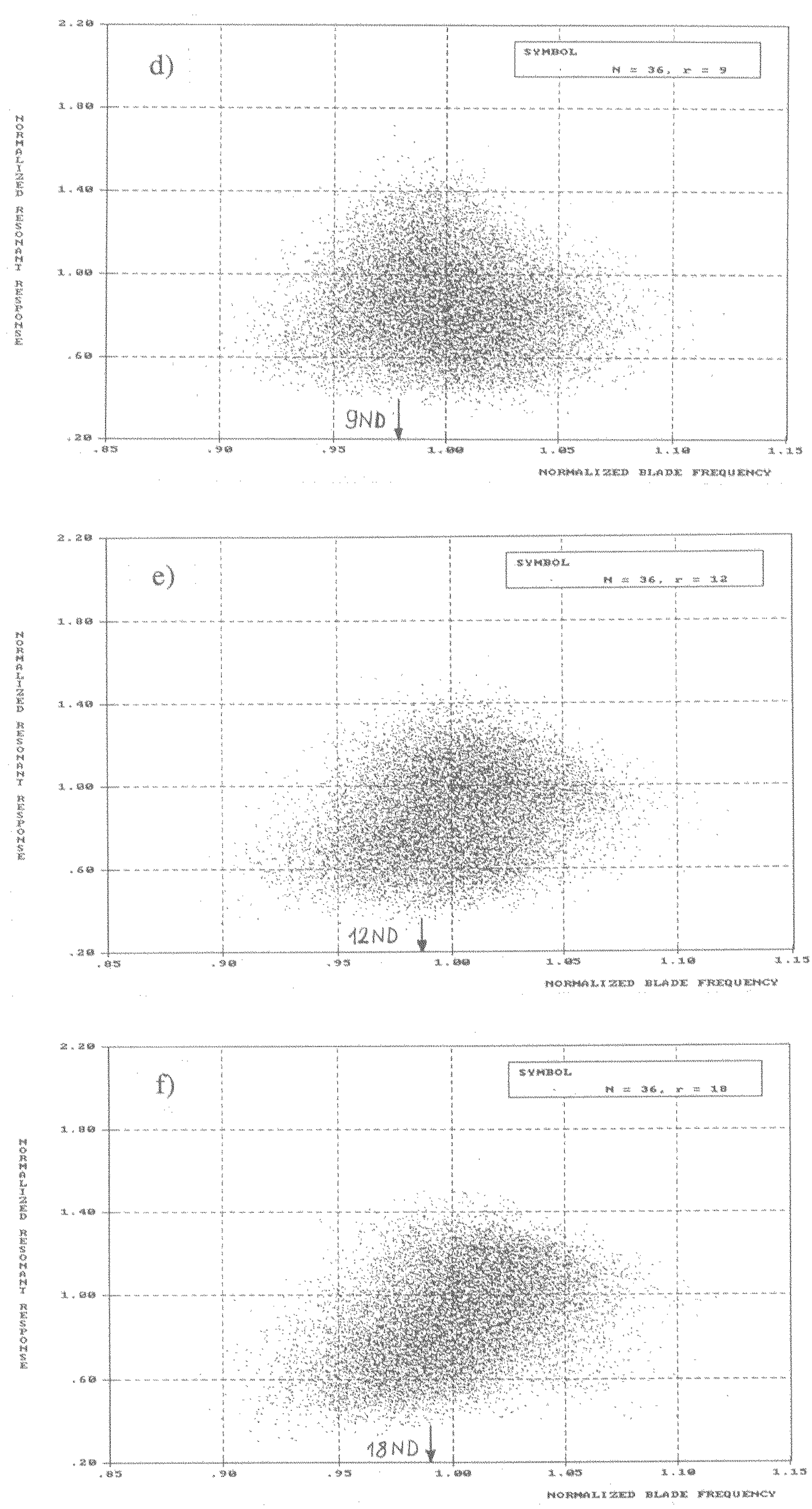


**Fig. 6.4** Resonant response versus blade frequency for various EO excitations.

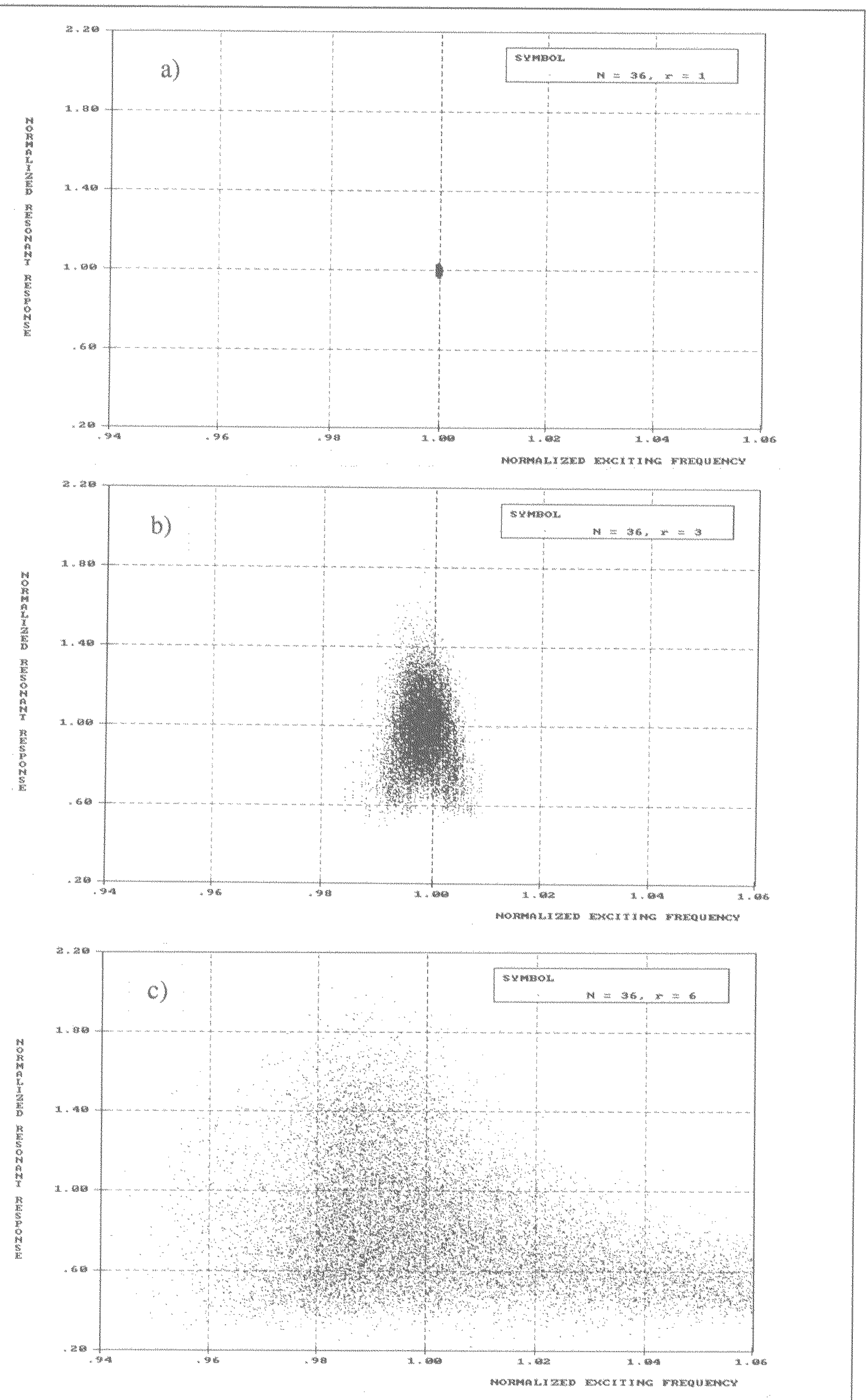


**Fig. 6.5** continued...

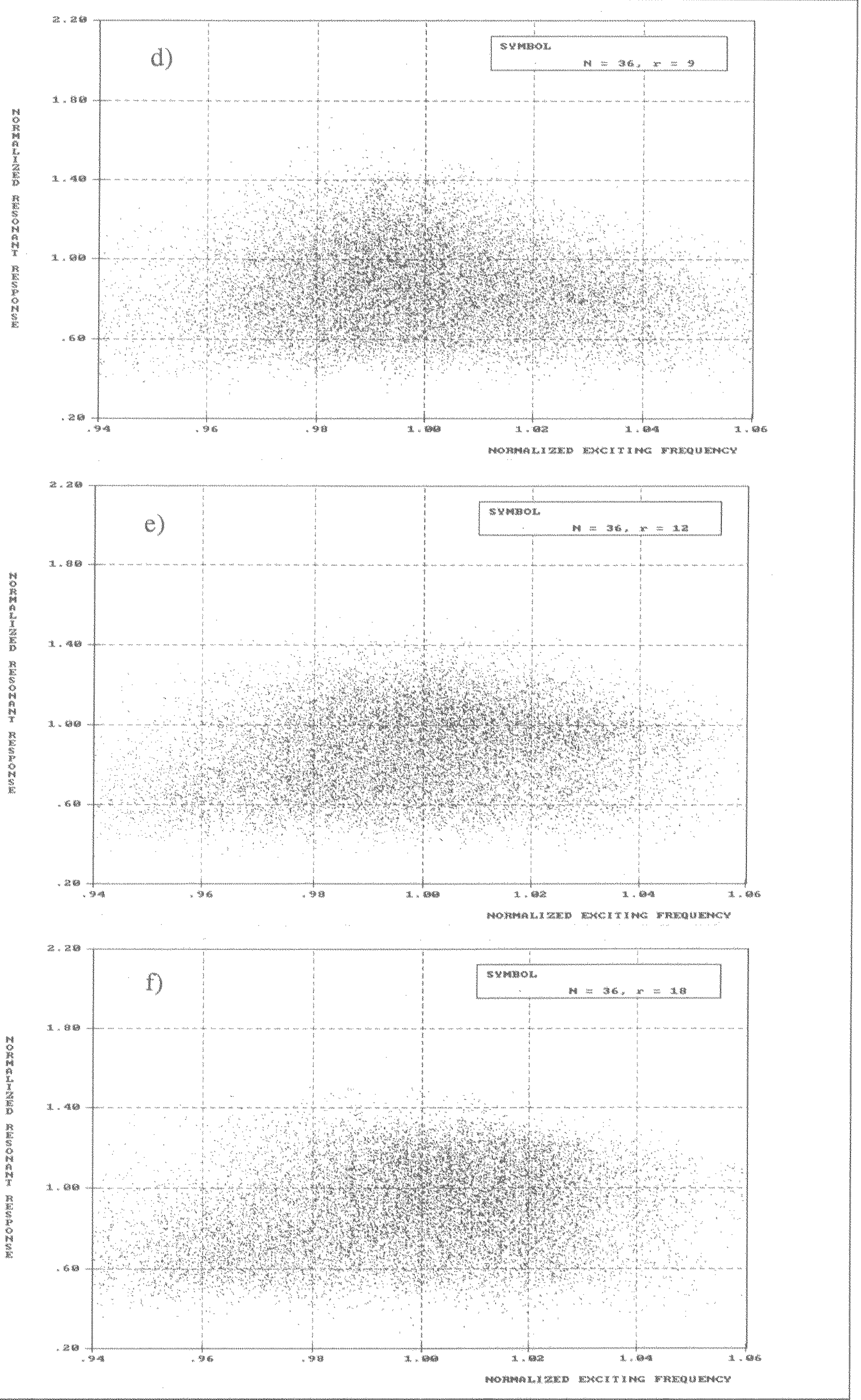


**Fig. 6.5** Resonant response versus excitation frequency for various EO excitations.

### 6.5.3 Critical Blade and Critical Excitation Frequency

Results presented in Figs. 6.4 and 6.5 help us to visualize the statistical characteristics of mistuned bladed discs when the mistuning pattern is random. In addition, one can also detect the blades with the highest responses together with the corresponding excitation frequencies. However, this information is not very useful for practical engine tests unless hundreds of bladed discs are to be tested: an extremely costly and hence very unlikely prospect.

It was thought that more could be learned about the critical blades if the properties of the 700 maximum-response blades (i.e. one per assembly) were analysed carefully. Several important characteristics of these blades are shown in Fig. 6.6 which is a plot of individual blade frequency versus resonant response for each of the 700 critical blades for various EO excitations. The first and very obvious result is that mistuning always increases the maximum resonant response levels from those experienced by a tuned system. The second feature is that every point in Fig. 6.6 represents a critical blade and the distribution of these points with respect to the blade frequency axis shows that there is no general rule for identifying the critical blade(s) according to their cantilever frequencies alone: almost any blade can become the critical blade, depending on the EO of the excitation and the specific distribution of blades around the disc. This explains why different blades have been identified as *critical* by different authors [**El-Bayoumy** and **Srinivasan** (1975), **Ewins** and **Han** (1984) **Afolabi** (1985a)]. The present results show that seemingly conflicting conclusions drawn by other researchers concerning the identification of the critical blade, and the degree of worsening caused by mistuning, are in fact conclusions derived from studying *specific* mistuning patterns under *specific* EO excitations. The third and final observation is that there is a group of blades (according to their cantilever frequencies) which are more prone to bear the maximum response and this range depends on the EO of the excitation. For instance, it is appropriate to monitor blades whose cantilever frequencies are, in round numbers,

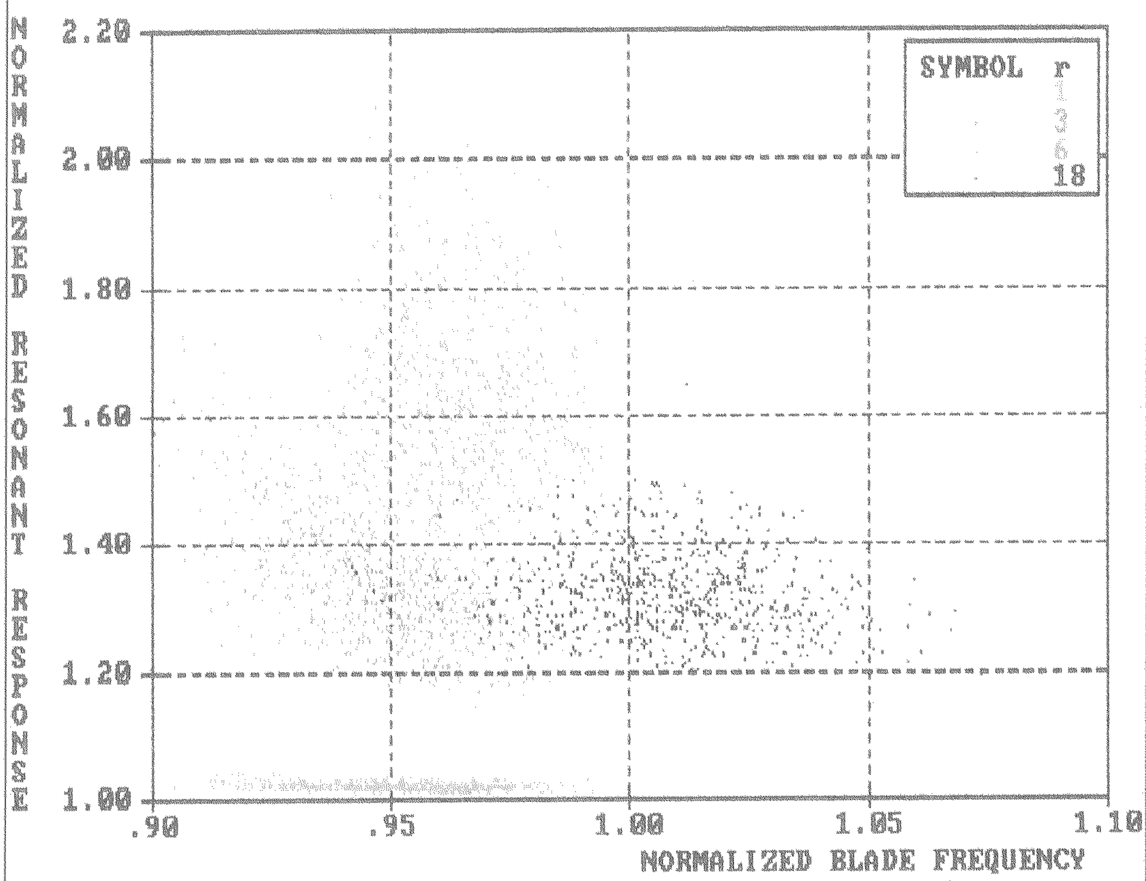


**Fig. 6.6** Resonant response versus blade frequency for 700 critical blades corresponding to 700 bladed discs simulated. (N=36)

between 90% to 98% of that of the tuned blade when r=3. However, there is no point in instrumenting the same blades if the engine is to be tested under 18 EO excitation. This time, blades with frequencies between 97% to 105% of that of tuned blades must be instrumented.

A better estimate of the critical excitation frequency can be derived from Fig. 6.7 which shows the correlation between the maximum response amplitude of each critical blade and the excitation frequency at which that maximum occurs for different EO excitation, the excitation frequency being normalized to the rND natural frequency of the tuned system. Another observation which can be made from Fig. 6.7 is that, even for a constant EO excitation, the excitation frequency at which the critical blade reaches

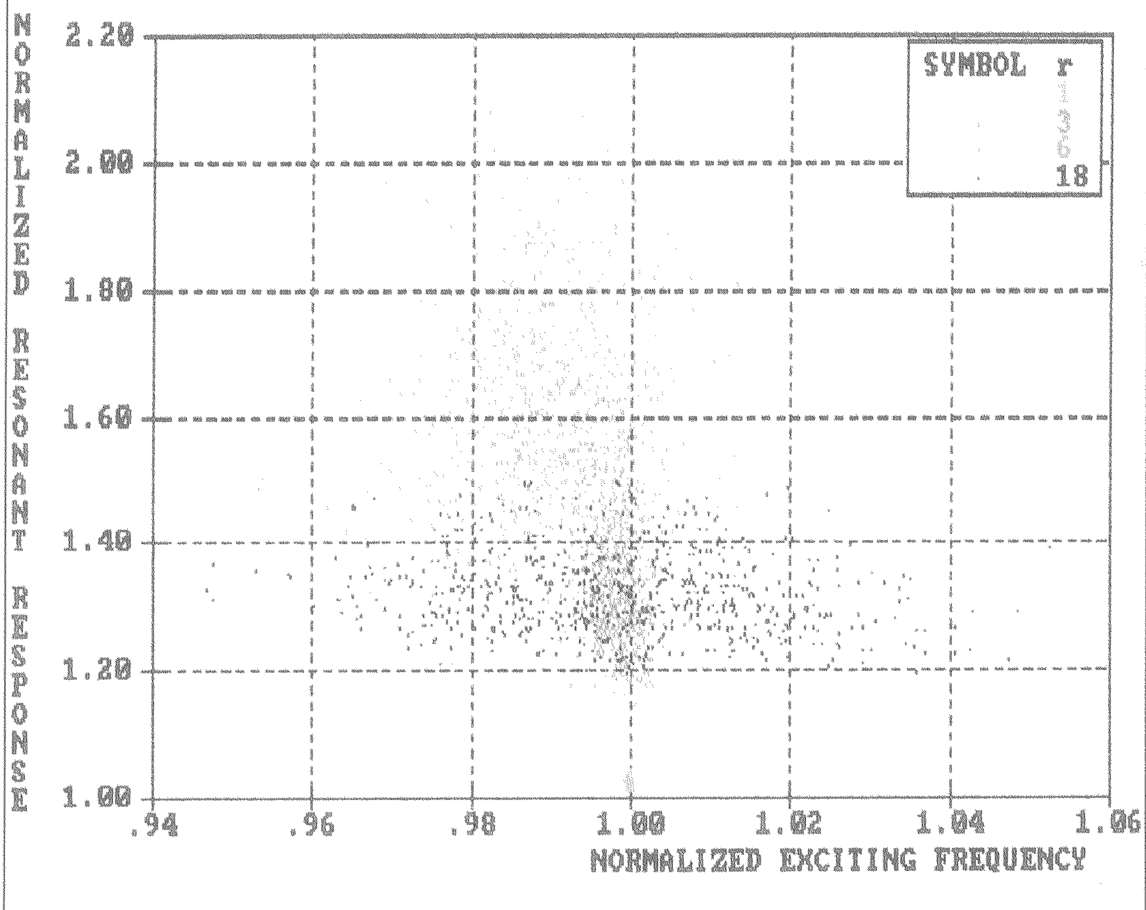


**Fig. 6.7** Resonant response versus excitation frequency for 700 critical blades corresponding to 700 bladed discs simulated. (N=36)

resonance changes from disc to disc. However, it is possible to determine the frequency range which must be considered for maximum response. This frequency range gets wider as the EO increases and its centre frequency is slightly lower than the rND natural frequency of the tuned system.

Many of the characteristics of the critical blade and the critical excitation frequency can be conveniently summarized by Fig. 6.8 where an excellent correlation between excitation frequency and critical blade can be observed for various EO excitations.

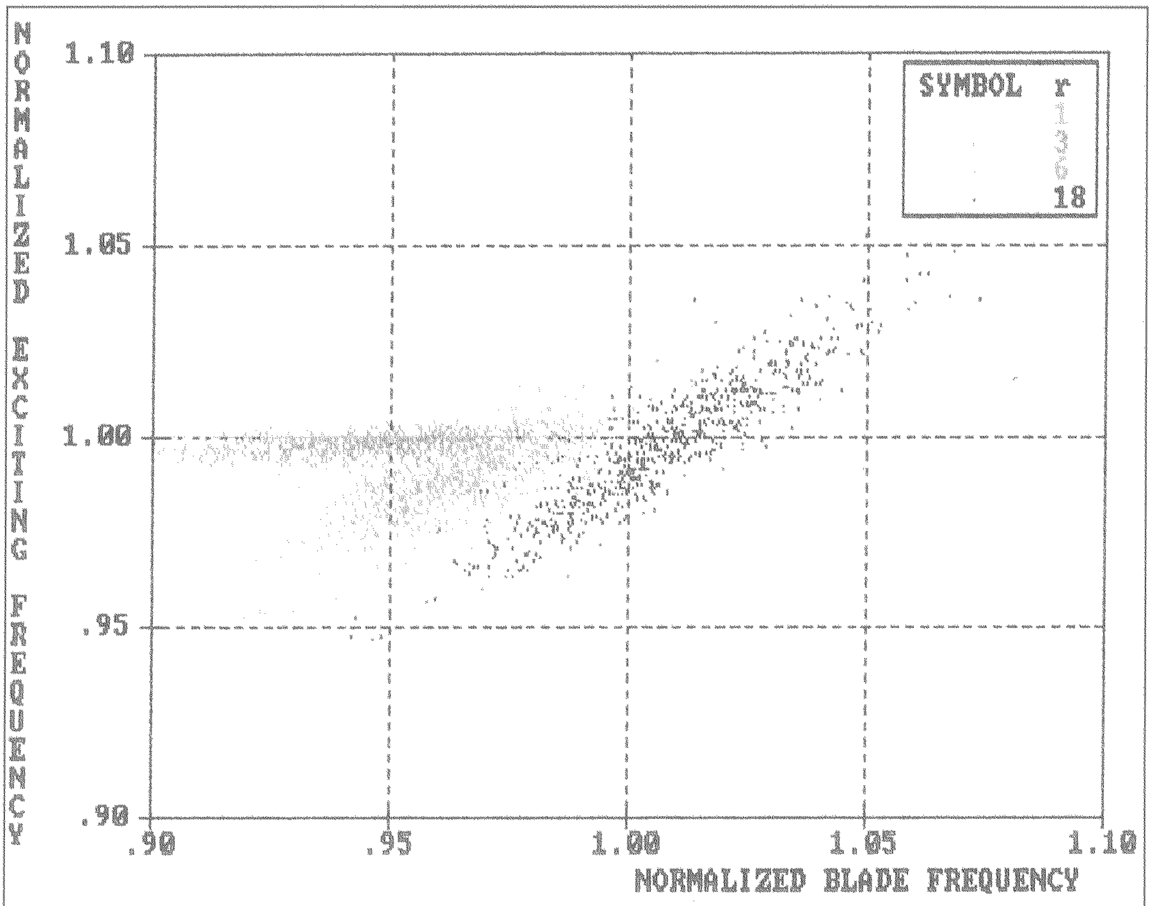


**Fig. 6.8** Excitation frequency versus blade frequency for 700 critical blades corresponding to 700 bladed discs simulated. (N=36)

### 6.5.4 Probability and Cumulative Density Functions of Resonant Response

Probability and cumulative density functions (pdf and cdf respectively) are very important parameters in describing the statistical properties of a population. For our particular problem, the cdf of resonant responses of mistuned blades can readily be used to find the probability of the resonant response exceeding a certain value. The pdf, on the other hand, is very useful for presenting the statistical distribution of resonant responses.

25,000 resonant response data points under various EO excitation conditions were used to calculate the probability and cumulative density functions (pdf, cdf) of the resonant response and the results are presented in Figs. 6.9.a to 6.9.d. An inspection of the pdfs and cdfs in Figs. 6.9.a to 6.9.d reveals that there is no unique distribution which can describe the statistical characteristics of resonant responses under every EO excitation when the blades are randomly mistuned. Each pdf or cdf curve shown is different from the others, a result which implies that any assumption about the pdf of resonant responses without taking the excitation EO into consideration cannot represent the real distribution for the practical engineering cases.

Another important point is that none of the calculated distributions is Gaussian. (This can be seen from the general shape of the pdf, or from the cdf which would be a straight line if the distribution was normal.) The true and the corresponding normal distributions which have the same mean and standard deviation are plotted together in Figs. 6.10.a and 6.10.b for two different EO excitations. This finding has important implications for those approaches which are based on the assumption that the response distribution is normal [**Sinha** (1986), **Sinha** and **Chen** (1989)]. It is important to emphasize that the mean and the standard deviation used in plotting the normal distribution were the *true* values found from our numerical simulation. If they had been calculated by presuming that the distribution was normal, the discrepancy would have been more pronounced.

The pdf of the resonant response under 6EO excitation and the pdf of blade frequency are presented in Fig. 6.11. These clearly show that small variations in blade frequencies cause big scatter in resonant response levels.

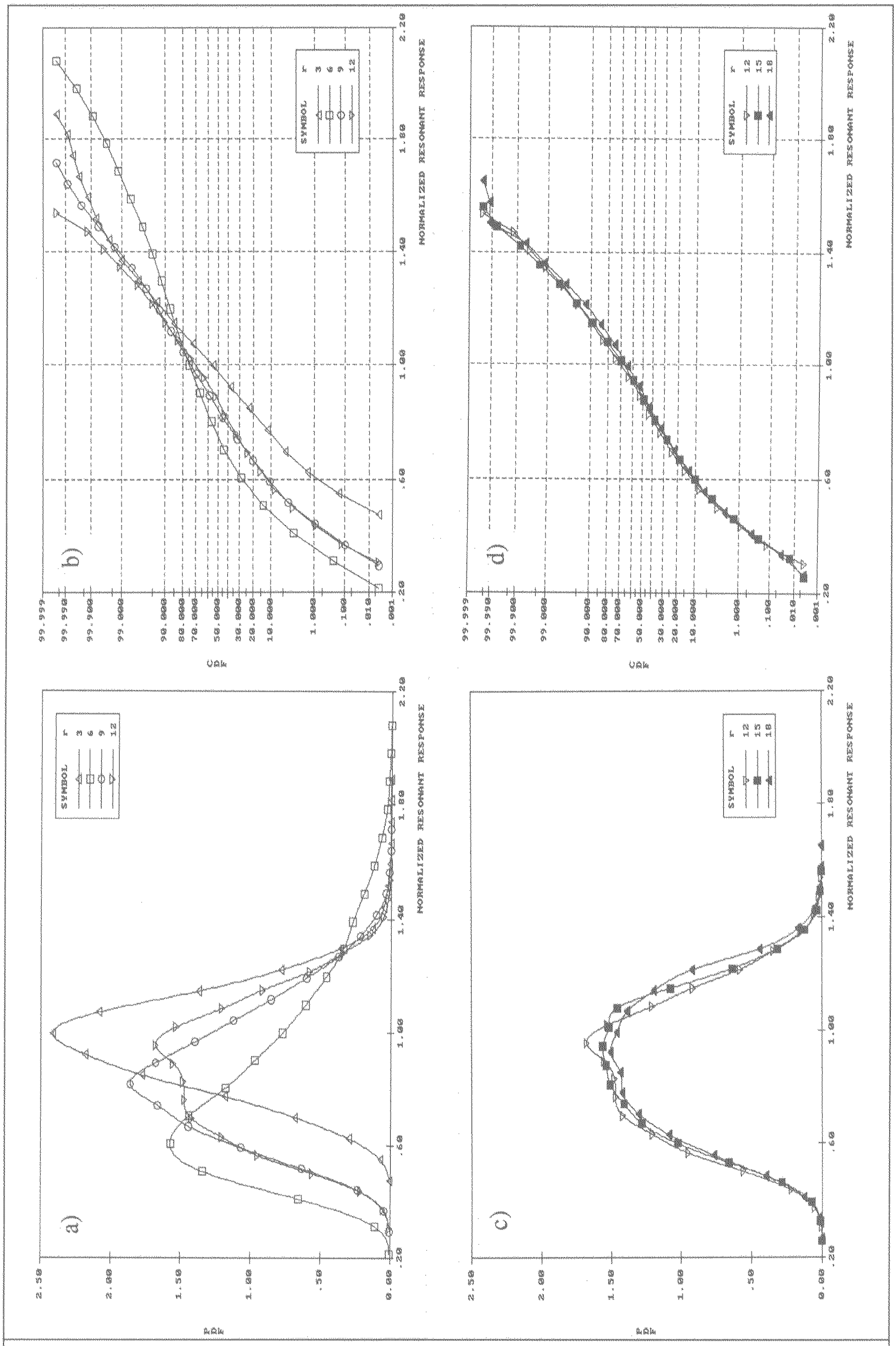


**Fig. 6.9** Probability and cumulative density functions of resonant response for various EO excitations.

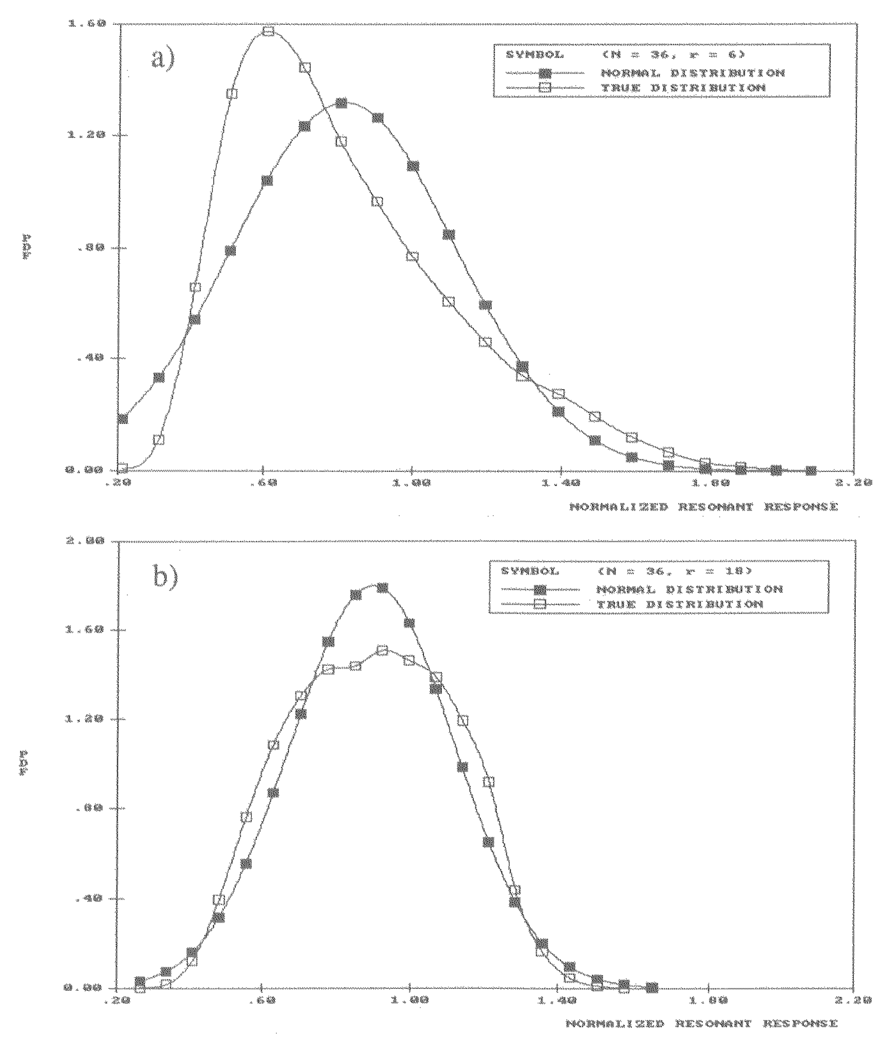


**Fig. 6.10** Probability density function of resonant response and normal distribution.

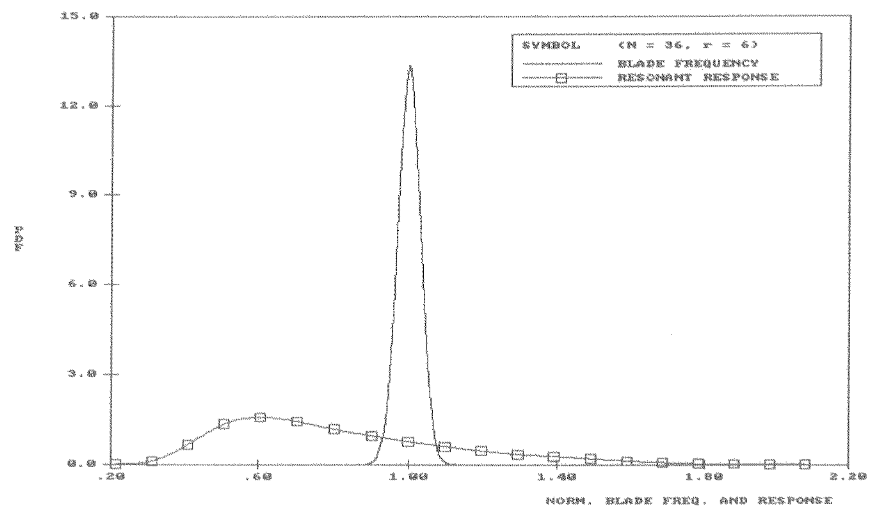


**Fig. 6.11** Probability density function of blade frequency and resonant response.

## 6.6 Effects of Blade Number and Engine Order of Excitation

Previous studies have traditionally been focussed on bladed discs with small numbers of blades without any justification that results found from such studies would reflect the behaviour of discs with larger blade numbers. Some researchers concluded that the effect of mistuning depended on the number of blades on the disc. "*...discs with a large number of blades can respond in quite a different way than those with only a few blades and that their behaviour cannot be simply inferred by studying the smaller systems....*" **Basu** and **Griffin** [1986]. However, our findings so far suggest that the underlying parameter for the forced vibration characteristics of bladed discs is the interblade phase angle of the forcing ($\theta_r = 2\pi r/N$) rather than the engine order of excitation (r) or the number of blades (N) individually. It was shown in chapter 2 that $\theta_r$ was sufficient to describe the *state* of the response levels for tuned bladed discs. Results presented in chapter 3 confirmed that this approach was also valid for alternate and single-blade mistuning cases. Therefore, it is now proposed to test the applicability of this finding for the general case of randomly mistuned assemblies.

First, it was decided to repeat the analysis made earlier for the 36-bladed disc for an *equivalent* (constant interblade phase angle)12-bladed disc in order to find if it was possible to obtain similar results by studying a smaller system. As before, resonant responses were calculated for 25000 blades and hence 2100 12-bladed discs were considered. Results are presented in Figs. 6.12.a to 6.12.d for various EO excitations (r=1,2,3 and 6). A close inspection of these figures reveals that the observed trends are very similar to those presented in Figs. 6.4.b, 6.4.c, 6.4.d and 6.4.f respectively. This is perhaps not surprising since the same EO excitation to blade number ratio was employed in both sets of figures. This ratio is simply the interblade phase angle $\theta_r$ multiplied by a constant. If we now turn our attention to the correlation between resonant response levels and excitation frequency, we also find very similar trends for the 36- and 12-bladed discs: results in Fig. 6.5 and 6.13 are once again unified by a common interblade phase angle. Discs with large numbers of blades seem to respond in a way very similar to those with fewer blades for the same interblade phase angle.

Further cases exemplifying the relationship between resonant response and blade frequency are presented in Figs 6.14.a to 6.14.d for discs with different numbers of blades (N=18,30,48,72) but all where $\theta_r = 60^o$. The corresponding probability density functions of the resonant responses are shown in Fig. 6.15 for each case. It is clear that very similar results are obtained for discs with different numbers of blades when $\theta_r$ is kept constant. It is pleasing to note that all the results showing the correlation between resonant response and blade frequency when $\theta_r = 60^o$ are very similar to Fig. 3 of **Griffin** and **Hoosac** (1984) for 72-bladed disc under 5EO (this corresponds to $\theta_r = 25^o$). This difference is believed to be due to different blade to disc coupling ratio used in the modelling of the bladed disc.

It is worth noting that **Basu** and **Griffin** (1986) reached the contradictory conclusion (i.e. the behaviour of discs with a large numbers of blades cannot be inferred by studying the smaller systems) by studying the effect of the number of blades only ( and hence keeping the EO excitation constant). However, if their results are inspected in terms of the interblade phase angle, the discrepancies disappear: it is seen that they are in complete agreement with the findings of the present work. Their results indicate that increasing the number of blades (N) has a similar effect to decreasing the EO of excitation (r). From the definition of the interblade phase angle ($\theta_r = 2\pi r/N$), it is immediately seen that both changes have the same effect of decreasing the interblade phase angle.

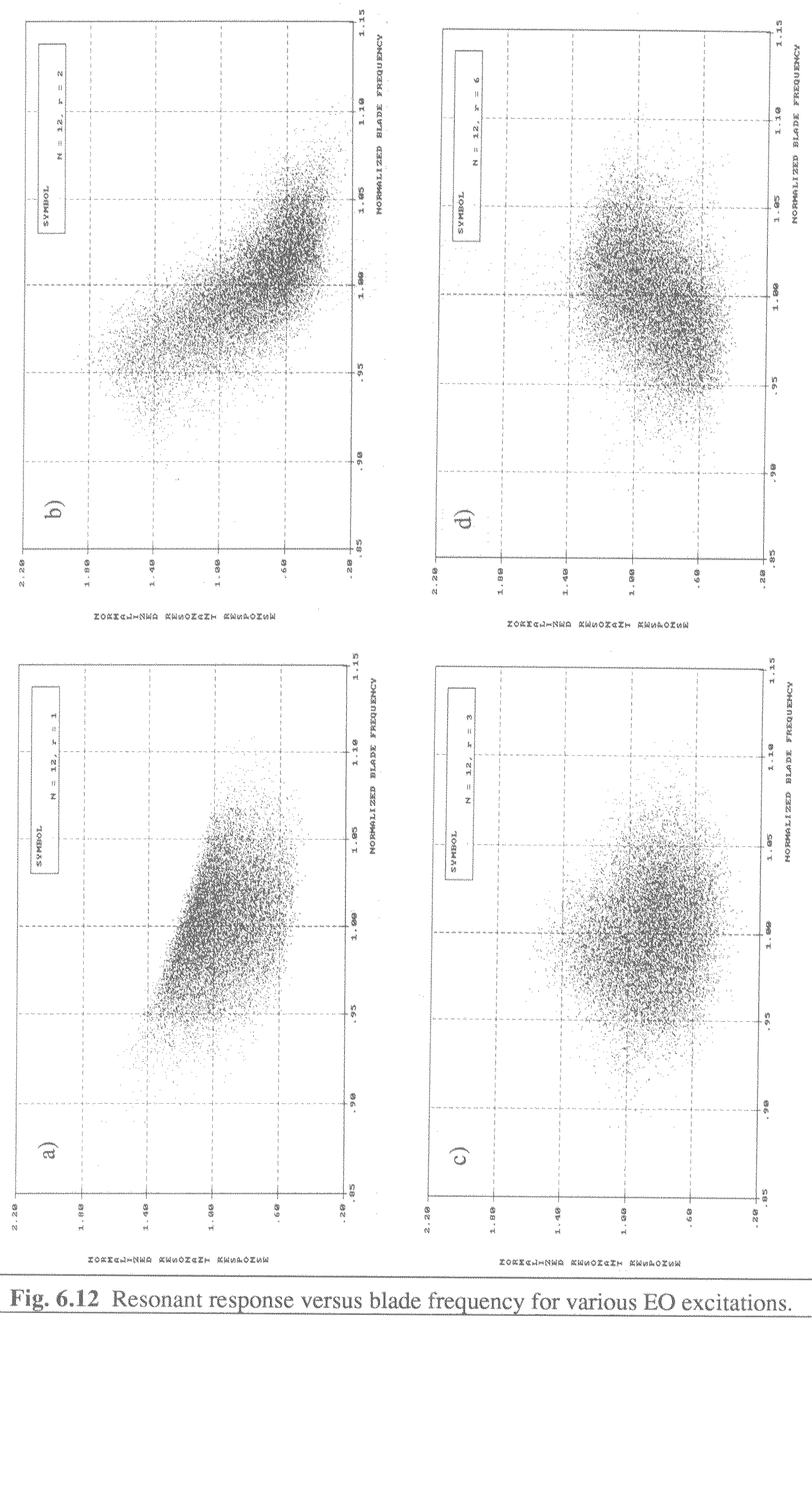


**Fig. 6.12** Resonant response versus blade frequency for various EO excitations.

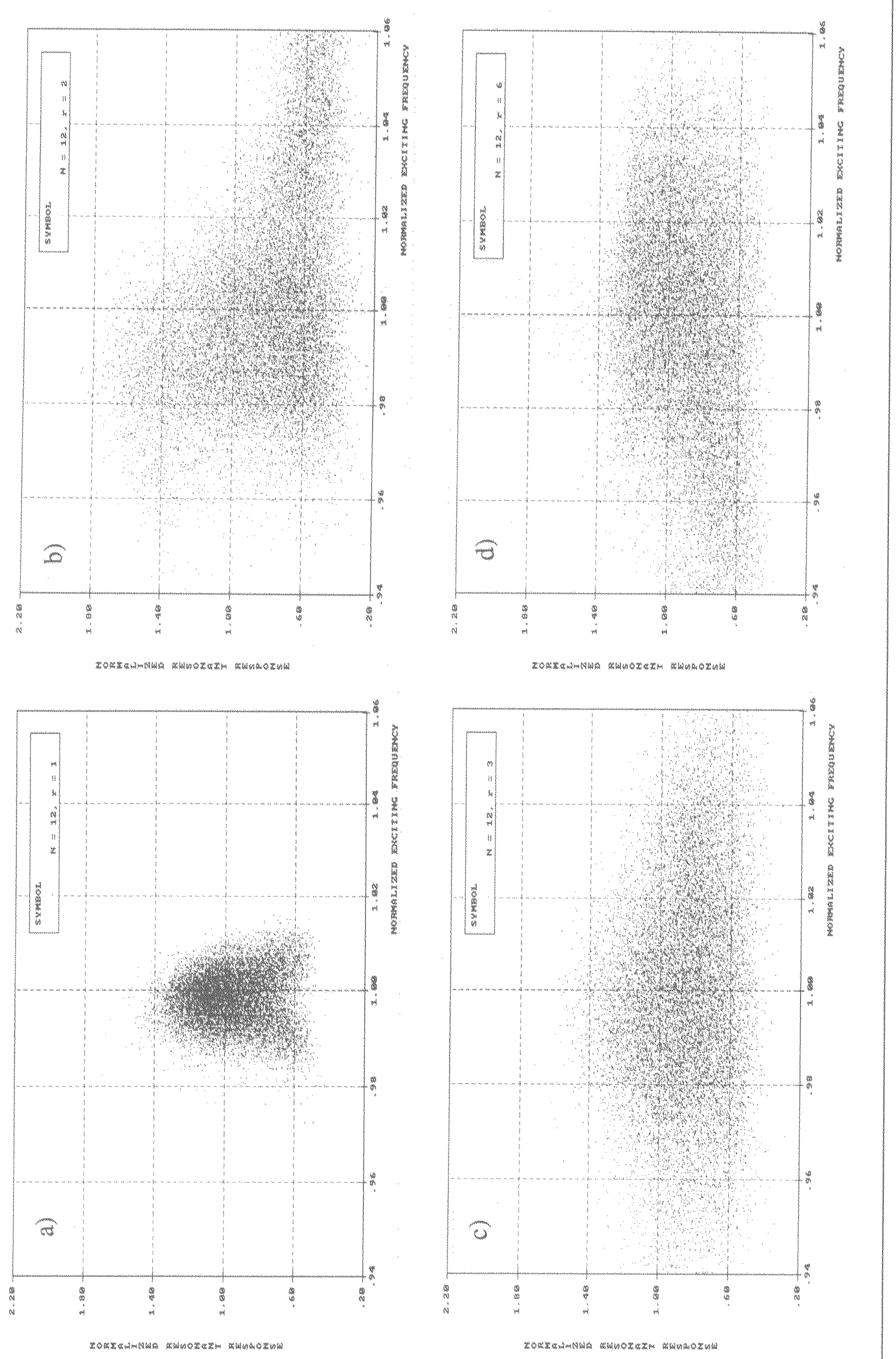


**Fig. 6.13** Resonant response versus excitation frequency for various EO excitations.

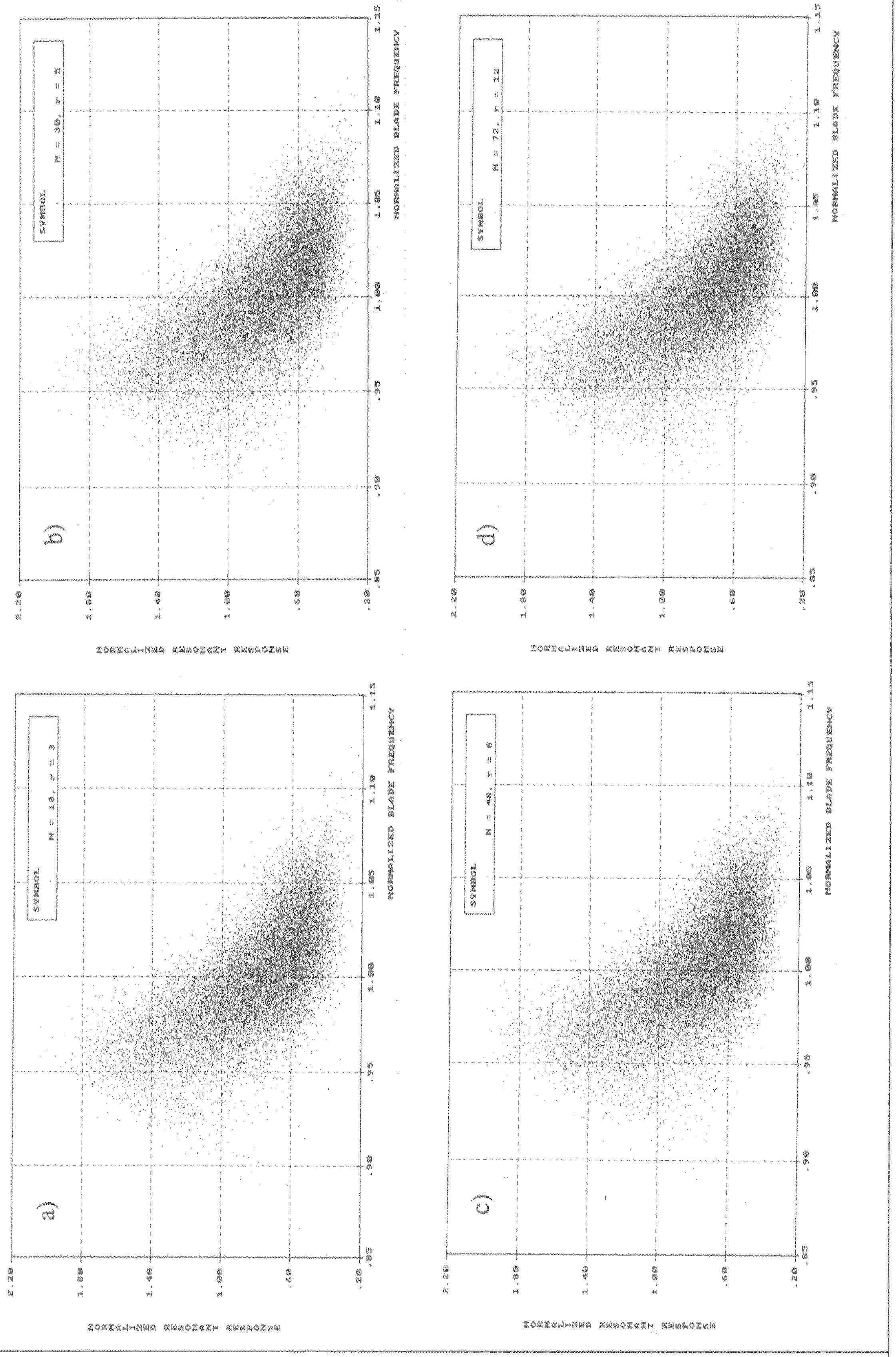


**Fig. 6.14** Resonant response versus blade frequency for a constant interblade phase angle ($\theta_r = 60^o$).

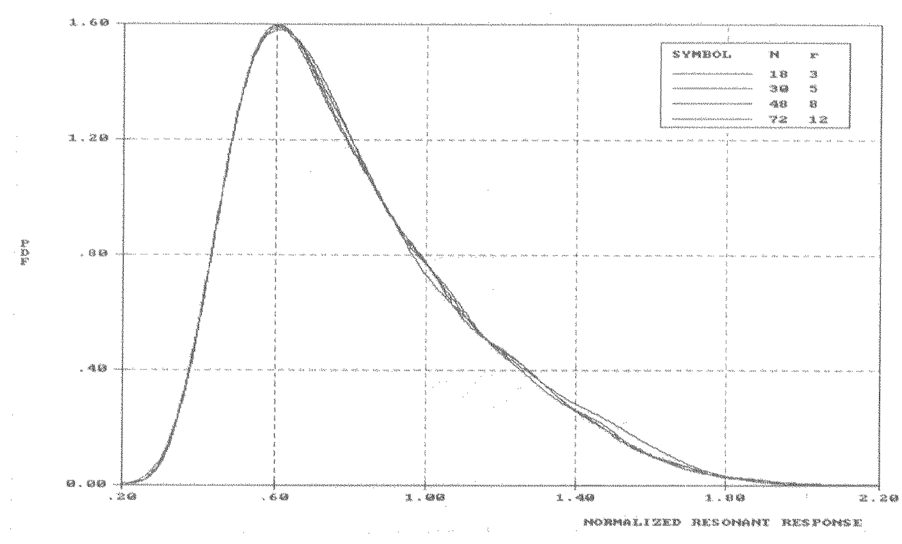


**Fig. 6.15** Probability density function of resonant response for a constant interblade phase angle($\theta_r$=60°).

## 6.7 Effects of Alternate Mistuning

As mentioned in chapter 3, a significant degree of alternate mistuning may already exist in bladed disc assemblies, probably due to dynamic balancing considerations. This type of mistuning was also found to be beneficial from an aeroelastic stability point of view [**Imregun** (1984)]. Therefore, a statistical investigation of the alternate mistuning pattern was considered appropriate.

Unlike the alternate mistuning simulation made by **Griffin** and **Hoosac** (1984), where low- and high-frequency blades were drawn from two distinct populations with different mean frequencies, the Gaussian-distributed blade population was assumed to be divided into two groups. Alternate mistuning was simulated by selecting low- and high-frequency blades alternately from the same blade population. A blade was considered to be low-frequency if its cantilever frequency was less than the mean value and vice-versa. Note that this does not require two separate stores for blades. The effects of such mistuning are summarised in Figs. 6.16.a to 6.16.c where the resonant

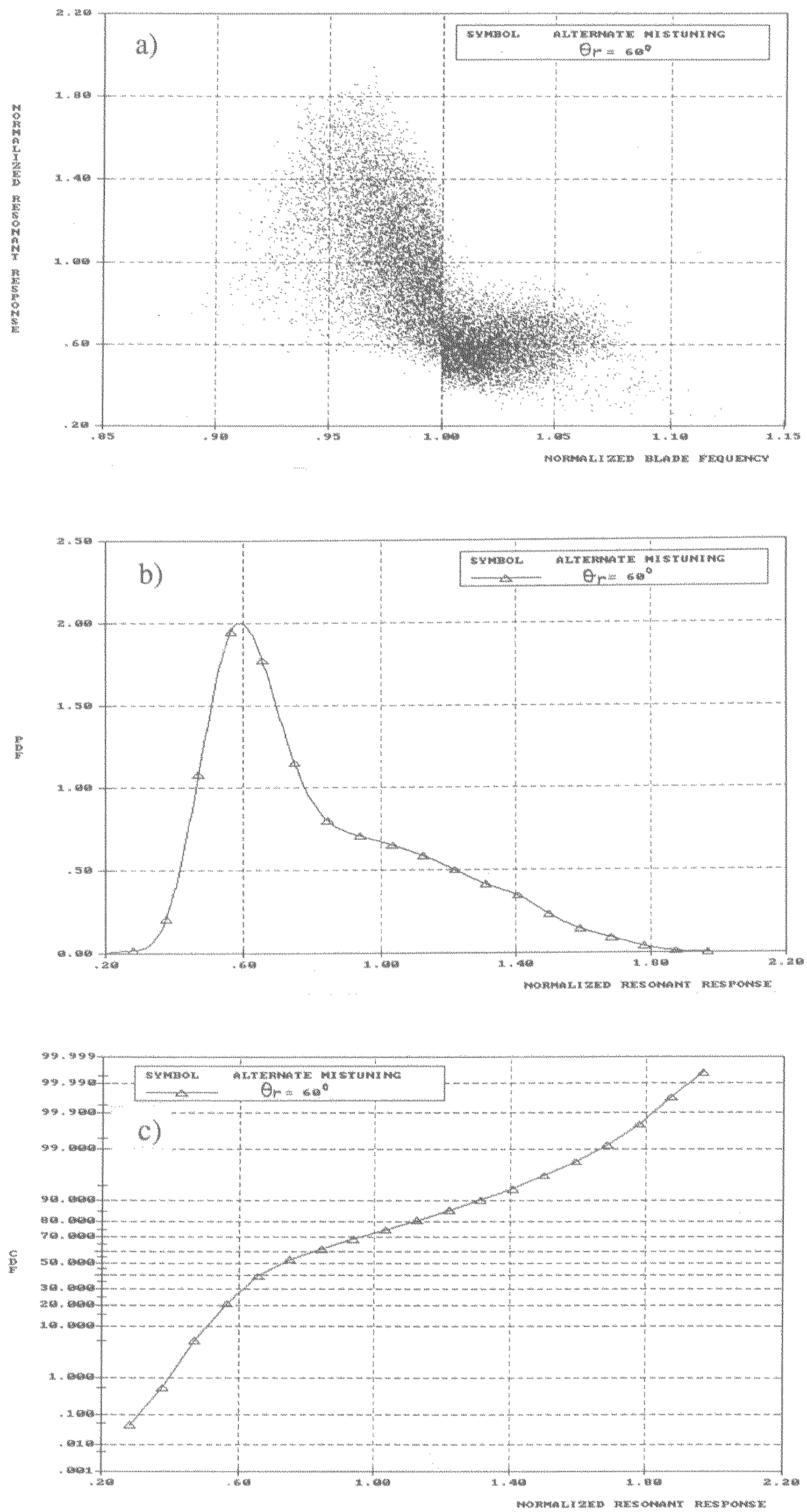


**Fig. 6.16** Resonant response versus blade frequency, pdf and cdf for alternate mistuning case.

response levels versus blade natural frequency and the corresponding probability and cumulative density functions are given for the case of $\theta_r = 60^o$. A comparison of Figs. 6.16.a and 6.14 reveals that there is a slight decrease in the resonant response.

## 6.8 Concluding Remarks

i) It has been found that the vibration response characteristics of a randomly mistuned bladed disc change with the engine order of excitation (r). When r is small, the worsening effect of mistuning seems to be small. At some intermediate values of r the worsening effect reaches a maximum and tends to decrease again as r increases further. The critical value of r seems to be dependent on blade to disc coupling and this observation warrants further investigation.

ii) The blade experiencing the highest response among N blades on a disc was determined for every individual assembly. An investigation of the properties of these critical blades showed that there were no general rules for identifying them according to blade cantilever frequency alone: the critical blade can be any blade depending on the EO of excitation. This explains why many apparently-conflicting conclusions were reached in previous studies In the light of the findings presented in this chapter they can be reconciled.

iii) A very good linear correlation has been found between the blades experiencing the maximum amplitude on every single disc and the excitation frequencies at which these blades will vibrate strongly. Such information can be used in deciding which blades to instrument and at which excitation frequency to test them. Results suggest that there is a range of critical blades classified according to their cantilever frequencies and as many blades as possible within this range should be instrumented in a practical engine test. This range depends on the EO of excitation and it also includes those blades with cantilever frequencies equal to the rND tuned system natural frequency. However, this rND frequency is not necessarily the mean of that blade frequency range requiring instrumentation.

iv) The resonant response increase over that of tuned system is the most commonly used parameter to measure the worsening effect of mistuning and conflicting conclusions on this value have been reached by several authors. These differences were usually attributed to the different models used in the various studies. However, for the same amount of mistuning and using the same model, it has been demonstrated that the magnitude of the worsening effect can vary from an increase of less than 5% to over 110% since this effect depends very strongly on the EO of the excitation.

v) The probability and the cumulative density functions of the resonant response show that the response distribution is not normal and that the overall shape of the distribution changes with the EO of the excitation.

vi) As for the tuned bladed disc, and for the alternate and single blade mistuning cases, a simple parameter, interblade phase angle, is of paramount importance to study the response characteristics of randomly mistuned bladed discs. The dynamic behaviour of discs with a large number of blades can be predicted by studying smaller systems with fewer blades and this offers huge savings in computation time.

vii) Alternate mistuning was simulated by selecting low- and high-frequency blades alternately from the same blade population. Results suggest that such mistuning may decrease resonant response slightly when compared with that of random mistuning.

# CHAPTER 7

# STATISTICAL ANALYSIS OF RANDOM MISTUNING: AN INVERSE APPROACH

**About This Chapter**

*So far, all mistuning analyses have focused on bladed discs with predetermined configurations and sought answers to the question "what is the A% response increase of a mistuned system for B% mistuning?" However, the question which needs to be addressed is: "what degree of blade-to-blade variation is acceptable if only A% response increase with respect to the tuned system response (design value) is allowable?" Although the statistical analysis presented in the previous chapter can be used to answer that question indirectly, such studies are expensive and are not practical since they are based on trial-and-error. An alternative approach is required which can solve the above-formulated inverse problem to predict the relationship between the allowable response increase and the amount of mistuning due to manufacturing tolerances. This chapter is devoted to this purpose.*

## 7.1 Introduction

One of the basic problems in vibration analysis is the determination of natural frequencies, mode shapes and response amplitudes of a *known* structure. A different class of problems, the so-called inverse problems, are concerned with the construction of a mathematical model for specified eigenvalues and eigenvectors [**Gladwell** (1986)]. In the context of this investigation, inverse problems are concerned with the determination of structural parameters which can satisfy specified responses (design values) under known excitation conditions.

A particular problem which is of considerable importance to the turbomachinery industry is the determination of acceptable manufacturing tolerances for an A% allowable increase in resonant response from that of the tuned system. The current determination of these tolerances is usually based on past experience rather than on engineering analysis. Although a statistical analysis based on the direct approach presented in the previous chapter can be used for this purpose, such a procedure can be very expensive and lengthy since it requires searching for the required tolerances by a trial-and-error approach. (The resonant response increase caused by a certain degree of mistuning needs to be calculated and, if found unacceptable, another solution must be sought for a different degree of mistuning.) Therefore, what is required is a method which is able to predict the permissible scatter in the blade cantilever frequencies for an allowable response increase due to mistuning.

Such a method has been developed and is presented in this chapter for predicting the permissible variations in blade-alone cantilever frequencies when response levels are prescribed. The responses were specified randomly within the acceptable limits and the corresponding distribution of blade cantilever frequencies was determined for many bladed disc assemblies. The allowable manufacturing tolerances were then estimated from the scatter of blade cantilever frequencies obtained in the case of hundreds of bladed discs.

It is believed that the method developed can be applied to the determination of physical parameters such as mass, stiffness and damping elements in any structural model if the response levels are given or known at a sufficient number of coordinates and when the harmonic forces applied to the structure are known.

## 7.2 Theoretical Background

The theory presented in this section deals with the determination of the unknown structural parameters when responses to known excitations are specified at a number of coordinates. The basic theory is also extended to find the blade cantilever frequencies when the magnitudes of the blade response levels are known.

### 7.2.1 Basic Theory

Consider a general mechanical system with m degrees of freedom and u unknown structural parameters. The equations of motion can be written as:

$$([K+iD] - \omega^2 [M] + i\omega [C])_{mxm} \{\hat{q}\}_{mx1} - \{\hat{f}\}_{mx1} = \{0\} \qquad (7.1.a)$$

where all symbols have their customary meanings. The matrix equation given above can be decomposed into real and imaginary parts, thus giving 2m real equations. Furthermore, one can write these 2m real equations explicitly at s excitation frequencies which gives $n = 2sm$ functional relations to set to zero for v unknowns ($\gamma_j$, j=1, 2, ..., v) as:

$$g_i (\gamma_1, \gamma_2, \gamma_3, ..., \gamma_v) = 0 \qquad i = 1, 2, 3, ..., n \qquad (7.1.b)$$

where

| | |
|---|---|
| $g$ | = is a known function of $\gamma_1, \gamma_2, \gamma_3, \ldots, \gamma_v$ |
| $\gamma_1, \gamma_2, \gamma_3, \ldots, \gamma_v$ | = are unknown structural parameters and unknown response levels |
| $v$ | = is the total number of unknowns (unknown structural parameters (u) plus unknown response levels (n) i.e., v=u+n) |

If some (u) of the structural parameters are unknown, n functional relations obtained from the equations of motion cannot be solved without further information since the number of unknowns is greater than the number of equations (v>n). However, if the real and imaginary parts of the response levels are known at w coordinates and at s excitation frequencies, where w<m and 2sw>u, then the problem will be over-determined, (n>v=u+2s(m-w)), and a solution can be obtained for the u unknown structural parameters and the 2s(m-w) unknown response levels.

The unknowns ($\gamma_j$, j=1, 2, ..., v) in the above functional relations can be solved iteratively using the Newton-Raphson Method [**Press et al**. (1986)] which converges very rapidly to a root if there is one, or diverges totally, indicating that no root exists in the vicinity of the search. Let vector $\{\gamma\}$ contain the initial estimates of unknowns $\gamma_j$. Each of the functions $g_i$ can then be expanded in a Taylor series in the neighbourhood of vector $\{\gamma\}$ as:

$$g_i(\{\gamma\} + \{\delta\gamma\}) = g_i(\{\gamma\}) + \sum_{j=1}^{v} \frac{\partial g_i}{\partial \gamma_j} \delta\gamma_j + O(\{\delta\gamma\}^2) \tag{7.2}$$

where $\{\delta\gamma\}$ is a correction vector for the initial estimates. By neglecting second- and higher-order terms in Eq. (7.2), a set of linear equations can be obtained for $\{\delta\gamma\}$ which moves all functions closer to zero simultaneously. This can be written in matrix form as:

$$[S]_{n\mathrm{x}v}\,\{\delta\gamma\}_{v\mathrm{x}1} = -\{R\}_{n\mathrm{x}1} \tag{7.3}$$

where

$$[S] = \begin{bmatrix} \frac{\partial g_1}{\partial\gamma_1} & \frac{\partial g_1}{\partial\gamma_2} & \frac{\partial g_1}{\partial\gamma_3} & \cdot & \cdot & \cdot & \frac{\partial g_1}{\partial\gamma_v} \\ \frac{\partial g_2}{\partial\gamma_1} & \frac{\partial g_2}{\partial\gamma_2} & \frac{\partial g_2}{\partial\gamma_3} & \cdot & \cdot & \cdot & \frac{\partial g_2}{\partial\gamma_v} \\ \cdot & \cdot & \cdot & \cdot & \cdot & \cdot & \cdot \\ \cdot & \cdot & \cdot & \cdot & \cdot & \cdot & \cdot \\ \frac{\partial g_n}{\partial\gamma_1} & \frac{\partial g_n}{\partial\gamma_2} & \frac{\partial g_n}{\partial\gamma_3} & \cdot & \cdot & \cdot & \frac{\partial g_n}{\partial\gamma_v} \end{bmatrix}; \quad \{\delta\gamma\} = \begin{Bmatrix} \delta\gamma_1 \\ \delta\gamma_2 \\ \delta\gamma_3 \\ \cdot \\ \cdot \\ \cdot \\ \delta\gamma_v \end{Bmatrix}; \quad \{R\} = \begin{Bmatrix} g_1\{\gamma\} \\ g_2\{\gamma\} \\ \cdot \\ \cdot \\ g_n\{\gamma\} \end{Bmatrix}$$

The matrix [S] and the residual vector {R} are formed using the assumed/corrected values of the unknown vector $\{\gamma\}$ and Eq. (7.3) is solved for $\{\delta\gamma\}$ which is then added to the assumed/corrected solution vector as follows:

$$\{\gamma\}^{new} = \{\gamma\}^{old} + \{\delta\gamma\} \tag{7.4}$$

and this process is repeated until convergence is obtained. (How to obtain [S] will be clearer in the next section since its explicit form for a specific bladed disc problem is given **Appendix** V)

A summary of the proposed method is given in Fig. 7.1.

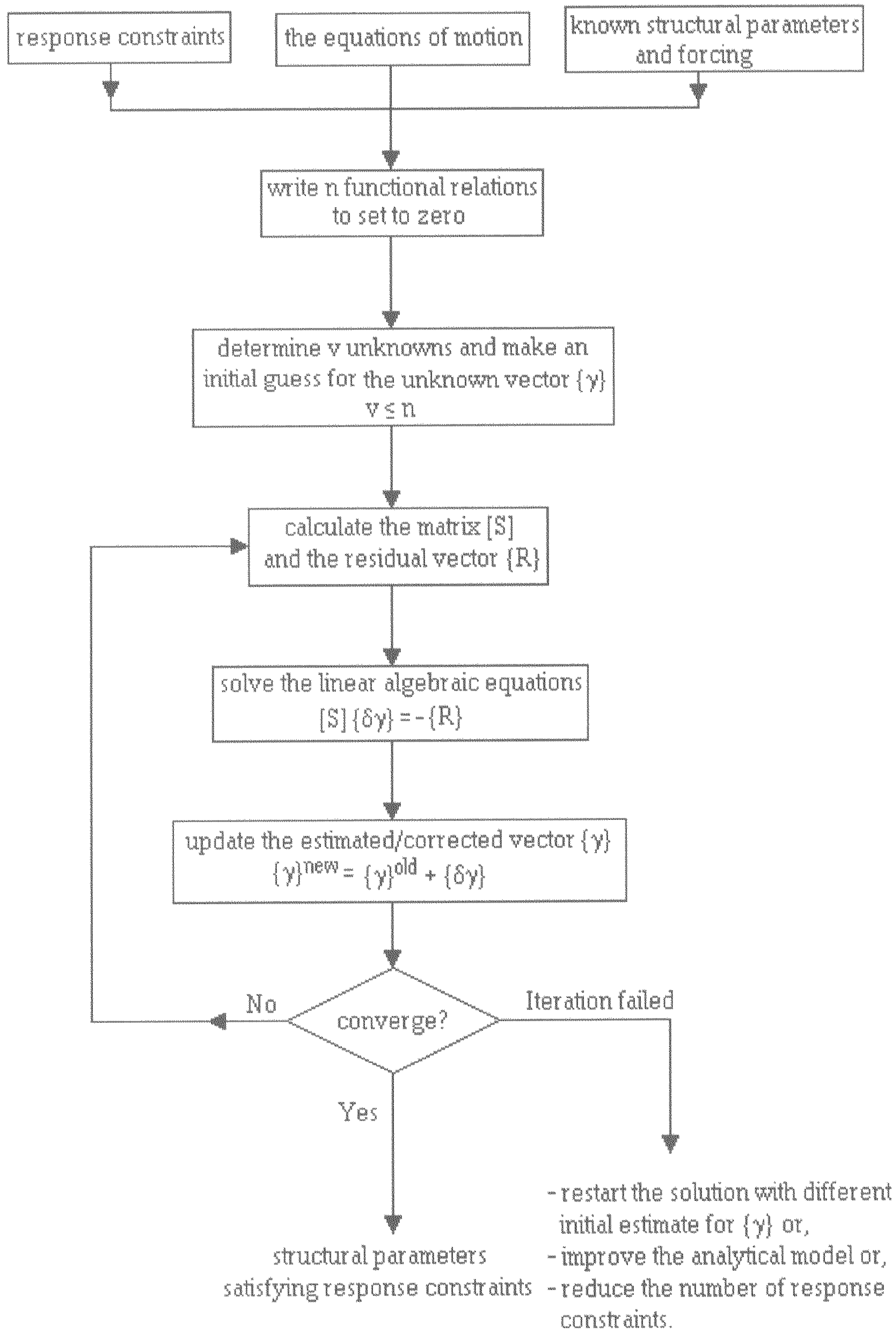


**Fig. 7.1** Flowchart for determination of structural parameters.

### 7.2.2 Determination of a Set of Blade Cantilever Frequencies

The bladed disc model used in chapters 3, 4 and 6 will also be used in the present investigation. Accordingly, the equations of motion for the $j^{th}$ sector are the same as before except that the forcing term representing the engine order (EO) excitation now appears on the left hand side of the equation.

$$\ddot{x}_j + 2\zeta G_j \dot{x}_j + G_j^2 (1+i\eta)(x_j - y_j) - \frac{f_j(t)}{m} = 0 \tag{7.5.a}$$

$$\frac{M_d}{m} \ddot{y}_j + G_j^2 (1+i\eta)(y_j - x_j) + \frac{k_g}{m} y_j + \frac{K_d}{m}(2y_j - y_{j+1} - y_{j-1}) = 0 \tag{7.5.b}$$

Assuming harmonic responses of the form

$$x_j = X_j e^{i(\omega t)} \tag{7.6.a}$$

$$y_j = Y_j e^{i(\omega t)} \tag{7.6.b}$$

and inserting these into the equations of motion gives:

$$-\omega^2 X_j + i\, 2\zeta G_j \omega X_j + G_j^2 (1+i\eta)(X_j - Y_j) - \frac{F_o}{m} e^{i((j-1)\theta_r)} = 0 \tag{7.7.a}$$

$$-\omega^2 \frac{M_d}{m} Y_j + G_j^2 (1+i\eta)(Y_j - X_j) + \frac{k_g}{m} Y_j + \frac{K_d}{m}(2Y_j - Y_{j+1} - Y_{j-1}) = 0 \tag{7.7.b}$$

where $\theta_r = 2\pi r/N$ and $F_o$ is the amplitude of the EO excitation.

The response amplitudes of the $j^{th}$ blade and disc sector at any exciting frequency $\omega_\ell$ can be separated into real and imaginary parts as:

$$X_j(\omega_\ell) = {}_R X_j(\omega_\ell) + i\, {}_I X_j(\omega_\ell) \tag{7.8.a}$$

$$Y_j(\omega_\ell) = {}_R Y_j(\omega_\ell) + i\, {}_I Y_j(\omega_\ell) \tag{7.8.b}$$

Substituting Eq. (7.8) into Eq. (7.7) and separating into real and imaginary parts gives 4 real functional relations, $g_i$, to set to zero for each sector at every exciting frequency $\omega_\ell$:

$$g_{5s(j-1)+5\ell-4} = -\,\omega_\ell^2\,{}_RX_j(\omega_\ell) - 2\zeta G_j\,\omega_\ell\,{}_IX_j(\omega_\ell) + G_j^2\,({}_RX_j(\omega_\ell) - \eta\,{}_IX_j(\omega_\ell) - {}_RY_j(\omega_\ell) + \eta\,{}_IY_j(\omega_\ell)) - \frac{F_o}{m}\cos(\frac{2\pi(j-1)r}{N}) = 0 \qquad (7.9.a)$$

$$g_{5s(j-1)+5\ell-3} = -\,\omega_\ell^2\,{}_IX_j(\omega_\ell) + 2\zeta G_j\,\omega_\ell\,{}_RX_j(\omega_\ell) + G_j^2\,({}_IX_j(\omega_\ell) + \eta\,{}_RX_j(\omega_\ell) - {}_IY_j(\omega_\ell) - \eta\,{}_RY_j(\omega_\ell)) - \frac{F_o}{m}\sin(\frac{2\pi(j-1)r}{N}) = 0 \qquad (7.9.b)$$

$$g_{5s(j-1)+5\ell-2} = -\,\omega_\ell^2\,\frac{M_d}{m}\,{}_RY_j(\omega_\ell) + G_j^2\,({}_RY_j(\omega_\ell) - \eta\,{}_IY_j(\omega_\ell) - {}_RX_j(\omega_\ell) + \eta\,{}_IX_j(\omega_\ell)) + \frac{k_g}{m}\,{}_RY_j(\omega_\ell) + \frac{K_d}{m}\,(2\,{}_RY_j(\omega_\ell) - {}_RY_{j+1}(\omega_\ell) - {}_RY_{j-1}(\omega_\ell)) = 0 \qquad (7.9.c)$$

$$g_{5s(j-1)+5\ell-1} = -\,\omega_\ell^2\,\frac{M_d}{m}\,{}_IY_j(\omega_\ell) + G_j^2\,({}_IY_j(\omega_\ell) + \eta\,{}_RY_j(\omega_\ell) - {}_IX_j(\omega_\ell) - \eta\,{}_RX_j(\omega_\ell)) + \frac{k_g}{m}\,{}_IY_j(\omega_\ell) + \frac{K_d}{m}\,(2\,{}_IY_j(\omega_\ell) - {}_IY_{j+1}(\omega_\ell) - {}_IY_{j-1}(\omega_\ell)) = 0 \qquad (7.9.d)$$

where $\ell$=1,2,3,...,s and j=1,2,3,....N and the subscript of g indicates equation numbering. In addition to response levels of the blades and disc sectors, the cantilever frequency of each blade, $G_j$, is also unknown in the above equations, a feature which makes the problem both non-linear (the unknowns are multiplied by each other) and under-determined. Therefore, additional information is needed to solve the problem.

For our particular problem, no explicit data are available for the values of the real and imaginary parts of the response levels, the only allowable assumption being that their magnitudes lie within prescribed limits. Specifying the magnitude of the vibration level for the $j^{th}$ blade at excitation frequency $\omega_\ell$, ${}_MX_j(\omega_\ell)$, brings one additional equation relating the real and imaginary parts of the blade response to the magnitude of the vibration level assumed and can be written as:

$$g_{5s(j-1)+5\ell} = {}_R X_j^2(\omega_\ell) + {}_I X_j^2(\omega_\ell) - {}_M X_j^2(\omega_\ell) = 0 \tag{7.9.e}$$

As additional equations of this form do not introduce any new unknowns, their inclusion can result in the system of non-linear equations becoming determined or over-determined, depending on the number of excitation frequencies at which the magnitudes of the blades' vibration levels are specified.

Equation (7.9) now presents 5sN functional relations with (4s+1)N unknowns, the unknowns being 4sN real and imaginary parts of responses and N blade-alone frequencies for $\ell$=1,2,3,...s and j=1,2,3,...,N. Note that the functional relations to set to zero in Eq. (7.9) are numbered from 1 to 5sN (This is the reason why '5' appears in the subscript of g.) All unknowns in Eq. (7.9) can now be written in vector form as:

$$\{\gamma\} = \left\{ \begin{array}{c} G_1 \\ \{U_1\} \\ G_2 \\ \{U_2\} \\ G_3 \\ \{U_3\} \\ \cdot \\ \cdot \\ G_N \\ \{U_N\} \end{array} \right\} \tag{7.10}$$

where

$G_j$ = is the $j^{th}$ blade's cantilever frequency; and

$$\{U_j\} = \{{}_RX_1(\omega_1), {}_IX_1(\omega_1), {}_RY_1(\omega_1), {}_IY_1(\omega_1), {}_RX_1(\omega_2), {}_IX_1(\omega_2), {}_RY_1(\omega_2), {}_IY_1(\omega_2), \cdots, {}_RX_1(\omega_s), {}_IX_1(\omega_s), {}_RY_1(\omega_s), {}_IY_1(\omega_s)\}^T$$

It is now possible to find the vector of unknowns, $\{\gamma\}$, by using the solution technique described previously in section 7.2.1: first, a solution is assumed for the unknown vector $\{\gamma\}$ and then a correction vector $\{\delta\gamma\}$ is obtained by solving the system of linear equations given below:

$$[S]_{5sNx(4s+1)N} \{\delta\gamma\}_{(4s+1)Nx1} = - \{R\}_{5sNx1} \tag{7.11}$$

where

$[S]$ = is the coefficient matrix, the explicit form of which is given in **Appendix V**;
$\{\delta\gamma\}$ = is the correction vector in Eq. (7.10);
$\{R\}$ = $\{g_1(\{\gamma\}), g_2(\{\gamma\}), g_3(\{\gamma\}), \ldots, g_{5sN}(\{\gamma\})\}^T$

The assumed/corrected solution is updated using Eq. (7.4) until convergence is achieved.

## 7.3 Structural Parameters

The structural parameters listed in Table 6.1 of the previous chapter were also used in this investigation, with the exception of the coefficient of dispersion for blade frequencies which is now an unknown rather than one of the input data, as previously.

Unless stated otherwise, results were obtained for a 12-bladed disc under 2$^{nd}$ engine-order excitation.

## 7.4 Some Computational Aspects

When dealing with a non-linear inverse problem, one is faced with several numerical difficulties such as ill-conditioning, poor convergence, non-uniqueness and non-existence of the solution. However, it must be said at the outset that our objective here is not to focus on these numerical problems, but to note them and to find acceptable solutions with emphasis on the engineering aspects of the problem.

### 7.4.1 Formation and Balancing of the [S] Matrix

As can be seen from Eq. (7.9), the non-linear algebraic equations were numbered from 1 to 5sN. Although numbering these functional relations can be quite arbitrary, this numbering, together with the resulting ordering of the unknowns in vector $\{\gamma\}$, can become quite important during the solution stage, an inefficient numbering resulting in a not banded [S] matrix which causes the iterative solution either to diverge or to require extra iterations. Hence, the numbering of the functional relations must be made in such a way that the matrix [S] is as banded as possible.

Another problem lies in the [S] matrix itself which can be very ill-conditioned. Indeed, the individual elements of the [S] matrix contain both response (very small numbers) and structural parameter (relatively large numbers) terms and, hence, the *condition number* of the matrix [S] can become very large (Condition number is an indicator of how much a matrix is ill-conditioned. A matrix is ill-conditioned if its condition number is too large.)

It may be necessary to balance the [S] matrix before the solution stage in order to overcome the ill-conditioning problem mentioned above. For our bladed disc problem, the balancing operation was performed by rescaling certain columns and rows of the [S] matrix. Rows numbered as $5s(j-1)+5\ell$ were multiplied by a large number (say,

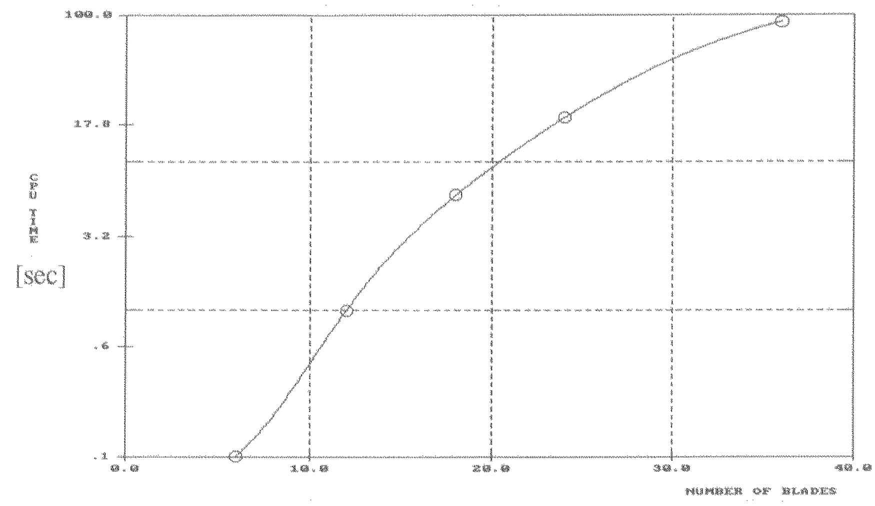


**Fig. 7.2** CPU time required for single iteration for different number of blades. (Blade responses were specified at 3 excitation frequencies.)

1.0E10). The corresponding rows in vector {R} were multiplied by the same number. Further elements, located at those columns numbered as 4s(j-1)+j, were also multiplied by a large number (say, 1.0E7).

Such numerical techniques, i.e., making the [S] matrix as banded as possible and balancing it, improved the solution procedure remarkably: first, initially non-converging cases started to yield a solution; second, the number of iterations required decreased; and finally, it became possible to use a Pseudo-Inverse routine instead of a Singular Value Decomposition one, a change which reduced the required computation time by an order of magnitude. After these improvements, the CPU time required for a single iteration on an IBM RS-6000 model 530 workstation was recorded for several cases with different numbers of blades when the blade responses were specified at 3 excitation frequencies and results are presented in Fig. 7.2.

### 7.4.2 Convergence and Uniqueness of the Solution

Before proceeding any further, it is appropriate to highlight some problems which occur when solving inverse problems: the iteration process may not always converge to

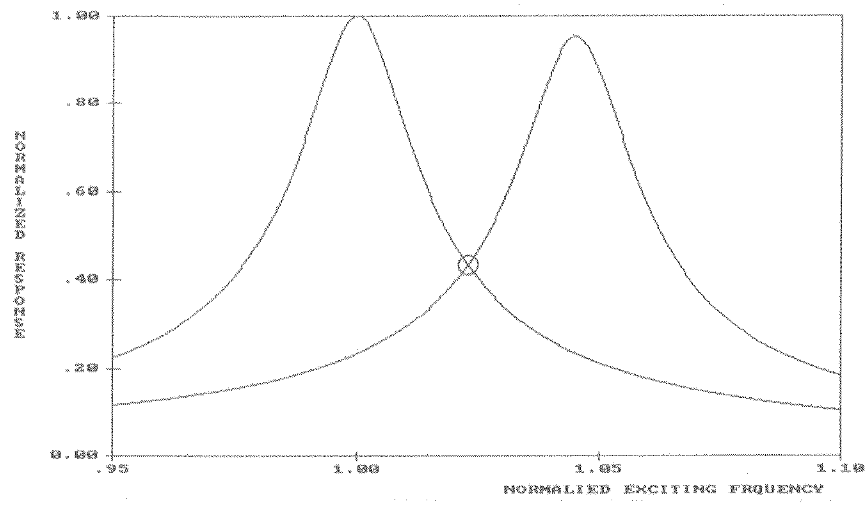


**Fig. 7.3** Two tuned systems satisfying the specified response levels at one excitation frequency.

a solution and, even if it does, that solution may not be unique. Therefore, one might obtain either no solution at all or a solution which can be one of the many possibilities.

In order to understand whether a solution is physically acceptable, let us first consider a tuned bladed disc assembly. If the magnitudes of all blade responses are specified to be equal at one excitation frequency only, there will be more than one tuned system which will satisfy that constraint. This is illustrated in Fig. 7.3 where tuned blade responses are shown against excitation frequency for two different tuned bladed discs. As can be seen, both of these tuned systems satisfy the required response level where the two curves intersect at the specified excitation frequency. Under such circumstances, the solution may converge to either of these tuned systems depending on the initial guess for the unknown vector $\{\gamma\}$. However, the blade cantilever frequencies of a tuned system can be found uniquely if the magnitudes of all the tuned blade responses are specified for at least two excitation frequencies. A typical example for such a case is given in Fig. 7.4 in which blade response magnitudes were specified at two different excitation frequencies. The blade cantilever frequencies were initially assumed to be different from each other and, as can be seen from Fig. 7.4, they all converged to the same correct value, 182 Hz, after five iterations.

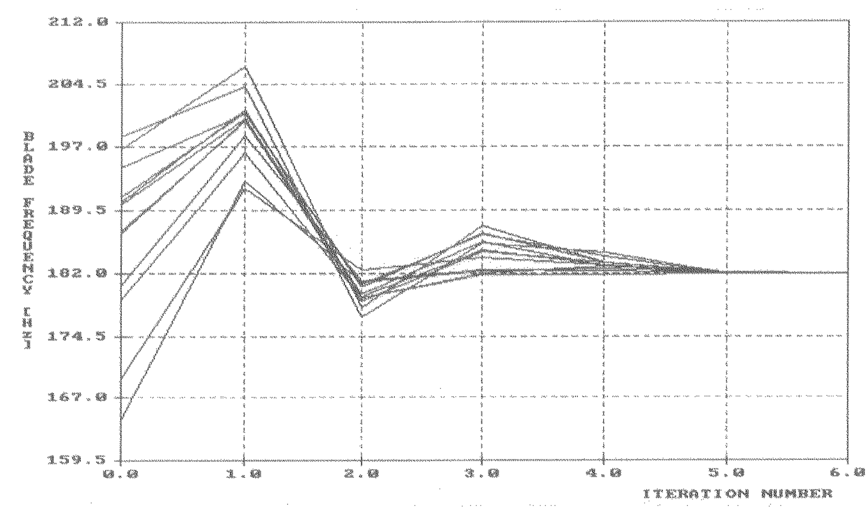


**Fig. 7.4** Convergence rate is very fast and the solution is unique when the tuned blade responses are specified at more than one excitation frequency.

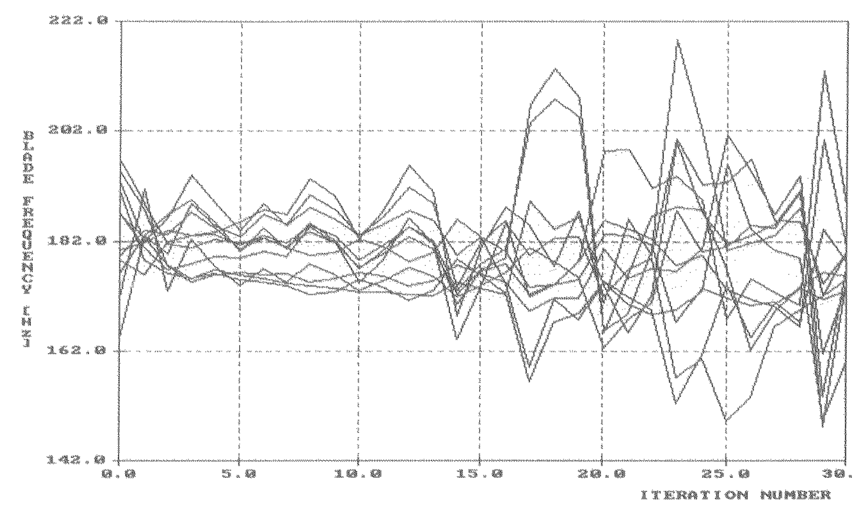


**Fig. 7.5** Iteration for tuned blade frequencies fails when the tuned blade responses are specified to be greater than the tuned resonant response level.

A case where the iteration would not converge to a solution can also be demonstrated easily for a tuned bladed disc system. If all tuned blade response levels are specified to be greater than the tuned resonant response level, no solution will exist for a set of blade cantilever frequencies which can yield such response levels. A typical example is shown in Fig. 7.5, the non-convergence here suggesting that such a system is physically impossible.

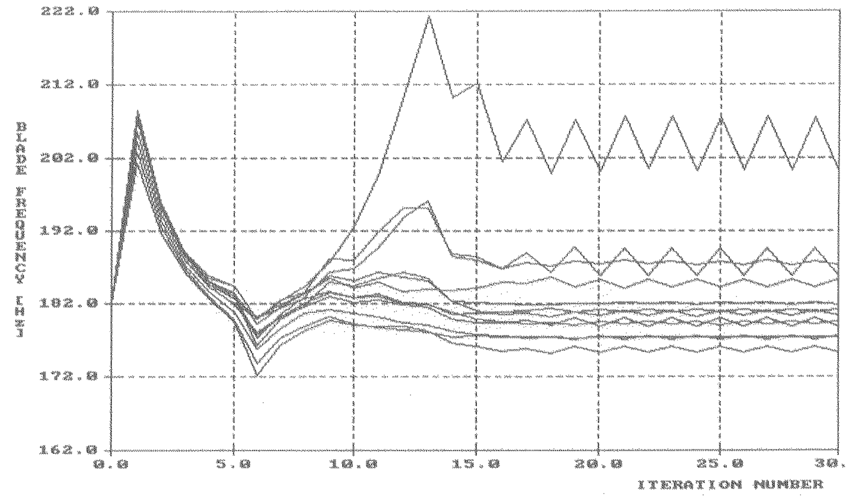


**Fig. 7.6** Iteration for mistuned blade frequencies fails when most of the blade responses are specified to be greater than the tuned resonant response level.

Similar results can also be obtained for mistuned bladed discs. Again, there may not be a physical system satisfying the assumed magnitudes of mistuned blade response levels. Some iteration results for mistuned blade cantilever frequencies are presented in Fig. 7.6 showing that a set of blade cantilever frequencies cannot be found if the assumed response levels are *not correct*. Preliminary case studies showed that such iteration failures happen (i) when the response levels for a large number of mistuned blades are assumed to be higher than the tuned resonant response level, or (ii) when the mean of the mistuned blade response levels exceeds the tuned resonant response level. However, the iterative solution process for the unknown vector $\{\gamma\}$ converges if the magnitudes of the response levels of a small number of mistuned blades are allowed to exceed the tuned resonant response level. A typical convergence path is illustrated in Fig. 7.7, the convergence rate being relatively slow when compared with that for the tuned system plotted in Fig. 7.4. The reason for this slower convergence is that although tuned blade cantilever frequencies constituted an adequate guess for mistuned blade cantilever frequencies, the initial guesses for the real and imaginary parts of the response amplitudes were extremely poor and there was no simple way of making good initial guesses for them.

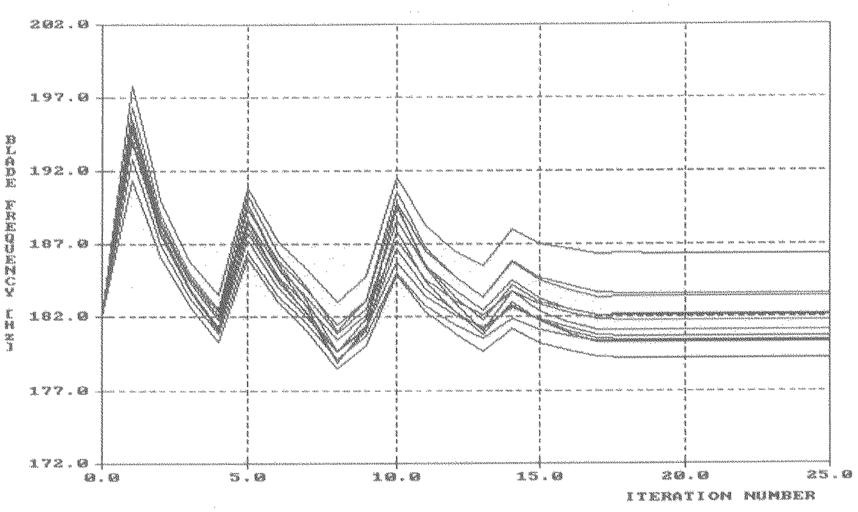


**Fig. 7.7** A typical convergence rate for mistuned blade cantilever frequencies.

As in the case of the tuned system, there may be more than one mistuned system which can satisfy the assumed response levels at a given excitation frequency. Of course, specifying the magnitudes of the mistuned blade responses at several excitation frequencies increases the possibility of finding a unique mistuned system. Unfortunately, the designer has no such data available. At a single excitation frequency, it is possible to choose the magnitudes of mistuned blade response levels randomly within specified limits. However, if responses are to be specified at several excitation frequencies, they cannot be drawn in a completely random manner. In order to make this point clearer, let us consider Fig. 6.3.a of the previous chapter where the response levels of mistuned blades are plotted against the excitation frequency for a particular mistuning configuration. Once the response levels are specified at a given excitation frequency, it is not possible to predict them at some other frequency without full knowledge of the system parameters. If they are drawn randomly at more than one excitation frequency, the chance of guessing the *correct* response levels is extremely low and the iteration process will usually fail to converge, indicating that there is no such system. (This is analogous to not being able to find a single-degree-of-freedom system subjected to harmonic excitation which can satisfy randomly-guessed response levels at three different excitation frequencies.)

**Table 7.1**. Verification of the inverse solution.

| Blade No: | Inverse Solution: Input Blade Res. (normalized) | Inverse Solution: Output Blade Freq. (normalized) | Direct Solution: Input Blade Freq. (normalized) | Direct Solution: Output Blade Res. (normalized) | Differ. [%] |
|---|---|---|---|---|---|
| 1 | 0.7857 | 1.0133 | 1.0133 | 0.7830 | 0.34 |
| 2 | 0.9143 | 0.9942 | 0.9942 | 0.9138 | 0.05 |
| 3 | 1.1766 | 0.9952 | 0.9952 | 1.1761 | 0.04 |
| 4 | 0.7220 | 1.0214 | 1.0214 | 0.7214 | 0.08 |
| 5 | 0.7721 | 1.0129 | 1.0129 | 0.7722 | -0.01 |
| 6 | 1.0230 | 0.9942 | 0.9942 | 1.0220 | 0.10 |
| 7 | 0.7830 | 1.0086 | 1.0086 | 0.7828 | 0.02 |
| 8 | 0.9804 | 1.0042 | 1.0042 | 0.9792 | 0.12 |
| 9 | 0.9243 | 0.9973 | 0.9973 | 0.9227 | 0.17 |
| 10 | 1.3000 | 0.9853 | 0.9853 | 1.2954 | 0.36 |
| 11 | 0.8393 | 1.0458 | 1.0458 | 0.8433 | -0.47 |
| 12 | 0.7204 | 1.0356 | 1.0356 | 0.7220 | -0.22 |

Blade response is normalized to the tuned blade's resonant response level (design value) and the blade natural frequency is normalized to the tuned blade first cantilever frequency, i.e.,182 Hz. ($\omega_{ex}$ = 2ND tuned system natural frequency)

The validation of the results obtained from the inverse solution was straightforward. The output of the inverse solution (blade cantilever frequencies) was used as input to the direct solution described in the previous chapter and a one-to-one correspondence was expected in recomputed and specified blade response levels. A typical example is presented in Table 7.1 where the difference between the response levels is less than 0.5% in all cases. If necessary, the numerical results can be improved further by tightening the convergence criteria.

In the next section it will be shown how the required tolerance for the cantilever frequencies of the mistuned blades was determined in spite of the non-uniqueness of the solution.

## 7.5 Results

It is clear from the previous chapter that, for a given A% acceptable response increase due to mistuning, the allowable manufacturing tolerances would depend on the excitation frequency, on the engine-order (EO) of excitation, and on the number of blades. In this chapter, however, we seek to find the allowable manufacturing tolerances for the blade cantilever frequencies in the worst possible case. It is proposed to use some of the results found in the previous chapter:

i) a bladed disc with a small number of blades can simulate the dynamic behaviour of discs with a large number of blades. This is a very important consideration from computation cost point of view. The number of blades was kept constant at 12 during this study;

ii) for the particular bladed disc assembly being studied, the maximum resonant response increase due to mistuning happens when the interblade phase angle of the forcing is about $60^{\circ}$. Therefore, all the results in this chapter were obtained under second engine order (2EO) excitation for this 12-bladed disc. This information was useful since it removed the need for solving the inverse problem for various engine order excitations, as had been done in the previous chapter;

iii) the most responsive blades among blades from hundreds of bladed discs, experience the maximum response levels when the excitation frequency is close to the natural frequency of the tuned system critical mode (the 'critical mode' is the one corresponding to the critical interblade phase angle.) This mode is the 2ND mode for the 12 bladed disc being studied. This finding from chapter 6 allowed determination of the required manufacturing tolerance by considering blade response levels at this specific excitation frequency only.

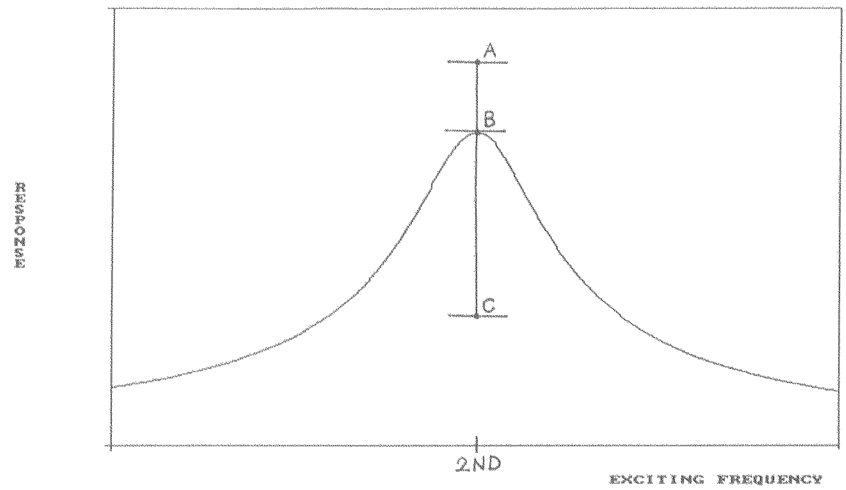


**Fig. 7.8** The magnitudes of mistuned blade response levels are chosen by a "semi-random" way within a specified range at 2ND natural frequency of the tuned system.

### 7.5.1 Required Tolerances for 30% Resonant Response Increase

At the 2ND tuned system natural frequency, the magnitudes of all the mistuned blade responses were chosen in a *semi-random* manner within a specified range shown in Fig. 7.8 where the response level of the tuned system provides the reference curve. The upper bound of this range, point A in Fig. 7.8, corresponds to the maximum allowable response increase of 30% above the tuned resonant response level for this particular case. Point B represents the resonant response level of the tuned system and point C is the lower bound which is determined by trial-and-error, as will be explained later. Sampling of the response levels is termed *semi-random* because at least 1 and at most 3 (out of 12) blade response levels were forced to lie between points A and B while the corresponding positions on the disc were totally random. (This was to simulate a typical case where only a few mistuned blades experience higher response levels than those of the tuned system.) The worst blade response level was set to the maximum allowable response level of 30% in order to ensure that every mistuned system determined had at least one blade experiencing the highest allowable response increase. The response levels of the remaining blades were randomly selected between points B and C.

As mentioned before, setting the lower response bound, point C, was required in order to simulate the real case although a suitable value for the lower response bound was not known a priori. After some deliberation, it was recalled that the upper and lower bounds for mistuned blade response levels would converge towards to the same value with decreasing mistuning and, in the limit, they would coincide with point B. Therefore, point C is expected to decrease with increasing allowable response increase. By making use of this information, the lower bound was determined by trial-and-error as follows: first, a lower bound which is slightly lower than point B was assumed; then, the value of the lower bound was decreased until a reasonable number of sampled response levels between lower and upper bounds yield solutions. It should be noted that the required tolerance for a given allowable upper response level can also be obtained without setting any limit to the position of point C. However, this would require much more sample size than necessary when a suitable value is assigned.

After a value for the lower response bound was determined, the magnitudes of the mistuned blade response levels were specified randomly within these limits (points A, B and C) as described previously and the solution technique developed in this chapter was applied to find a mistuned system satisfying the prescribed response levels at the 2ND natural frequency of the tuned system. However, even if such a mistuned system can be found, the response levels of some of its blades may well exceed the allowable response increase at some **other** excitation frequencies. A typical example for such a situation is illustrated in Fig. 7.9 where the response levels of all 12 blades are shown against the excitation frequency. It is immediately seen that the response level of one of the blades exceeds the 30% limit at some excitation frequencies between 1.0 and 1.1 of the normalized excitation frequency. Perhaps more importantly, there is no guarantee that the maximum response level will not exceed the allowable value when the same set of blades are rearranged around the disc. All these observations indicate

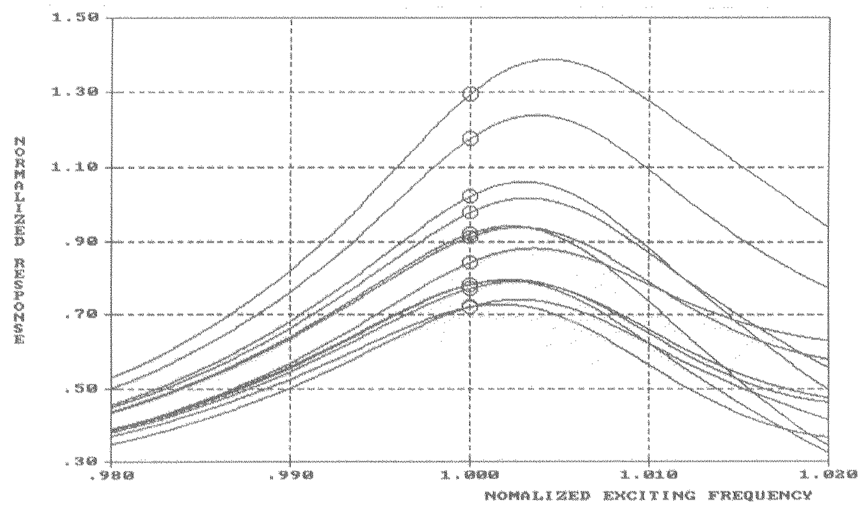


**Fig. 7.9** Response levels of some blades may exceed the allowable response increase at some other excitation frequencies.

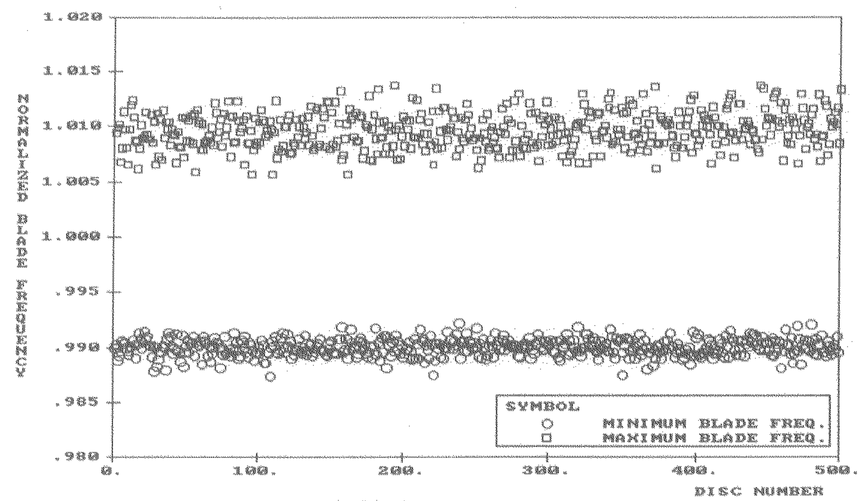


**Fig. 7.10** The Minimum and the maximum blade frequencies for 500 bladed discs which satisfy 30% response increase.

that a statistical approach with a large enough sample size must be used to address the inverse problem.

Configurations for 500 bladed discs, each having a blade experiencing a maximum of 30% response increase were determined using the solution technique described in section 7.2.2. The maximum and the minimum blade frequencies for each bladed disc were found and are plotted in Fig. 7.10 by normalizing all values to the tuned blade cantilever frequency of 182 Hz. Using the data of Fig. 7.10, the tolerance value which

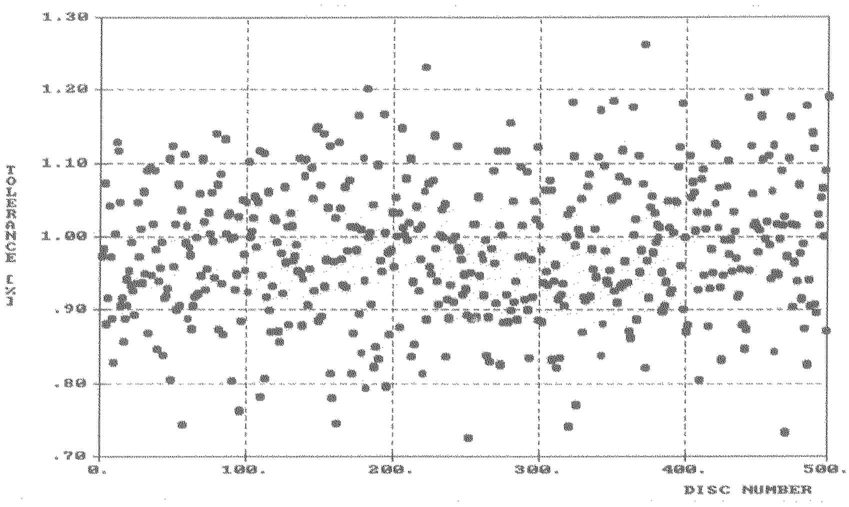


**Fig. 7.11** Tolerances obtained form 500 bladed discs determined.

was defined as $(G_{max}-G_{min})/2\bar{G}$ was calculated for each determined bladed disc configuration and the results are presented in Fig. 7.11. The tolerance values obtained from 500 bladed discs show that a blade-to-blade cantilever frequency variation of as little as 0.73% can cause a 30% response increase. Therefore, to ensure blade response levels lower than 130% of the tuned system resonant response, the manufacturing tolerances are required to be tight enough such that the individual blade cantilever frequencies should be between $(1\pm0.0073)\mathrm{x}\bar{G}$.

This result, found from the inverse solution, was checked by using the direct approach. The acceptable degree of blade-to-blade variation for a 30% response increase, ±0.73%, was used as an input value to the direct solution described in the previous chapter. The individual blade cantilever frequencies were selected randomly from a normal population (mean = $\bar{G}$ = 182 Hz, standard deviation = $\sigma$ = $0.0073\mathrm{x}\bar{G}$) and they were rejected if they were outside the range $(1\pm0.0073)\mathrm{x}\bar{G}$ (i.e., $G_j$ was rejected if it was outside the range $\bar{G}\pm\sigma$) and this procedure was repeated until all 12 blades' cantilever frequencies were specified. The direct solutions were obtained for more than 2100 12-bladed discs and the statistical results are summarized in Figs. 7.12.a and 7.12.b. As can be seen, only one blade's response out of 25000 exceeds the 30% limit with a value of 31.6%.

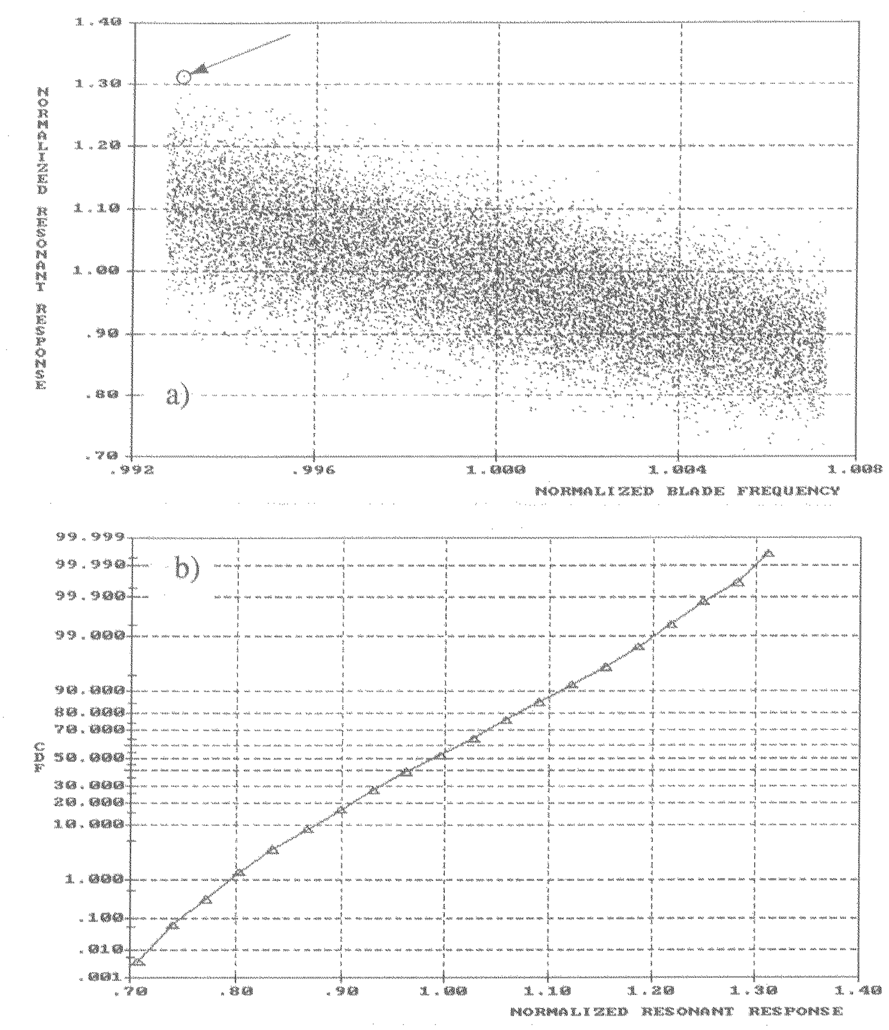


**Fig. 7.12** Verification of the result by direct solution.

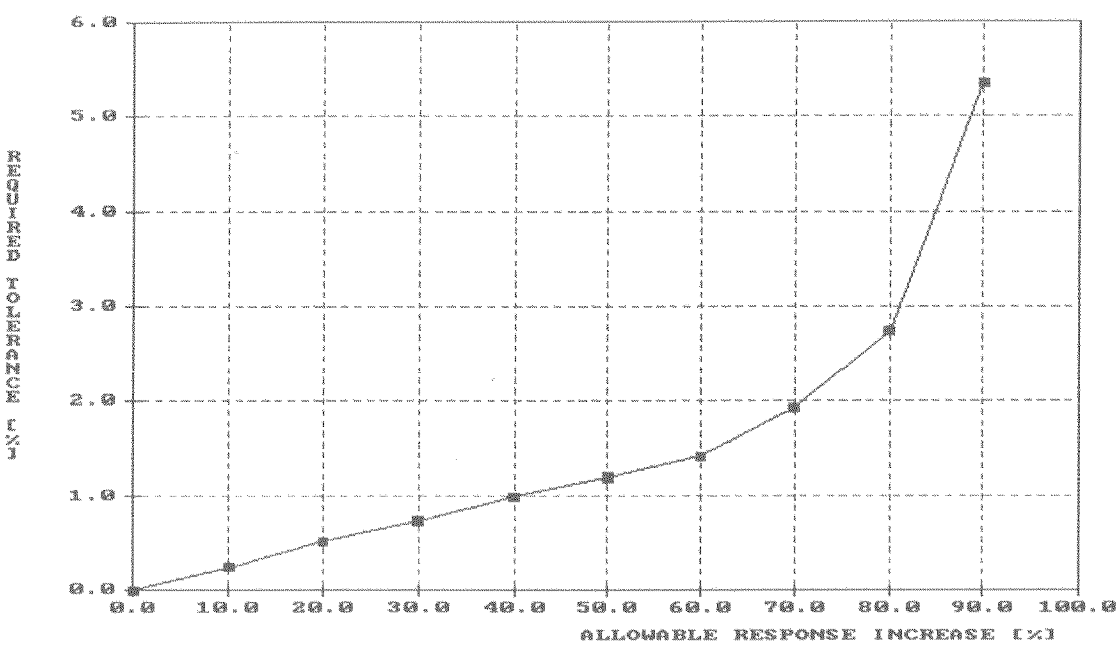


**Fig. 7.13** Required tolerance in blade-alone cantilever frequency versus allowable response increase due to mistuning.

### 7.5.2 Relationship Between Allowable Response Increase and Required Tolerance

The procedure described above for determining the required manufacturing tolerances for 30% response increase was repeated for various values of allowable response increase, up to 90%, and the corresponding tolerances were determined. Results are summarized in Fig. 7.13 and it is seen that the relationship between these two parameters is almost linear up to 60% allowable response increase, after which the threshold tolerance values increases very sharply. Thus, if the value of an acceptable response increase is to be reduced from say 90% to 80% of the tuned system level, the required tolerance in blade-alone frequency needs to be tightened almost by a factor of two (i.e., from $\pm 5.4\%$ to $\pm 2.8\%$ of blade cantilever frequency.) Therefore, results presented in Fig. 7.13 suggest that if considerable improvement is to be achieved in reducing the worsening effect of the mistuning, the blade-to-blade cantilever frequency variations should be kept to less than 2% in this case so that any further improvement (tightening) in manufacturing tolerance decreases the worsening effect of the mistuning proportionally.

## 7.6 Concluding Remarks

i) A method has been developed for determining the appropriate structural parameters of a model when response levels are specified at some coordinates under known excitation conditions.

ii) The method was used to find the required manufacturing tolerance for a specified allowable worsening effect due to mistuning and the result was verified using the direct approach described in the previous chapter.

iii) A relationship between the required manufacturing tolerance and the response increase due to mistuning has been determined by solving the inverse problem for various values of allowable response increase. The results found here suggest that for the case studied this relationship is almost linear up to 60% allowable response increase, after which the required tolerance does not need to be tightened proportionally. Therefore, if considerable improvement is to be made in reducing the worsening effect of the mistuning, the manufacturing tolerance should be lowered to less than 2% in this case. However, it should be kept in mind that these results were obtained from studying a bladed disc with a given degree of blade-to-disc coupling ratio and damping properties and, hence, it is difficult to generalize the numerical values.

iv) Finally, it is believed that the method proposed can also be used for model updating purposes.

# CHAPTER 8

# CONCLUSIONS AND SUGGESTIONS FOR FURTHER WORK

**About This Chapter**

*This chapter is an attempt to summarize and unify the conclusions of the preceding chapters. One conclusion - inevitable in such a research project - is that there remains some questions which are still unresolved. Accordingly, some suggestions for further research are proposed in the light of the present work.*

## 8.1 Conclusions

The work described in this thesis represents an effort to improve the basic understanding of the response characteristics of mistuned bladed discs. To this end, several analytical models based on both deterministic and statistical approaches have been developed and used with success to conduct qualitative and quantitative studies in order to understand the consequences of mistuning.

The main findings of this investigation are listed below.

i) The analytical formulation where the response levels are expressed as explicit functions of coefficients in the equations of motion for tuned and alternate mistuning assemblies brings huge savings in computational time. Moreover, the antiresonance frequencies, which cannot be identified from an eigensolution, can also be determined in any coordinate response using the proposed formulation.

ii) Results on single blade mistuning have shown that high levels of damping can suppress the effect of mistuning. It has also been found that damping caused by a fatigue crack in any one blade can have a marked effect on the response levels of that blade.

iii) A general method for predicting fatigue life under forced vibration has been developed. It has been found that the inclusion of frequency- and/or crack-dependence into the stress intensity factor yields significantly lower fatigue life predictions than estimated fatigue life when they are ignored, especially when the excitation frequency is in the vicinity of a mode of vibration. The technique was applied to a bladed disc assembly with a fatigue-cracked blade. The findings suggest that the coincidence of excitation frequency with the new natural frequencies of the system due to fatigue crack should be avoided for prolonged fatigue life.

iv) For a given bladed disc, the worst blade under a certain EO excitation may not be the critical one under some other EO excitations and there are no general rules for identifying the critical blades according to their cantilever frequencies alone. This explains why many apparently-conflicting conclusions were reached in previous studies and these have now been reconciled in the light of the findings presented in this thesis.

v) For the same amount of mistuning and using the same model, it has been demonstrated that the magnitude of the worsening effect can vary from an increase of less than 5% to over 110% since this worsening effect depends very strongly on the EO of the excitation (r). When r is 'small', the worsening effect of mistuning seems to be small. At some intermediate values of r the worsening effect reaches a maximum and tends to decrease again as r increases further. The critical value of r seems to be dependent on blade-to-disc coupling and this observation requires further investigation.

vi) A very good linear correlation between the blades experiencing the maximum amplitude and the excitation frequencies at which these blades vibrate strongly has been found. Such information can be used in deciding which blades to instrument and at which excitation frequency to test them. Results suggest that there is a range of critical blades classified according to their cantilever frequencies and as many blades as possible within this range should be instrumented in a practical engine test. This range depends on the EO excitation and it also includes those blades with cantilever frequencies equal to the rND tuned system natural frequency. However, this rND frequency is not necessarily the mean of that blade frequency range requiring instrumentation.

vii) A simple parameter, interblade phase angle $\theta_r=2\pi r/N$, is of paramount importance when studying the response characteristics of mistuned bladed discs. There is no need to conduct parametric studies by changing r and N individually since the combined effects can be found from $\theta_r$ directly. This is a huge saving in computing time since (a) far fewer cases need to be investigated and (b) the dynamic behaviour of large systems can be deduced from that of much smaller systems.

viii) The probability and cumulative density functions of the resonant response show that the response distribution is not normal and, furthermore, that there is no unique distribution which can represent the statistical characteristics of mistuned blade forced response under all EO excitations.

ix) An inverse method has been developed to determine acceptable blade-to-blade variations for response levels not to exceed A% of the tuned system response. The method was used to find the a relationship between the required manufacturing tolerance and the allowable response increase due to mistuning. The results found in this thesis suggest that this relationship is almost linear up to 60% allowable response increase, after which the required tolerance increases very sharply. Therefore, if considerable improvement is to be made in reducing the worsening effect of the mistuning, the manufacturing tolerance should be lowered to less than 2%. However, it should be kept in mind that results in Fig. 7.13 were obtained from studying a bladed disc with a specific blade-to-disc coupling ratio and damping properties and, hence, care must be taken in generalising this result to other assembly configurations.

## 8.2 Suggestions for Further Studies

Notwithstanding that a number of achievements have been made towards the understanding of the mistuning effects, there is still work to be done before the effects of mistuning can be fully predicted and controlled. Areas which now need particular attention are:

i) experimental verification of the findings of this thesis in order to clarify certain important points such as the effect of EO excitation and the interblade phase angle on the consequences of mistuning;

ii) a detailed investigation of damping mistuning caused by unsteady aerodynamic forces as well as blade-to-disc and blade-to-shroud joints;

iii) the development of an analytical method for the statistical investigation of mistuning in an attempt to prevent the need for expensive numerical simulations;

iv) the determination of the critical interblade phase angle causing the worst mistuning effect without having to calculate the resonant response levels of hundreds of bladed discs for various interblade phase angles and

v) more accurate modelling of blade and disc geometry.

# APPENDIX I

# CIRCULANT MATRIX THEORY AND APPLICATION TO A TUNED BLADED DISC

The purpose of this appendix is to derive analytically Eq. (2.21) of chapter 2 which was obtained by observation in the light of several case studies. Although a short review of circulant matrices is presented below, the interested reader should consult **Davis** (1979) for more details.

## AI.1 Eigenvalues and Eigenvectors of Circulant Matrices

A matrix of the form:

$$[C] = \begin{vmatrix} c_o & c_1 & c_2 & c_3 \cdots & c_{n-2} & c_{n-1} \\ c_{n-1} & c_o & c_1 & c_2 \cdots & c_{n-3} & c_{n-2} \\ c_{n-2} & c_{n-1} & c_o & c_1 \cdots & c_{n-4} & c_{n-3} \\ & & & \cdot & & \\ & & & \cdot & & \\ c_2 & c_3 & c_4 & c_5 \cdots & c_o & c_1 \\ c_1 & c_2 & c_3 & c_4 \cdots & c_{n-1} & c_o \end{vmatrix}_{nxn} \tag{AI.1}$$

is called a *circulant matrix* of order n. Let $r_j$ be a root of the scalar equation $r^n = 1$ and let

$$\kappa_j = c_0 + c_1 r_j + c_2 r_j^2 + \ldots\ldots + c_{n-1} r_j^{n-1} \tag{AI.2}$$

Then, $\kappa_j$ satisfies the following set of equations:

$$
\begin{aligned}
c_0 + c_1 r_j + c_2 r_j^2 + \ldots\ldots + c_{n-1} r_j^{n-1} &= \kappa_j \\
c_{n-1} + c_0 r_j + c_1 r_j^2 + \ldots\ldots + c_{n-2} r_j^{n-1} &= \kappa_j r_j \\
c_{n-2} + c_{n-1} r_j + c_0 r_j^2 + \ldots\ldots + c_{n-3} r_j^{n-1} &= \kappa_j r_j^2 \\
&. \\
&. \\
c_1 + c_2 r_j + c_3 r_j^2 + \ldots\ldots + c_0 r_j^{n-1} &= \kappa_j r_j^{n-1}
\end{aligned}
\tag{AI.3}
$$

It is seen that Eq. (AI.3) is of the form:

$$[C]\{\psi_j\} = \kappa_j \{\psi_j\} \tag{AI.4}$$

It follows that $\kappa_j$ is an eigenvalue of [C] with associated eigenvector:

$$\{\psi_j\} = \{1, r_j, r_j^2, \ldots\ldots, r_j^{n-1}\}^T \tag{AI.5}$$

## AI.2 Application to a Tuned Bladed Disc (Model A)

The matrix equation which needs to be solved is:

$$[Z]\{\hat{q}\} = \{\hat{f}\} \tag{AI.6}$$

where [Z], $\{\hat{q}\}$ and $\{\hat{f}\}$ are given by Eq. (2.16), (2.17) and (2.18) respectively. The size of the square matrix [Z] is N (i.e. n=N) where N is the number of blades. The scalar equation $r^N=1$ has N distinct solutions which are given below:

$$r_j = e^{i\theta_j}, \qquad j=0,1,2,\ldots\ldots,N-1 \tag{AI.7}$$

where

$$\theta_j = \frac{2\pi j}{N} \tag{AI.8}$$

Circulant Matrix Theory gives the eigenvectors and the eigenvalues of [Z] respectively as:

$$\{\psi_j\} = \{1, e^{i\theta j}, e^{i2\theta j}, e^{i3\theta j}, \ldots\ldots, e^{i(N-1)\theta j}\}^T \tag{AI.9}$$

$$\kappa_j = A + Be^{i\theta j} + 0 + 0 + \ldots..+ 0 + Be^{i(N-1)\theta j} = A + B(e^{i\theta j} + e^{i(N-1)\theta j}) \tag{AI.10}$$

Eq. (AI.10) can be further simplified since $N\theta_j = 2\pi j$

$$\kappa_j = A + B(e^{i\theta j} + e^{-i\theta j}) = A + 2B\cos(\theta_j) \tag{AI.11}$$

Note that the $j^{th}$ eigenvector given in Eq. (AI.9) is identical to the force vector $\{\hat{f}\}$ given in Eq. (2.18) for jEO excitation. Therefore, $\{\hat{f}\}$ in Eq. (AI.6) can be replaced by $\{\psi_j\}$ which gives:

$$[Z]\{\hat{q}\} = \{\psi_j\} \tag{AI.12}$$

Multiplying both sides by $[Z]^{-1}$ in above equation yields

$$\{\hat{q}\} = [Z]^{-1}\{\psi_j\} \tag{AI.13}$$

Since [Z] is a circulant matrix, it satisfies the following equation:

$$[Z]\{\psi_j\} = \kappa_j\{\psi_j\} \tag{AI.14}$$

Eq. (AI.14) can be rearranged to give:

$$\frac{1}{\kappa_j}\{\psi_j\} = [Z]^{-1}\{\psi_j\} \tag{AI.15}$$

It is seen that the right hand sides of Eq. (AI.13) and Eq. (AI.15) are equal hence:

$$\{\hat{q}\} = \frac{1}{\kappa_j}\{\psi_j\} \tag{AI.16}$$

Inserting the values of $\{\hat{q}\}$, $\kappa_j$ and $\{\psi_j\}$ yields the required answer:

$$\left\{\begin{matrix} X_1 \\ X_2 \\ X_2 \\ \cdot \\ \cdot \\ X_N \end{matrix}\right\} = \frac{1}{A + 2B\cos(\theta_j)} \left\{\begin{matrix} 1 \\ e^{i\theta j} \\ e^{i2\theta j} \\ \cdot \\ \cdot \\ e^{i(N-1)\theta j} \end{matrix}\right\} \tag{AI.17}$$

It is seen from Eq. (AI.17) that the response level $X_1$ is the same as in Eq. (2.21) when j is equal to EO excitation, which is the required result.

# APPENDIX II

# THE ROOTS OF A CUBIC EQUATION

Substituting the coefficients in Eq. (2.43) into Eq. (2.36) and equating the resulting expression to zero yields the following frequency equation for the r nodal diameter modes.

$$\lambda^3 + a_1 \lambda^2 + a_2 \lambda + a_3 = 0 \tag{AII.1}$$

the solution for three real and distinct roots is

$$\lambda_1 = 2\sqrt{-Q}\cos\left(\frac{1}{3}\phi + \frac{2\pi}{3} a_1\right) - \frac{1}{3} a_1 \tag{AII.2}$$

$$\lambda_2 = \sqrt{-Q}\cos\left(\frac{1}{3}\phi\right) - \frac{1}{3} a_1 \tag{AII.3}$$

$$\lambda_3 = \sqrt{-Q}\cos\left(\frac{1}{3}\phi + \frac{4\pi}{3} a_1\right) - \frac{1}{3} a_1 \tag{AII.4}$$

where

$$\cos(\phi) = \frac{R}{\sqrt{-Q^3}} \tag{AII.5}$$

$$R = \frac{3a_2 - a_1^2}{9} \tag{AII.6}$$

$$Q = \frac{9a_1a_2 - 27a_3 - 2a_1^3}{54} \tag{AII.7}$$

# APPENDIX III

# NATURAL FREQUENCY AND DAMPING CHANGES PRODUCED BY FATIGUE CRACKS[1]

(The experimental data presented in this appendix are used in chapters 3 and 4.)

791

## NATURAL FREQUENCY AND DAMPING CHANGES PRODUCED BY FATIGUE CRACKS

M. IMREGUN and K. Y. SANLITURK
Department of Mechanical Engineering
Imperial College of Science, Technology and Medicine
Exhibition Road, London, SW7 2BX, U.K.

***Abstract***

*The changes in the natural frequency and structural damping of free-free beams due to the presence of fatigue cracks have been investigated experimentally. It has been shown that the presence of a fatigue crack in such beams decreases the natural frequencies considerably and increases the damping by an order of magnitude when the initial damping is light. It is hoped that results from this study will allow a more realistic assessment of forced response characteristics of bladed-disk systems, especially when there is mistuning due to a crack defect in a single blade.*

## 1. Introduction

Reliable design of engineering components requires a thorough understanding of the mechanisms involved in fatigue crack formation and growth. Non-destructive testing (NDT) studies have shown that many physical parameters correlate with the nature and amount of defects present in a structure (**refs 1, 2**). For vibration analysis in particular, damping values and natural frequencies of a structure are known to be very sensitive to cracks (**refs 3-5**) but there is a lack of reliable experimental data to provide guidelines as to how these variations occur. The vibration amplitudes introduced in the measurements of one or both of these properties are usually so small that the stresses produced are negligible. Therefore, damping level and/or natural frequency measurements in order to detect the presence of possible defects are shown to be quick and attractive methods in NDT (**refs 6-8**).

[1] Reproduced from the **Proceedings of the 15th International Seminar on Modal Analysis**, Leuven, Belgium, 19-21 September 1990, pp. 791-805.

There is also a growing interest in the prediction of *dynamic* fatigue life using crack growth rate data. Although fatigue-life prediction methods are also well established (**refs 9-12**), almost all of them require predetermined stresses or strains around a fatigue crack. Prediction of these stresses or strains usually brings no complication provided that the frequency spectrum of the applied force is far below the natural frequencies of the structure under study so that a static force assumption is adequate. Unfortunately, for most rotating machinery components, this is not the case. For such applications, dynamic stresses or strains should be determined via vibration analysis which in turn requires stiffness and damping variation produced by fatigue cracks. Another important engineering area, where stiffness and damping variation caused by a fatigue cracks is of paramount importance, is the determination of the dynamic characteristics of systems comprising elements with defects . This problem will be addressed shortly in a forthcoming paper.

## 2. Theory : Damping Measurements

Damping is the removal of energy from a vibratory system and a convenient way of quantifying is to introduce the specific damping ratio $\gamma$, defined as the ratio of the energy lost to the peak potential energy stored in the system during each cycle. The specific damping ratio is related to other commonly used damping parameters by:

$$\gamma = 2\pi / Q = 2\delta = 2\pi\eta = 4\pi\zeta$$

where Q is the amplification factor, $\delta$ is the logarithmic decrement, and $\eta$ and $\zeta$ are the hysteretic damping coefficient and damping ratio respectively.

Damping estimation methods can be broadly divided into two groups; namely, time domain methods and frequency domain methods.

### 2.1 Time Domain Methods

As the name implies, time domain methods make use of the measured transient response signal directly. There are four well established techniques.

(i) The logarithmic decrement method: the logarithmic decrement, defined as the natural logarithm of the ratio of any two successive amplitudes, gives an estimate of damping from simple measurements of successive oscillation amplitudes. The application of this method to continuous structures requires the isolation of the particular modes of interest using a very narrow band filter.

(ii) The envelope method: this method is a refined version of (i) where an exponential envelope is fitted through all available oscillation peaks. Damping is then estimated from the rate of decay of this envelope.

(iii) Complex exponential method: this is a method based on multi-degree of freedom curve-fitting in time domain. As the method is based on the system's impulse response function, its present application is limited to the models incorporating viscous damping only.

(iv) Ibrahim's time domain method (**refs 13, 14**) : this method allows the determination of all modal parameters from a set of free vibration measurements in a single analysis. However, it may not be the most appropriate technique if damping is of primary interest (**ref 15**).

### 2.2 Frequency Domain Methods

Basic methods in this group include half power point method, circle-fit method, line-fit method and power spectrum method, the first three methods being based on the frequency response functions (FRF) of a structure. The half-power point method, perhaps the simplest technique of all, predicts the damping level of the mode concerned using the natural frequency of that mode and two other frequencies at the half power points. (The half power points on an FRF are two points on either side of a natural frequency with magnitudes of $1/\sqrt{2}$ times that of the resonance peak.)

The circle- and line-fitting methods have almost become the standard tools for extracting modal parameters from measured FRFs. The circle-fit method uses the fact that a Nyquist plot of an FRF translates into a circle around resonance, the diameter of which provides a measure of the damping. A plot of the imaginary part of the inverse FRF against frequency on the other hand gives a straight line which forms the basis of the line-fit method. The damping level is then estimated from the slope of that line.

A new method of damping measurement, the power spectrum method, was proposed by Cawley and Sarsentis (**ref 8**). The impulse time history of a structure is recorded and divided into a series of sub-records each of which is subjected to a Fourier Transform. The resonant peaks of such successive records in frequency domain are plotted against

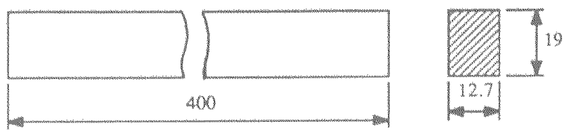


Fig.(1) Test specimen (All dimensions are in mm and not to scale)

time and the structural damping for each mode is obtained from this decay curve. The technique does not require the transient signal to die away within the measurement time.

## 3. Experimental Procedure

### 3.1 Description of Test Specimen

Experiments reported in this study were carried out on freely-supported rectangular bars. As shown in **Fig. (1)**, the test specimens were rectangular mild steel bars with nominal dimensions of $400 \times 19.0 \times 12.7$ mm. The dimensions of the bars were chosen such that the resulting FRFs showed clear and well-separated modes which were easy to identify. Fatigue cracks were produced under cyclic loading by using a 60 kN capacity of Dowty hydraulic testing machine.

There is no doubt that testing as many specimens as possible would provide better and more reliable data. However, as time and cost factors had to be weighted carefully, it was decided to consider 20 specimens only.

### 3.2 Description of the Experimental Setup

The two experimental setups shown in **Fig. (2)** were used throughout the investigation for FRF measurements. In the first case the structure was excited via an hammer. The signals from the accelerometer and force gauge were amplified and fed into a spectrum analyser, the output of which was fed into a micro computer for subsequent modal analysis. In the second case, a sine wave was generated by a frequency response analyser, amplified through a power amplifier and used to excite the structure via an electromagnetic shaker. The magnitude and phase of the amplified signals of force gauge and accelerometer were recorded by the analyser at each discrete frequency and transferred to the computer for post-processing.

### 3.3 Preliminary Tests

Before attempting to measure the natural frequencies and vibration damping levels of the bars, it was necessary to decide which type of excitation to use and which analysis method to apply for modal parameter identification. However, from the outset, it is worth mentioning that the purpose of these preliminary tests was not to find the limitations, advantages and shortcomings of various measuring techniques and analysis methods but to select the best options for this particular application.

It was decided to carry out preliminary tests on a test bar free of defects in order to assess the repeatability of the measurements. The initial idea of testing clamped-free bars was dropped because of the non-repeatability of clamping conditions.

One of the bars was tested first using sine excitation via a shaker. A washer was soldered to the bar for shaker attachment and the bar was supported on loops of fine string which were positioned at the nodes of the first flexural mode of vibration. The smallest shaker, force gauge and accelerometer available were attached very near the ends of the specimen for a point measurement in the direction of the smaller thickness. Initial measurements were made with a large frequency step to locate the first four natural frequencies. Zoom measurements were then carried out around each of these natural frequencies for accurate determination of the modal parameters. Measured data were analysed by using both circle- and line-fitting techniques which gave almost identical results and these are listed in **Table 1**.

Another set of measurements were carried out using impact testing, the excitation and response points and supporting strings' positions remaining at the same locations as before. Because of the very high frequency resolution required to analyse this lightly-damped rectangular bar, zoom measurements had to be made around each resonance. FRFs obtained from those measurements were then transferred to an IBM PC compatible microcomputer and the modal parameters for the first four modes were identified using once again circle- and line-fitting techniques. Results are given in **Table 2**.

As can be seen from **Tables 1** and **2**, natural frequencies obtained via sine sweep measurements are lower than those acquired by impact testing. This is almost certainly due to the mass effect of the force gauge attached to the bar. On the other hand, damping levels obtained from sine sweep measurements are much higher than those given by impact testing. It is believed that the main reason for obtaining high level of damping using sine sweep is the interaction between the specimen, the shaker and the force gauge.

After identifying the natural frequencies and damping levels of the test bar using two different measurement techniques, it was decided to focus on impact testing for the remainder of the experimental programme. Since every method of measuring the damping was bound to introduce some additional damping, a method which gives lower levels of damping seems to be preferable from this view point.

Although zoom measurements in impact testing seemed appropriate for the purpose of acquiring reliable data, this procedure was very time consuming (four modes per each bar and at least five averages for each mode meant about 800 tappings for the 20-bar set with and without fatigue cracks). It was therefore decided to investigate the possibility of using some other technique of damping identification. One possibility was to apply an exponential window to the time histories of response and force signals prior to the Fourier transform and to subtract the artificial damping introduced by this windowing right at the end. This procedure could have given the *correct* damping levels for each mode from a single measurement. However results were unrepeatable since the added damping due to exponential windowing was significantly higher than the true damping in the structure. Another possibility of determining the modal damping from a single measurement was to apply the power spectrum method of **reference (8)**. In this method, a Hanning window is applied to each of the successive segments of free time response data before carrying out a Fourier transform and it is claimed that this causes the leakage to be contained within the spectral points close to the resonance. Experimental results, however, showed that this was not the case. FRFs obtained from an actual transient responses with and without Hanning windows are shown in **Figs. (3a)** and **(3b)**. In the first case, a zoom measurement was carried out such a way that the response signal died away within the measurement time so that no windowing was necessary. In the second case, a typical measurement without zoom was made (because of very low level of damping the signal did not die away within the measurement time) and a Hanning window was applied to the time signal before carrying out a Fourier Transform. The true FRF, plotted in **Fig. (3a)**, shows no noise at all while the FRF obtained from the windowed signal exhibits clear signs of leakage with a totally distorted shape. This finding is also verified in **reference (16)**.

After this second round of preliminary tests, it was decided to carry out the rest of the experiments using impact testing with frequency zooming in spite of the process being slow. This decision was taken in the light of repeatability and the introduction of the least amount of artificial damping. In order to achieve a further reduction in artificial damping supporting strings were moved to the nodal lines of the mode being measured. The identification of these nodal lines was very easy by moving the tapping position of the hammer and observing the resulting FRF at the same time.

Impact measurements were then carried out for all 20 bars and the acquired FRF data were analysed to determine natural frequencies and damping levels for the first four modes of vibration using both circle- and line-fitting techniques which again gave very similar results. As can be seen from Table 3, natural frequencies and damping levels of the defect-free bars differ slightly from one bar to the next. Natural frequency variations are believed to be caused by minor differences in bars' geometric properties while variations in damping levels are probably due to small differences in surface properties (grease, finish etc.).

### 3.4 Fatigue Crack Formation and Testing of Bars with Cracks

There is no doubt that one of the most important factors affecting the vibration properties of a bar with a defect is the location of the crack. Although it would be desirable to make measurements on bars with different crack locations, this would be very costly and it was therefore decided to fix the crack position at some location away from the nodal lines of the first four modes of vibration as shown in **Fig. (4)**.

An initial notch of about 0.5 mm depth was introduced on each bar using a saw-cut. A very sharp saw cutter was then used to sharpen the tip of the notch. Cracks with various depths were formed by subjecting the bars to three-point bend fatigue loading in a Dowty 60 kN hydraulic testing machine. Since the exact profile of the notches across the cross section of the bars could not be controlled, it was not possible to predict the number of cycles required for crack initiation under a given level of loading. The relationship between the amplitude of stress applied, the number of cycles required for crack initiation and the crack growth rate were determined using an iterative method. For this purpose, bar no 20 was loaded first into the testing machine. A stress level of 250 $MN/m^2$ was applied first. The frequency of the sinusoidal excitation was kept at 30 Hz throughout crack formation. After 300,000 stress cycles, there was no sign of crack initiation, probably because of the size of the initial notch being too small. Then the stress level applied was increased and the specimen was kept under load for another 50,000 cycles. If there was still no sign of crack initiation, the stress level was increased further. At the end of this process, it was found that about 45,000 cycles were required for a crack initiation at 350 $MN/m^2$ stress level. Since the applied stress was displacement controlled, the force required for the same deflection with a crack was less than that without a crack. Thus, the area loss due to crack propagation was accomplished by the decreasing force applied.

In order to have a different crack depth for each bar, the desired depth was marked on each bar prior to stress loading. Fatigue crack growth was then observed through an optical instrument mounted on a two-dimensional traverse. Loading was stopped as soon as the crack depth had reached the required level. The number of cycles required for fatigue crack formation on each bar is given in **Table 4** together with the equivalent crack depth and percentage cross section removed. (The equivalent crack depth was measured after all the vibration measurements were completed.) The area around the fatigue crack was heated using a torch until the colour of the heated area changed to blue (tempered) and the bars were then soaked into liquid nitrogen and broken using the same hydraulic testing machine.

Since the scope of this study is to investigate the effects of fatigue crack on dynamic properties of a structure, care was taken to carry out all vibration measurements under as identical conditions as possible. However, there were still some factors which made measurements much more difficult when the bars had cracks. First of all, the fatigue cracks caused some degree of non-linearity which in turn depended on the crack depth. Secondly, although all modes were initially well-separated and in one direction only fatigue cracks caused coupling between coordinate directions. These problems created considerable difficulty during measurements and subsequent analyses. For minimising the errors and non-linearity effects, the magnitude of the impact force was kept as small as possible and special care was taken to apply the impact force in one direction in order not to excite the modes in the other direction. Because of these difficulties, zoom measurements for some of the modes had to be repeated several times. Once satisfactory FRFs were obtained, the natural frequencies and damping levels for the first four modes of 20 fatigue-cracked bars were obtained via modal analysis and results are listed in **Table 5**. After all vibration measurements were completed, the bars were broken for crack depth and area determination as described before.

## 4. Results

The percentage natural frequency change for each mode ( $100 * (\omega_{without\ crack} - \omega_{with\ crack}) / \omega_{without\ crack}$ ) is plotted against the percentage cross section removed (100 *

Crack area / Total area) in **Fig. (5)**. The natural frequency decrease is very small up to 20 % cross section removed, from which point it increases parabolically with increasing crack depth and this observation is valid for each mode. The susceptibility of the natural frequency of a particular mode to being affected by a crack is certainly related to the crack position and to the stress pattern of each mode. A close inspection of **Figs. (4)** and **(5)** reveals that it also depends on the proximity of the crack to high stress areas.

Another set of results is presented in **Figs. (6a)** to **(6d)** where the variation of damping with crack depth is shown. Unlike the natural frequency, the damping increases with increasing crack depth. Once again, the effect of the fatigue crack up to 20 % cross section removed is negligible, the resulting damping being comparable to initial damping levels. However, after that point there is a sudden increase and a maximum is reached around 60 % removed cross-section. The trend then levels off and damping starts to decrease again, indicating that the opposite surfaces lose rubbing action during vibration. As for the natural frequency, the susceptibility of the damping level of a particular mode being affected by a crack is related to the proximity of the crack to high stress areas.

The information in **Figs. (5)** and **(6)** is replotted in **Fig. (7)** in a different format: defining the relationship between the natural frequency reduction and damping increase caused by fatigue cracks, this perhaps being the most useful form for the mathematical modelling of fatigue crack effects. Remembering that the fatigue cracks cause almost no mass change to the bars, any frequency reduction can be interpreted as a modal stiffness change for each of the modes measured.

Finally, it is worth noting that although this experimental study was conducted with 20 rectangular bars, results in **Figs. (5)** to **(7)** refer to 18 bars only. Two specimens, Nos 11 and 18, were excluded from the final analysis. Bar No 11 was accidentally deformed plastically during the adjustment of the cyclic load while No 18 exhibited uncharacteristic behaviour. When the specimens were broken it was seen that No 18 had two distinct crack surfaces, the reason being that during crack generation under cyclic loading this bar had to be removed from loading and reloaded again. At that time, it was thought that this would not effect the crack behaviour. However, results clearly show that it did.

## 5. Concluding Remarks

(i) Before attempting any measurements on bars with and without fatigue cracks, it was necessary to find out the most suitable method of measurement. The critical parameter was the level of energy dissipation which showed marked variations depending on the measurement setup and technique used. Although exact damping levels of the bars were unknown, it is believed that measurements which gave both repeatable and lower damping values were the best for the purpose of this work since the amount of artificial damping was kept as a minimum.

(ii) The natural frequency and damping level changes produced by fatigue cracks were investigated experimentally. It is believed that this type of data leading to *dynamic* fatigue crack growth rate is very useful for life predictions of beam-like structures such as turbomachinery blades.

(iii) It was further found that:
-position of the fatigue crack is one of the primary factors affecting change in damping levels,
-the presence of a marked (more than 20% of total depth) fatigue crack in a structure decreases the structure's natural frequencies considerably and increases its energy dissipation by an order of magnitude if the initial damping is light.

## 6. References


**1-Halmshaw R.,** "Non-Destructive Testing", Metallurgy and Materials Science, Edward Published By Arnold Ltd., London 1987

**2-Hull J. B., Joh V. B.,** " Non-Destructive Testing", Published By Macmillan Education Ltd. London 1988

**3-Chan T. S.,** "Change of Damping Due to a Crack", Imperial College, MSc Thesis, 1982

**4-Okuba T.,** "Damping Changes Produced by Cracks", Imperial College, MSc Thesis, 1985

**5-Cawley P., Ray R.,** "A Comparison of the Natural Frequency Changes Produced by Cracks and Slots", J. Vib. Acous. Stress and Rel. in Des, July 1988, Vol.110, pp. 366-370

**6-Uygur E. M.,** "Research Technique in Non-Destructive Testing" (Sharp R. S. Edition), Vol.4, Academic Press, London

**7-Adams R. D., Cawley P.,** "Research Technique in Non-Destructive Testing" (Sharp R. S. Edition), Vol.8, pp.303-360, Academic Press, London

**8-Cawley P., Sarsentis N.,** "A Quick Method for the Measurement of Structural Damping", Mechanical Systems and Signal Processing, 2(1), pp.39-47, 1988

**9-Wei R. P.,Stephens R. I.,** ASME , "Fatigue Crack Growth Under Spectrum Loads", Special Technical Publication, No.595, May 1976

**10-Duggan T. V., Byrne J.,**"Fatigue as a design criterion", The Macmillan Press Ltd.,1979

**11-Pook L. P.,** "The Role of Crack Growth in Metal Fatigue", Published by the Metal Society, London, 1983

**12-Halford G. R., et. al.,** " Fatigue Life Prediction Modelling for Turbine Hot Section Materials", Journal of Engineering for Gas Turbines and Power, April 1989, Vol. 111, pp.279-285

**13-Ibrahim S. R., Mikuleik E. C.,** "A Method for the Direct Identification of Vibration Parameters from Free Responses", Shock and Vibration Bulletin, 47, 1977

**14-Pappa R. S., Ibrahim S. R.,** "A Parametric Study of the Ibrahim Time Domain Modal Identification Algorithm", Shock and Vibration Bulletin, 51(3), 1981

**15-Ewins D. J.,** "Modal Testing: Theory and Practice", Research Studies Press, 1984

**16-Hewlett Packard,** Application Note: The Fundamentals of Signal Analysis, No.243

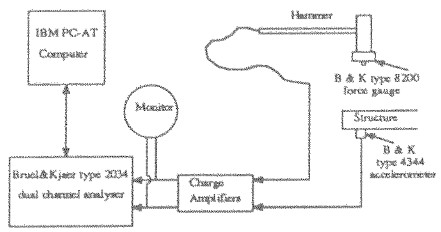


**Fig.(2a) Experimental setup for Impact Testing.**

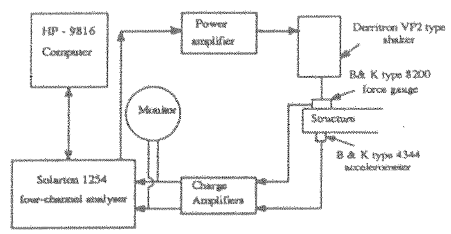


**Fig. (2b) Experimental setup for sine sweep testing**

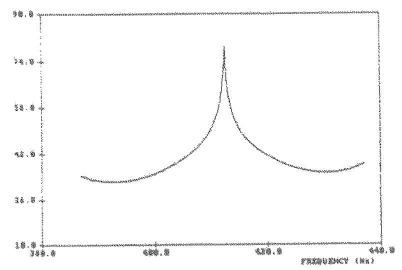

Fig. (3a) FRF from raw transient signal. No windowing.

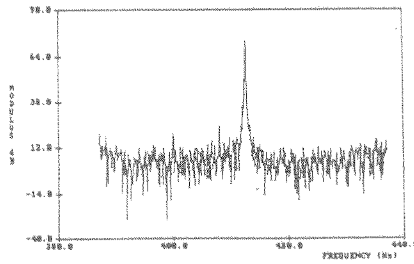

Fig. (3b) FRF from Hanning windowed transient signal.

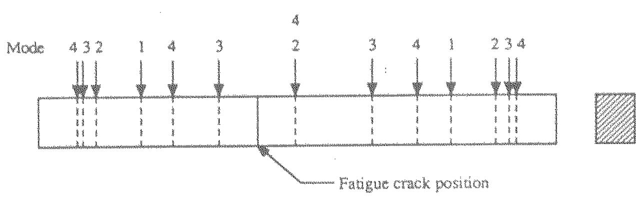


Fig. (4) Crack position and nodal points along the specimen

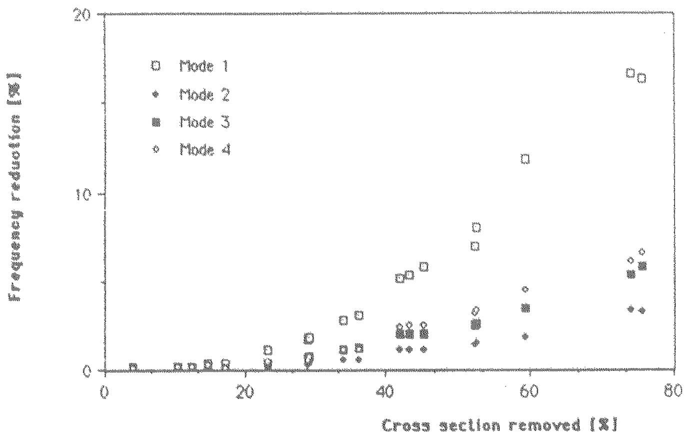


Fig. (5) Natural frequency change vs removed cross-section area

803

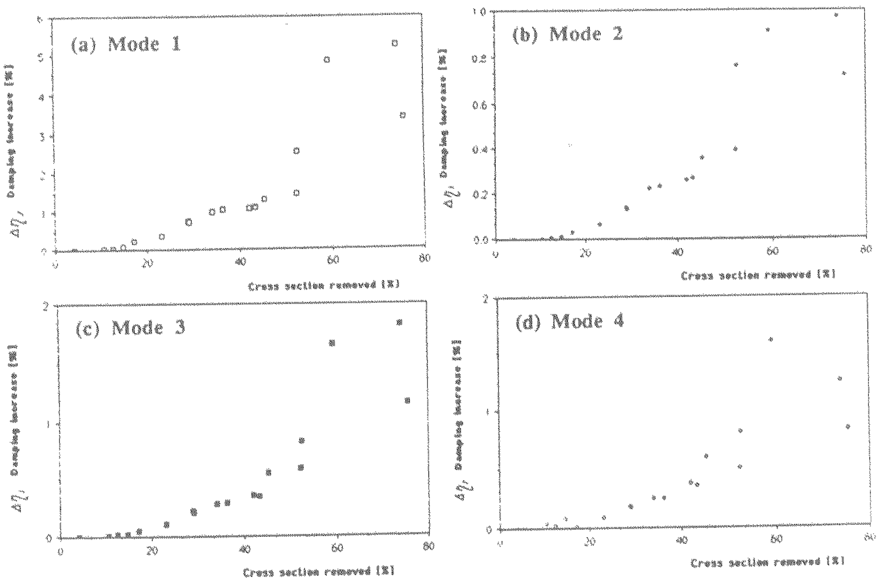


Fig. (6) Damping change vs removed cross-section area

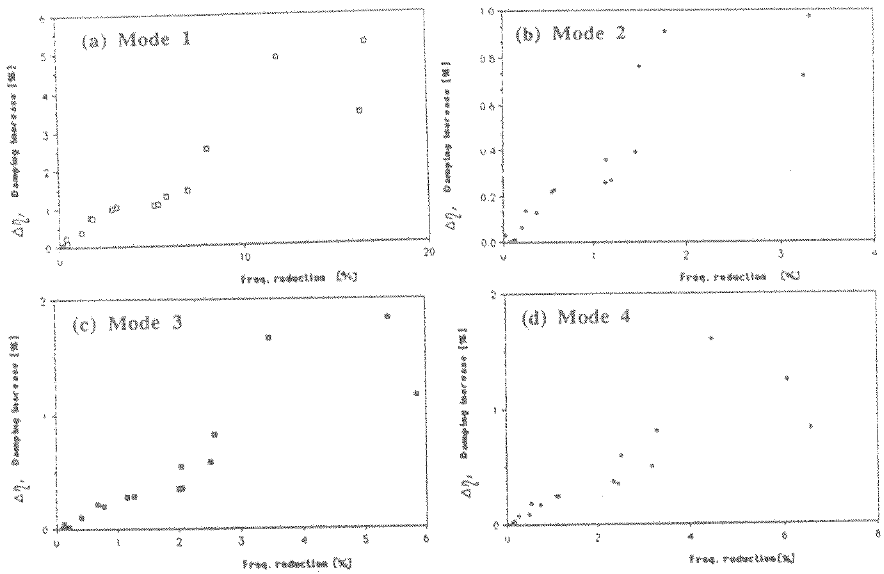


Fig. (7) Relationship between frequency reduction and damping increase

Table 1. Natural frequency and damping levels of test bar using sine sweep testing

| Mode | Frequency [Hz] | Damping $\eta$ [%] |
|---|---|---|
| 1 | 395 | 0.142 |
| 2 | 1080 | 0.280 |
| 3 | 2074 | 0.940 |
| 4 | 3465 | 1.172 |

Table 2. Natural frequencies and damping levels of test bar using Impact Testing

| Mode | Frequency [Hz] | Damping $\eta$ [%] |
|---|---|---|
| 1 | 412 | 0.050 |
| 2 | 1131 | 0.070 |
| 3 | 2198 | 0.090 |
| 4 | 3593 | 0.190 |

Table 3. Natural frequencies and damping levels of bars without fatigue cracks

| Bar | Mode 1 | | Mode 2 | | Mode 3 | | Mode 4 | |
|---|---|---|---|---|---|---|---|---|
| No | $\omega_1$ [Hz] | $\eta_1$ [%] | $\omega_2$ [Hz] | $\eta_2$ [%] | $\omega_3$ [Hz] | $\eta_3$ [%] | $\omega_4$ [Hz] | $\eta_4$ [%] |
| 1 | 413.9 | 0.044 | 1134.4 | 0.062 | 2204.2 | 0.058 | 3601.1 | 0.134 |
| 2 | 410.6 | 0.046 | 1125.1 | 0.065 | 2186.5 | 0.055 | 3572.5 | 0.125 |
| 3 | 412.5 | 0.044 | 1130.8 | 0.064 | 2197.5 | 0.057 | 3590.5 | 0.125 |
| 4 | 413.9 | 0.042 | 1134.0 | 0.063 | 2203.5 | 0.055 | 3600.0 | 0.112 |
| 5 | 410.4 | 0.046 | 1124.4 | 0.062 | 2185.5 | 0.054 | 3571.3 | 0.130 |
| 6 | 412.0 | 0.044 | 1129.4 | 0.062 | 2194.8 | 0.058 | 3586.0 | 0.123 |
| 7 | 411.5 | 0.045 | 1127.8 | 0.066 | 2191.2 | 0.052 | 3580.2 | 0.122 |
| 8 | 411.9 | 0.040 | 1128.4 | 0.070 | 2193.2 | 0.065 | 3584.2 | 0.123 |
| 9 | 415.2 | 0.040 | 1138.0 | 0.058 | 2210.8 | 0.055 | 3611.4 | 0.113 |
| 10 | 411.8 | 0.042 | 1128.6 | 0.070 | 2193.5 | 0.060 | 3584.4 | 0.121 |
| 11 | 409.8 | 0.052 | 1123.0 | 0.065 | 2181.8 | 0.055 | 3566.3 | 0.148 |
| 12 | 413.2 | 0.043 | 1132.5 | 0.061 | 2200.5 | 0.058 | 3595.0 | 0.157 |
| 13 | 412.2 | 0.041 | 1129.8 | 0.063 | 2195.5 | 0.057 | 3587.6 | 0.118 |
| 14 | 412.1 | 0.040 | 1129.3 | 0.063 | 2195.0 | 0.055 | 3586.9 | 0.124 |
| 15 | 411.9 | 0.041 | 1129.0 | 0.068 | 2194.2 | 0.057 | 3584.4 | 0.116 |
| 16 | 413.8 | 0.041 | 1133.8 | 0.061 | 2203.2 | 0.056 | 3600.0 | 0.134 |
| 17 | 410.6 | 0.043 | 1125.0 | 0.062 | 2186.2 | 0.063 | 3572.0 | 0.128 |
| 18 | 412.6 | 0.043 | 1131.0 | 0.068 | 2197.6 | 0.063 | 3590.5 | 0.132 |
| 19 | 413.5 | 0.043 | 1133.1 | 0.065 | 2201.8 | 0.062 | 3597.0 | 0.140 |
| 20 | 412.5 | 0.042 | 1130.6 | 0.068 | 2197.2 | 0.060 | 3590.5 | 0.125 |
| Min | 409.8 | 0.040 | 1123.0 | 0.058 | 2181.8 | 0.052 | 3571.3 | 0.112 |
| Max | 415.2 | 0.052 | 1138.0 | 0.070 | 2210.8 | 0.063 | 3611.4 | 0.157 |
| Mean | 412.3 | 0.043 | 1129.9 | 0.064 | 2195.7 | 0.058 | 3587.6 | 0.127 |
| S D | 1.361 | 0.003 | 3.784 | 0.003 | 7.232 | 0.003 | 11.482 | 0.011 |

S D = Standard deviation.

Table 4. Description of fatigue cracks on bars

| Bar No | No. of stress cycles applied | Equivalent crack depth [mm] | Area removed [%] |
|---|---|---|---|
| 1 | 0 | 0.50 | 3.94 |
| 2 | 63000 | 1.32 | 10.39 |
| 3 | 68000 | 1.59 | 12.52 |
| 4 | 73000 | 1.85 | 14.57 |
| 5 | 70000 | 2.16 | 17.01 |
| 6 | 94000 | 2.93 | 23.07 |
| 7 | 120000 | 3.70 | 29.13 |
| 8 | 123000 | 3.65 | 28.74 |
| 9 | 129000 | 4.30 | 33.86 |
| 10 | 122000 | 4.60 | 36.22 |
| 11 | Plastic deformation occured during fatigue crack formation. | | |
| 12 | 108000 | 5.32 | 41.89 |
| 13 | 90000 | 5.50 | 43.31 |
| 14 | 90000 | 5.75 | 45.28 |
| 15 | 109000 | 6.68 | 52.60 |
| 16 | 180000 | 6.65 | 52.36 |
| 17 | 114000 | 7.55 | 59.45 |
| 18 | 108000 | 8.00 | 63.00 |
| 19 | 157000 | 9.60 | 75.60 |
| 20 | 807000 | 9.40 | 74.02 |

Table 5. Natural frequencies and damping levels of bars with a fatigue crack

| Bar | Mode 1 | | Mode 2 | | Mode 3 | | Mode 4 | |
|---|---|---|---|---|---|---|---|---|
| No | $\omega_1$ [Hz] | $\eta_1$ [%] | $\omega_2$ [Hz] | $\eta_2$ [%] | $\omega_3$ [Hz] | $\eta_3$ [%] | $\omega_4$ [Hz] | $\eta_4$ [%] |
| 1 | 413..2 | 0.05 | 1133.5 | 0.06 | 2202.2 | 0.06 | 3597.3 | 0.13 |
| 2 | 409.7 | 0.07 | 1124.2 | 0.06 | 2184.2 | 0.07 | 3567.2 | 0.17 |
| 3 | 411.6 | 0.08 | 1129.6 | 0.07 | 2195.0 | 0.07 | 3589.0 | 0.14 |
| 4 | 412.4 | 0.13 | 1132.5 | 0.07 | 2199.0 | 0.07 | 3590.5 | 0.19 |
| 5 | 409.0 | 0.28 | 1124.1 | 0.09 | 2183.0 | 0.10 | 3568.0 | 0.14 |
| 6 | 407.1 | 0.40 | 1127.0 | 0.12 | 2186.0 | 0.17 | 3568.0 | 0.21 |
| 7 | 404.2 | 0.80 | 1123.5 | 0.20 | 2174.6 | 0.25 | 3553.0 | 0.30 |
| 8 | 405.0 | 0.81 | 1125.5 | 0.21 | 2178.7 | 0.28 | 3564.0 | 0.31 |
| 9 | 403.5 | 1.04 | 1131.8 | 0.28 | 2185.4 | 0.34 | 3571.6 | 0.36 |
| 10 | 399.0 | 1.10 | 1122.1 | 0.30 | 2165.9 | 0.35 | 3543.2 | 0.37 |
| 11 | Plastic Deformation occured during fatigue crack formation | | | | | | | |
| 12 | 391.8 | 1.13 | 1119.7 | 0.32 | 2155.6 | 0.41 | 3510.2 | 0.53 |
| 13 | 390.0 | 1.16 | 1116.3 | 0.33 | 2151.7 | 0.40 | 3499.3 | 0.47 |
| 14 | 388.2 | 1.37 | 1116.4 | 0.42 | 2150.4 | 0.60 | 3496.0 | 0.71 |
| 15 | 378.8 | 2.60 | 1112.0 | 0.83 | 2138.2 | 0.89 | 3465.7 | 0.92 |
| 16 | 385 | 1.50 | 1117.2 | 0.45 | 2148.2 | 0.64 | 3485.0 | 0.63 |
| 17 | 361.8 | 4.88 | 1104.9 | 0.97 | 2110.7 | 1.72 | 3412.0 | 1.73 |
| 18 | 345.6 | 0.82 | 1093.0 | 0.17 | 2065.2 | 0.31 | 3552.0 | 0.33 |
| 19 | 346.0 | 3.47 | 1096.2 | 0.78 | 2073.0 | 1.22 | 3360.0 | 0.96 |
| 20 | 343.7 | 5.26 | 1093.0 | 1.04 | 2079.0 | 1.89 | 3372.0 | 1.37 |

# APPENDIX IV

# DERIVATION OF $\beta_{ij}(\omega)$ FOR A CANTILEVER BEAM

$\beta_{ij}(\omega)$ referred in chapter 4 is defined as the ratio of the stress at point i to the response at point j.

$$\beta_{ij}(\omega) = \frac{\sigma(s)|_{s=s_i}}{q(s)|_{s=s_j}} \tag{AIV.1}$$

The deflection equation per unit force for a uniform cantilever beam shown in Fig. AIV.1 is given by **Bishop** and **Johnson** (1979):

$$q(s) = \frac{(\sin\lambda L+\sinh\lambda L)(\cos\lambda s-\cosh\lambda s)-(\cos\lambda L+\cosh\lambda L)(\sin\lambda s-\sinh\lambda s)}{2EI\lambda^3(1+\cos\lambda L+\cosh\lambda L)} \tag{AIV.2}$$

where

$$\lambda^4 = \frac{\rho A\omega^2}{EI}$$

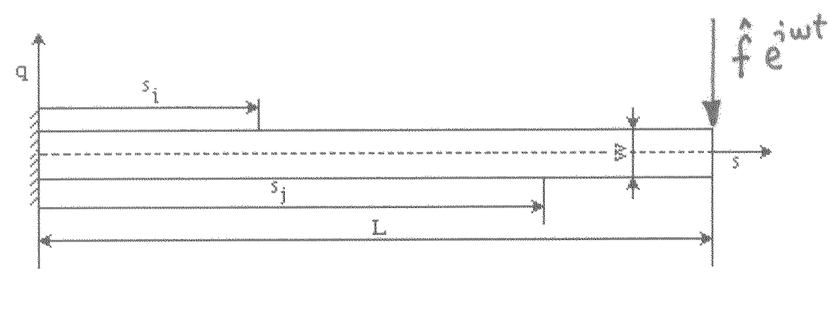


**Fig. AIV.1** A cantilever beam.
(Cantilever beam's dimensions : 19.0*12.7*400 mm, $s_i$ = 17.0 mm, $s_j$ =400 mm)

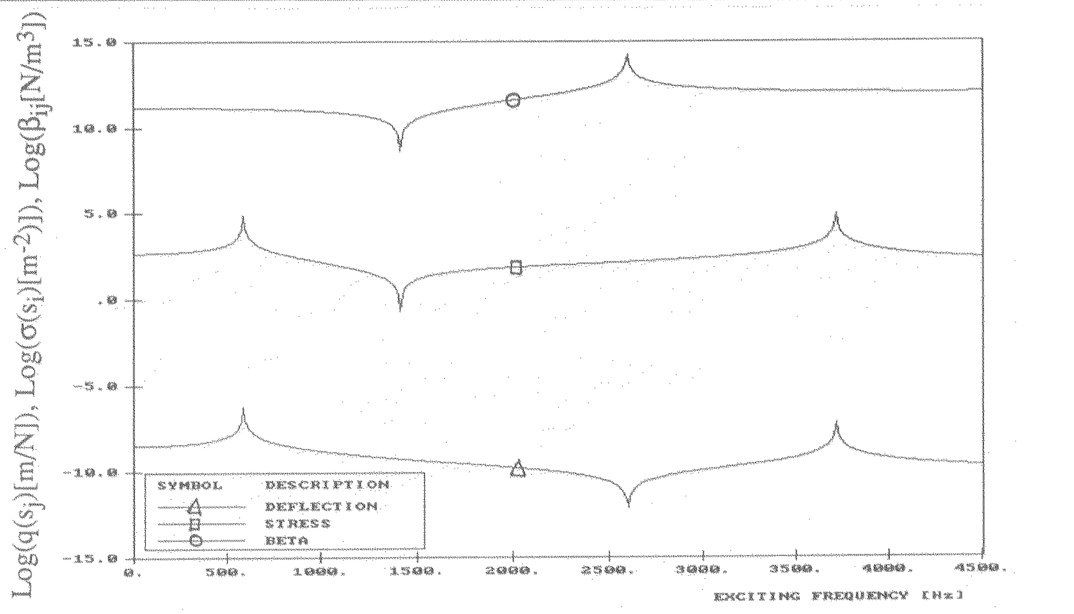


**Fig. AIV.2** $q(s_j)$, $\sigma(s_i)$ and $\beta_{ij}(\omega)$ versus frequency.

and all variables have their customary meanings. The stress at the beam surface can be found from:

$$\sigma(s) = \frac{Ew}{2} \frac{d^2q(s)}{ds^2} \tag{AIV.3}$$

where w is the thickness of the cantilever beam. Using (AIV.2) and (AIV.3), the stress parameter $\beta_{ij}(\omega)$ can be written as:

$$\beta_{ij}(\omega) = \frac{E\lambda^2 w}{2} \frac{\left[ (-\cos\lambda s_i - \cosh\lambda s_i) - \dfrac{\cos\lambda L+\cosh\lambda L}{\sin\lambda L+\sinh\lambda L}(-\sin\lambda s_i - \sinh\lambda s_i) \right]}{\left[ (\cos\lambda s_j - \cosh\lambda s_j) - \dfrac{\cos\lambda L+\cosh\lambda L}{\sin\lambda L+\sinh\lambda L}(\sin\lambda s_j - \sinh\lambda s_j) \right]} \tag{AIV.4}$$

The variations of $q(s_j)$ ,$\sigma(s_i)$ and $\beta_{ij}(\omega)$ with respect to frequency are plotted in Fig. AIV.2.

# APPENDIX V

# ELEMENTS OF THE MATRIX [S]

The elements of the matrix $[S]_{5sNx4(s+1)N}$ are given by

$$S_{ir,ic} = \frac{\partial g_{ir}}{\partial \gamma_{ic}}$$

For $\ell$=1,2,3,...,s and j=1,2,3,...,N the non-zero elements of the [S] matrix in Eq. (7.11) are:

$$\frac{\partial g_{5s(j-1)+5\ell-4}}{\partial \gamma_{4s(j-1)+j}} = \frac{\partial g_{5s(j-1)+5\ell-4}}{\partial G_j} = -2\zeta\omega_\ell\, {}_IX_j(\omega_\ell)+2G_j({}_RX_j(\omega_\ell)-\eta\, {}_IX_j(\omega_\ell)-{}_RY_j(\omega_\ell)+\eta\, {}_IY_j(\omega_\ell))$$

$$\frac{\partial g_{5s(j-1)+5\ell-4}}{\partial \gamma_{4s(j-1)+4\ell+j-3}} = \frac{\partial g_{5s(j-1)+5\ell-4}}{\partial {}_RX_j(\omega_\ell)} = -\ \omega_\ell^2 + G_j^2$$

$$\frac{\partial g_{5s(j-1)+5\ell-4}}{\partial \gamma_{4s(j-1)+4\ell+j-2}} = \frac{\partial g_{5s(j-1)+5\ell-4}}{\partial {}_IX_j(\omega_\ell)} = -\ 2\zeta G_j\, \omega_\ell - \eta G_j^2$$

$$\frac{\partial g_{5s(j-1)+5\ell-4}}{\partial \gamma_{4s(j-1)+4\ell+j-1}} = \frac{\partial g_{5s(j-1)+5\ell-4}}{\partial {}_RY_j(\omega_\ell)} = -\ G_j^2$$

$$\frac{\partial g_{5s(j-1)+5\ell-4}}{\partial \gamma_{4s(j-1)+4\ell+j}} = \frac{\partial g_{5s(j-1)+5\ell-4}}{\partial {}_IY_j(\omega_\ell)} = \eta G_j^2$$

$$\frac{\partial g_{5s(j-1)+5\ell-3}}{\partial \gamma_{4s(j-1)+j}} = \frac{\partial g_{5s(j-1)+5\ell-3}}{\partial G_j} = 2\zeta\omega_\ell\, {}_RX_j(\omega_\ell)+2G_j({}_IX_j(\omega_\ell)+\eta\, {}_RX_j(\omega_\ell)-{}_IY_j(\omega_\ell)-\eta\, {}_RY_j(\omega_\ell))$$

$$\frac{\partial g_{5s(j-1)+5\ell-3}}{\partial \gamma_{4s(j-1)+4\ell+j-3}} = \frac{\partial g_{5s(j-1)+5\ell-3}}{\partial {}_RX_j(\omega_\ell)} = 2\zeta G_j\, \omega_\ell + \eta G_j^2$$

$$\frac{\partial g_{5s(j-1)+5\ell-3}}{\partial \gamma_{4s(j-1)+4\ell+j-2}} = \frac{\partial g_{5s(j-1)+5\ell-3}}{\partial {}_IX_j(\omega_\ell)} = -\ \omega_\ell^2 + G_j^2$$

$$\frac{\partial g_{5s(j-1)+5\ell-3}}{\partial \gamma_{4s(j-1)+4\ell+j-1}} = \frac{\partial g_{5s(j-1)+5\ell-3}}{\partial_R Y_j(\omega_\ell)} = -\eta G_j^2$$

$$\frac{\partial g_{5s(j-1)+5\ell-3}}{\partial \gamma_{4s(j-1)+4\ell+j}} = \frac{\partial g_{5s(j-1)+5\ell-3}}{\partial_I Y_j(\omega_\ell)} = -G_j^2$$

$$\frac{\partial g_{5s(j-1)+5\ell-2}}{\partial \gamma_{4s(j-1)+j}} = \frac{\partial g_{5s(j-1)+5\ell-2}}{\partial G_j} = 2G_j\left({}_R Y_j(\omega_\ell) - \eta\, {}_I Y_j(\omega_\ell) - {}_R X_j(\omega_\ell) + \eta\, {}_I X_j(\omega_\ell)\right)$$

$$\frac{\partial g_{5s(j-1)+5\ell-2}}{\partial \gamma_{4s(j-1)+4\ell+j-3}} = \frac{\partial g_{5s(j-1)+5\ell-2}}{\partial_R X_j(\omega_\ell)} = -G_j^2$$

$$\frac{\partial g_{5s(j-1)+5\ell-2}}{\partial \gamma_{4s(j-1)+4\ell+j-2}} = \frac{\partial g_{5s(j-1)+5\ell-2}}{\partial_I X_j(\omega_\ell)} = \eta G_j^2$$

$$\frac{\partial g_{5s(j-1)+5\ell-2}}{\partial \gamma_{4s(j-1)+4\ell+j-1}} = \frac{\partial g_{5s(j-1)+5\ell-2}}{\partial_R Y_j(\omega_\ell)} = -\omega_\ell^2 \frac{M_d}{m} + G_j^2 + \frac{k_g}{m} + 2\frac{K_d}{m}$$

$$\frac{\partial g_{5s(j-1)+5\ell-2}}{\partial \gamma_{4s(j-1)+4\ell+j}} = \frac{\partial g_{5s(j-1)+5\ell-2}}{\partial_I Y_j(\omega_\ell)} = -\eta G_j^2$$

$$\frac{\partial g_{5s(j-1)+5\ell-2}}{\partial \gamma_{4s(j-2)+4\ell+j-2}} = \frac{\partial g_{5s(j-1)+5\ell-2}}{\partial_R Y_{j-1}(\omega_\ell)} = -\frac{K_d}{m}$$

$$\frac{\partial g_{5s(j-1)+5\ell-2}}{\partial \gamma_{4sj+4\ell+j}} = \frac{\partial g_{5s(j-1)+5\ell-2}}{\partial_R Y_{j+1}(\omega_\ell)} = -\frac{K_d}{m}$$

$$\frac{\partial g_{5s(j-1)+5\ell-1}}{\partial \gamma_{4s(j-1)+j}} = \frac{\partial g_{5s(j-1)+5\ell-1}}{\partial G_j} = 2G_j\left({}_I Y_j(\omega_\ell) + \eta\, {}_R Y_j(\omega_\ell) - {}_I X_j(\omega_\ell) - \eta\, {}_R X_j(\omega_\ell)\right)$$

$$\frac{\partial g_{5s(j-1)+5\ell-1}}{\partial \gamma_{4s(j-1)+4\ell+j-3}} = \frac{\partial g_{5s(j-1)+5\ell-1}}{\partial_R X_j(\omega_\ell)} = -\eta G_j^2$$

$$\frac{\partial g_{5s(j-1)+5\ell-1}}{\partial \gamma_{4s(j-1)+4\ell+j-2}} = \frac{\partial g_{5s(j-1)+5\ell-1}}{\partial_I X_j(\omega_\ell)} = -G_j^2$$

$$\frac{\partial g_{5s(j-1)+5\ell-1}}{\partial \gamma_{4s(j-1)+4\ell+j-1}} = \frac{\partial g_{5s(j-1)+5\ell-1}}{\partial_R Y_j(\omega_\ell)} = \eta G_j^2$$

$$\frac{\partial g_{5s(j-1)+5\ell-1}}{\partial \gamma_{4s(j-1)+4\ell+j}} = \frac{\partial g_{5s(j-1)+5\ell-1}}{\partial_I Y_j(\omega_\ell)} = -\,\omega_\ell^2 \frac{M_d}{m} + G_j^2 + \frac{k_g}{m} + 2\,\frac{K_d}{m}$$

$$\frac{\partial g_{5s(j-1)+5\ell-1}}{\partial \gamma_{4s(j-2)+4\ell+j-1}} = \frac{\partial g_{5s(j-1)+5\ell-1}}{\partial_I Y_{j-1}(\omega_\ell)} = -\,\frac{K_d}{m}$$

$$\frac{\partial g_{5s(j-1)+5\ell-1}}{\partial \gamma_{4sj+4\ell+j+1}} = \frac{\partial g_{5s(j-1)+5\ell-1}}{\partial_I Y_{j+1}(\omega_\ell)} = -\,\frac{K_d}{m}$$

$$\frac{\partial g_{5s(j-1)+5\ell}}{\partial \gamma_{4s(j-1)+4\ell+j-3}} = \frac{\partial g_{5s(j-1)+5\ell}}{\partial_R X_j(\omega_\ell)} = 2\,{}_R X_j(\omega_\ell)$$

$$\frac{\partial g_{5s(j-1)+5\ell}}{\partial \gamma_{4s(j-1)+4\ell+j-2}} = \frac{\partial g_{5s(j-1)+5\ell}}{\partial_I X_j(\omega_\ell)} = 2\,{}_I X_j(\omega_\ell)$$

# REFERENCES


[1] **Afolabi, H. D.** (1982)
*"Vibration of Mistuned Bladed Disc Assemblies"*, Ph.D Thesis, Imperial Colege, University of London.

[2] **Afolabi, H. D.** (1985a)
*"The Frequency Response of Mistuned Bladed Disk Assemblies"*, Proceedings of ASME on Vibration of Blades and Bladed Disk Assemblies.

[3] **Afolabi, H. D.** (1985b)
*"The Eigenvalue Spectrum of a Mistuned Bladed Disk"*, Proceedings of ASME on Vibration of Blades and Bladed Disk Assemblies.

[4] **Afolabi, H. D.** (1988a)
*"A Note on the Rogue Failure of Turbine Blades"*, Journal of Sound and Vibration, Vol. 122, No.3, pp 535-545.

[5] **Afolabi, H. D.** (1988b)
*"Vibration Amplitudes of Mistuned Blades"*, Trans. ASME, Journal of Turbomachinery, Vol. 110, Apr., pp 251-257.

[6] **Alawi, H.** (1989)
*"Fatigue Crack Growth Prediction Under Random Peaks and Sequence Loading"*, ASME, Journal of Engineering Materials and Technology, Vol.111, pp.339-344, Oct.

[7] **Armstrong, E. K., Christie, P. I.** and **Hague, W. M.** (1966)
*"Natural Frequencies of Bladed Discs"*, Proccedings of the Institute of Mechanical Engineers, Vol. 180, Part 3I.

[8] **Basu, P.** and **Griffin, J. H.** (1986)
*"The Effect of Limiting Aerodynamic and Structural Coupling in Models of Mistuned Bladed Disk Vibration"*, Trans. ASME, Journal of Vibration, Acoustics, Stress and Reliability in Design, Vol. 108, Apr., pp 132-139.

[9] **Beliven, D. O.** (1969)
*"On Frequencies of Elastic Beams with Random Imperfactions"*, Journal of Fnanklin Institute, Vol. 287, No.4, Apr., pp 294-304.

[10] **Bendiksen, O. O.** (1984)
*"Flutter of Mistuned Turbomachinery Rotors"*, Trans. ASME, Journal of Engineering for Gas Turbines and Power, Vol. 106, Jan., pp 25-33.

[11] **Bishop, R. E. D.** and **Johnson, D. J.** (1979)
*"The Mechanics of Vibration"*, Cambridge University Press.

[12] **Crawley, E. F.** and **Hall, K. C.** (1985) *"Optimization and Mechanism of Mistuning in Cascades"*, Trans. ASME, Journal of Engineering for Power, Vol. 107, Apr., pp 418-426.

[13] **Davies, O. L.** and **Goldsmith P. L.**(1972)
*"Statistical Methods in Research and Production"*, Oliver & Boyd press.

[14] **Davis, P. J.** (1979)
*"Circulant Matrices"*, John Wiley and Sons Puplication, New York.

[15] **Dowling, N. E.** (1983)
*"Fatigue Life Prediction for Complex Load Versus Time Histories"*, ASME, Journal of Engineering Materials and Technology, Vol.105, pp.207-214, July.

[16] **Dye, R. C. F.** and **Henry, T. A.** (1969)
*"Vibration Amplitudes of Compressor Blades Resulting from Scatter in Blade Natural Frequencies"*, Trans. ASME, Journal of Engineering for Power, July, pp 182-188.

[17] **Ealpole, R. E.** and **Myers R. H.**(1985)
*"Probability and Statistics for Engineers and Scientists"*, Macmillan Publishing Company.

[18] **El-Bayoumy, L. E.** and **Srinivasan, A. V.** (1975)
*"Influence of Mistuning on Rotor-Blade Vibration"*, AIAA Journal, Vol.13, No. 4, Apr., pp 460-464.

[19] **Ewalds, H. L.** and **Wanhill, R. J. H.** (1986)
*"Fracture Mechanics"*, Edward Arnold Ltd.

[20] **Ewins, D. J.** (1966)
*"The Vibration of Bladed Discs"*, Ph.D Thesis, University of Cambridge.

[21] **Ewins, D. J.** (1969,)
*"The Effect of Detuning Upon the Forced Vibration of Braded Disks"*, Journal of Sound and Vibration, Vol. 9, No. 1, pp 65-79.

[22] **Ewins, D. J.** (1973)
*"Vibration Characteristics of Bladed Disc Assemblies"*, Journal of Mechanical engineering Science, Vol. 12, No. 5, pp 165-186.

[23] **Ewins, D. J.** (1976)
*"An Experimental Investigation of the Forced Vibration of Bladed Discs due to Aerodynamic Excitation"*, Proceedings of ASME on Structural Dynamics Aspects of Bladed Disk Assemblies, Dec., pp 15-27.

[24] **Ewins, D. J.**(1973)
*"Vibration Characteristics of Bladed Disc Assemblies"*, Journal of Mechanical Engineering Science, Vol.15, No.3, pp.165-186.

[25] **Ewins, D. J.** (1984)
*"Modal Testing: Theory and Practise"*, Research Studies Press Ltd., England.

[26] **Ewins, D. J.** (1980)
*"Bladed Disc Vibration: A Review of Techniques and Characteristics"*, Int. Conf. of Recent Adv. Struct. Dynamics, Southampton, UK, pp 187-210.

[27] **Ewins, D. J.** (1991)
*"The Effects of Blade Mistuning on Vibration Response - A Survey"*, IFToMM 4th International Conference on Rotodynamics, Prague, Czechoslovakia, Aug.

[28] **Ewins, D. J.** and **Han, Z. S.** (1984)
*"Resonant Vibration Levels of a Mistuned Bladed Disk"*, Trans. ASME, Journal of Vibration, Acoustics, Stress and Reliability in Design, Vol. 106,pp 211-217.

[29] **Ewins, D. J.** and **Rao, Y. V. K. S.** (1976)
*"A Theoretical Study of the Damped Forced Vibration Response of Bladed Discs"*, Proceedings of ASME on Structural Dynamics Aspects of Bladed Disk Assemblies, Dec., pp 57-71.

[30] **Fabunmi, J. A.** (1980)
*"Forced Vibrations of a Single Stage Axial Compressor Rotor"*, Trans. ASME, Journal of Engineering for Power, Vol. 102, Apr., pp 322-328.

[31] **Findly, W. N.** and **Reed, R. M.** (1983)
*"Fatigue of Autofrettaged thick Tubes: Closed and Open Ended; As-Received and Honed"*, Journal Eng. Materials, Vol.105, PP. 195-205, July.

[32] **Fisher, B. C.** and **Sherratt, F.** (1977)
*"A Fracture Mechanics Analysis of Fatigue Crack Growth Data for Short Cracks"*, Fracture Mechanics in Engineering Practise, Edited by Stanley P., Applied Science Publisher Ltd, London.

[33] **Fong J. T.** (1979)
*"Fatigue Mechanisms"*, American Society for Testing and Materials.

[34] **Forman, R. G., Kearney, V. E.** and **Egle, R. M.** (1967)
*"Numerical Analysis of Crack Propagation in Cyclic Loaded Structures"*, ASME, Journal of Basic Engineering, Vol.89, No.3, pp.459-464.

[35] **Gibra, I. N.** (1973)
*"Probability and Statistical Inference for Scientists and Engineers"*, Prentice-Hall, Inc.

[36] **Gladwell, G. M. L.** (1986)
*"Inverse Problems in Vibrations"*, Martinus Nijhoff Publishers.

[37] **Griffin, J. H.** (1991)
*"Optimizing Instrumentation When Measuring Jet Engine Blade Vibration"*, ASME, Presented at the International Gas Turbine and Aeroengine Congress and Exposition, Orlando, FL, June 3-6, 91-GT-71.

[38] **Griffin, J. H.** (1980)
*"Friction Damping of Resonant Stresses in Gas Turbine Engine Airfoils."*, Trans. ASME, Journal of Engineering for Power, Vol. 102, Apr., pp 329-333.

[39] **Griffin, J. H.** and **Hoosac, T. M.** (1984)
*"Model Development and Statiscal Investigation of Turbine Blade Mistuning"*, Trans. ASME, Journal of Vibration, Acoustics, Stress and Reliability in Design, Vol. 106, pp 204-210.

[40] **Griffin, J. H.** and **Sinha, A.** (1985)
*"The Interaction Between Mistuning and Friction in the Forced Response of Bladed Disk Assemblies"*, Trans. ASME, Journal of Engineering for Gas Turbines and Power, Vol. 107, pp 205-211.

[41] **Huang, W. H.** (1982)
*"Vibration of Some Structures with Periodic Random Parameters"*, AIAA Journal, Vol. 20, No. 7, pp 1001-1008.

[42] **Ibrahim, R. A.** (1987)
*"Structural Dynamics with Parameter Uncertainties"*, ASME, Appl. Mech. Rev. Vol.20, No. 3, pp 309-328

[43] **Imregun, M.** (1984)
*"Structural and Aeroelastic Vibration Analysis of Bladed Systems"*,Ph.D Thesis, Imperial College, London.

[44] **James, L. A.** (1971)
*"The Effects of Frequency Upon the Fatigue Crack Growth of Type 304 Stainless Steel at 1000 F"*, Stress Analysis and Growth of Cracks, Proceedings of the National Symposium on Fracture Mechanics, Part 1, pp.218-230.

[45] **Kaza, K. R. V.** and **Kielb, R. E.** (1982a)
*"Coupled Bending-Bending-Torsion Flutter of a Mistuned Cascade with Nonuniform Blades"*, NASA Report No. TM-82813, May.

[46] **Kaza, K. R. V.** and **Kielb, R. E.** (1982b)
*"Flutter and Response of a Mistuned Cascade in Incompressible Flow"*, AIAA Journal, Vol. 20, No.8, Aug., pp 1120-1127.

[47] **Kaza, K. R. V.** and **Kielb, R. E.** (1984)
*"Flutter of Turbofan Rotors with Mistuned Blades"*, AIAA Journal, Vol. 22, No. 11, Nov., pp 1618-1625.

[48] **Kaza, K. R. V.** and **Kielb, R. E.** (1985)
*"Vibration and Flutter of Mistuned Bladed-Disk Assemblies"*, AIAA Journal of Propulsion and Power, Vol. 1, No. 5, Sept-oct., pp 336-344.

[49] **Kaza, K. R. V., Mehmed, O., Williams, M.** and **Moss, L.** (1987)
*"Analytical and Experimental Investigation of Mistuning in Propfan Flutter."*, NASA Report NO. TM-88959, Apr.

[50] **Kielb, R. E.** and **Kaza, K. R. V.** (1983)
*"Aeroelastic Characterstics of a Cascade of Mistuned Blades in Subsonic and Supersonic Flows"*, Trans. ASME, Journal of Vibration, Acoustics, Stress and Reliability in Design, Vol. 105, Oct., pp 425-433.

[51] **Kielb, R. E.** and **Kaza, K. R. V.** (1984)
*"Effects of Structural Coupling on Mistuned Cascade Flutter and Response"*, Trans. ASME, Journal of Engineering for Gas Turbines and Power, Vol. 106, Jan., pp 17-24.

[52] **Kissel, G. J.** (1988)
*"Randomly Disordered Periodic Structures"*, Proc. 3rd International Conference on Recent Advances in Structural Dynamics, 18-22 July, pp 45-54.

[53] **Leissa, A.** (1981) *"Vibrational Aspects of Rotating Turbomachinery Blades"*, ASME, Appl. Mech. Rev. Vol.34, No. 5, pp 629-635

[54] **Lin, Y. K.** (1967)
*"Probabilistic Theory of Structural Dynamics"*, McGraw-Hill Company, New York, USA.

[55] **MacBain, J. C.** and **Whaley, P. W.** (1984)
*"Maximum Resonant Response of Mistuned Bladed Disk"*, Trans. ASME, Journal of Vibration, Acoustics, Stress and Reliability in Design, Vol. 106, pp 218-223.

[56] **Menq, C. -H., Griffin, J. H.** and **Bielak, J.** (1986)
*"The Influence of a Variable Normal Load on the Forced Vibration of a Frictionally Damped Structure"*, Trans. ASME, Journal of Engineering for Gas Turbines and Power, Vol. 108, pp 301-305.

[57] **Muszynska, A.** and **Jones, D. I. G.** (1981)
*"A Parametric Study of Dynamic Response of a Discrete Model of Turbomachinery Bladed Bisk"*, An ASME, Publication, 81-DET-137.

[58] **Muszynska, A.** and **Jones, D. I. G.** (1983)
*"On Tuned Bladed Disk Dynamics: Some Aspects of Friction Related Mistuning"*, Journal of Sound and Vibration, Vol. 86, No. 1, pp 107-128.

[59] **Newman, J. C. Jr.** and **Raju, I. S.** (1981)
*"An Empirical Stress Intensity Factor Equation for the Surface Cracks"*, Engineering fracture mechanics, Vol.15, pp.185-192.

[60] **Omprakash, V.** and **Ramamurti, V.** (1988)
*"Analysis of Bladed Disk - A Review"*, The Shock and Vibration Digest, Vol. 20, No. 11, pp 14-21.

[61] **Paris, P. C.** and **Erdogan, F.** (1963)
*"A Critical Analysis of Crack Propagation Laws"*, Journal of Basic Engineering, 85,4, pp.528-534, Dec.

[62] **Paris, P. C.** and **Sih, G. C.** (1965)
*"Stress Analysis of Cracks"*, American Society of Testing and Materials, STP 381, pp.30-83.

[63] **Parzen, E.** (1960)
*"Modern Probability Theory and Its Application"*,John Wiley and Sons,Inc., New York, London, Sydney.

[64] **Pierre, C.** (1990)
*"Weak and Strong Vibration Localization in Disordered Structures: A Statistical Analysis"*, Journal of Sound and Vibration, Vol. 139, No.1, pp 111-132.

[65] **Pook, L. P.** (1983)
*"The Role of Crack Growth in Metal Fatigue"*, The Metal Society, London.

[66] **Press, W. H., Flannery, B. P., Teukolsky, S. A.** and **Vetterling W. T.** (1986)
*"Numerical Recipes: The Art of Scientific Computing"*, Cambridge University Press.

[67] **Ramamurti, V.** and **Balasubramanian, P.** (1984)
*"Analysis of Turbomachine Blades - A Survey"*, Shock and Vibration Digest, Vol. 16, No. 8, pp 13-28.

[68] **Rao, J. S.** (1973)
*"Natural Frequencies of Turbine Blading - A Survey"*, Shock and Vibration Digest, Vol. 5, No. 10, pp 15-22.

[69] **Rao, J. S.** (1977)
*"Turbine Blading Excitation and Vibration"*, Shock and Vibration Digest, Vol. 9, No. 3, pp 3-14.

[70] **Rao, J. S.** (1987)
*"Turbomachine Blade Vibration"*, Shock and Vibration Digest, Vol. 19, No. 5, pp 3-10.

[71] **Rolfe, S. T.** and **Barson, J. M.** (1977)
*"Fracture and Fatigue Control in Structures: Application of Fracture Mechanics"*, Prentice Hall Inc.

[72] **Sakamoto, H., Takezono, S.** and **Nakano, T.** (1988)
*"Effect of Stress Frequency on Fatigue Crack Initiation in Titanium"*, Engineering Fracture Mechanics, Vol.30, No.3, pp.373-382.

[73] **Sanliturk, K. Y.** and **Imregun, M.** (1991)
*"Theoretical Modelling of the Damping Produced by Fatigue Cracks"*, Proceedings of the 9th International Modal Analysis Conference, Florence, Italy, pp 1370-1374.

[74] **Sih, G. C.** ( 1973)
*"Handbook of Stress Intensity Factors"*, Institute of Fracture and Solid Mechanics", Lehigh University, Bethlehem.

[75] **Singh, M. P.** (1988)
*"Turbine Blade Dynamics: A Probabilistic Approach"*, ASME, Vibrations of Blades and Bladed Disk Assemblies, Book No. H00335.

[76] **Singh, M. P.** and **Ewins, D. J.** (1988)
*"A Probabilistic Analysis of Mistuned Bladed Turbine Disc"*, Proceedings of Inst. Mech. Engrs. International Conference on Vibrations in Rotating Machinery, Heriot-Watt University, Edinburgh, Sept., pp 143-150.

[77] **Sinha, A.** (1986)
*"Calculating the Statistics of Forced Response of a Mistuned Bladed Disk Assembly"*, AIAA Journal, Vol. 24, No.11, Nov., pp 1797-1801.

[78] **Sinha, A.** and **Chen, S.** (1989)
*"A Higher Order Technique to Compute the Statistics of Forced Response of a Mistuned Bladed Disk Assembly"*, Journal of Sound and Vibration, Vol. 130, No. 2, pp 207-221.

[79] **Sinha, A.** and **Griffin, J. H.** (1984)
*"Effects of Static Friction on the Forced Response of Frictionally Damped Turbine Blades"*, Trans. ASME, Journal of Engineering for Gas Turbines and Power, Vol. 106, pp 65-69.

[80] **Sinha, A., Griffin, J. H.** and **Kielb, R. E.** (1985)
*"Influence of Friction Dampers on Tortional Blade Flutter"*, ASME, Journal of Engineering for Gas Turbines and Power, No. 85-GT-170.

[81] **Sogliero, G.** and **Srinivasan, A. V.** (1980)
*"Fatigue Life Estimates of Mistuned Blades Via A Stochastic Approach"*, AIAA Journal, Vol. 18, No.3, Mar., pp 318-323.

[82] **Srinivasan, A. V.** (1980)
*"Influence of Mistuning on Blade Torsional Flutter"*, NASA Report, No. CR-165137.

[83] **Srinivasan, A. V.** (1984)
*"Vibrations of Bladed-Disk Assemblies - A Selected Survey"*, Trans. ASME, Journal of Vibration, Acoustics, Stress and Reliability in Design, Vol. 106, pp 165-168.

[84] **Srinivasan, A. V.** and **Fabunmi, J. A.** (1984)
*"Cascade Flutter Analysis of Cantilevered Blades"*, Trans. ASME, Journal of Engineering for Gas Turbines and Power, Vol. 106, Jan., pp 34-43.

[85] **Srinivasan, A. V.** and **Frye, H. M.** (1976)
*"Effects of Mistuning on Resonant Stresses of Turbine Blades"*, Proceedings of ASME on Structural Dynamics Aspects of Bladed Disk Assemblies, Dec., pp 57-71.

[86] **Stange, W. A.** and **MacBain, J. C.** (1983)
*"An Investigation of Dual Mode Phenomena in a Mistuned Bladed Disk"*, Trans. ASME, Journal of Vibration, Acoustics, Stress and Reliability in Design, Vol. 105, July, pp 402-407.

[87] **Stanley, P.** (1977)
*"Fracture Mechanics in Engineering Practise"*, Applied Science Publishers ltd., London.

[88] **Tada, H., Paris, P C.** and **Irwin, G. R.** (1973)
*"The Stress Analysis of Cracks Handbook"*, Del Research Corporation, Hellertown.

[89] **Takezono, S.** and **Satoh, M.** (1982)
*"Effects of Stress Frequency on Fatigue Crack Propagation in Titanium"*, ASME, Journal of Engineering Materials and Technology, Vol.104, pp.257-261, Oct.

[90] **Tobias, S. A.** and **Arnold, R. N.** (1957)
*"The Influence of Dynamical Imperfection on the Vibration of Rotating Disks"*, Proccedings of the Institute of Mechanical Engineers, Vol. 171, No.2, pp 669-690.

[91] **Wagner, J. T.** (1967)
*"Coupling of Turbomachine Blade Vibrations Through the Rotor"*, Trans. ASME, Journal of Engineering for Power, Vol. 89, No. 4, Oct., pp 502-513.

[92] **Wang, J. H.** and **Yau, H. L.** (1990)
*"Design of Blade-Shroud to Minimize the Sensitivity of Response to Preload Mistuning"*, IFToMM 3rd International Conference on Rotodynamics, Lyon, France, Sept., pp 535-540.

[93] **Wei, S. T.** and **Pierre, C.** (1990)
*"Statistical Analysis of the Forced Response of Mistuned Cyclic Assemblies"*, AIAA Journal, Vol. 28, No. 5, May, pp 861-868.

[94] **Whitehead, D. S.** (1966)
*"Effect of Mistuning on the Vibration of Turbomachine Blades Induced by Wakes"*, Joural of Mechanical Engineering Science, Vol. 8, No. 1, pp 15-21.

[95] **Whitehead, D. S.** (1976)
*"Research Note: Effect of Mistuning on Forced Vibration of Blades with Mechanical Coupling"*, Journal of Mechanical Science, Vol. 18, No.6, pp 306-307.

[96] **Wolfram, S.** (1988)
*"Mathematica: A System For Doing Mathematics"*, Addison-Westley Company.